Predicting Blast-Induced Damage for Open Pit Mines Using Numerical Modelling Software and Field Observations

by

Alexander K. Hall

A thesis submitted in partial fulfillment

of the requirements for the degree of

Master of Applied Science in Natural Resources Engineering (M.A.Sc.)

The Faculty of Graduate Studies

Laurentian University

Sudbury, Ontario, Canada

Thesis Defence Committee/Comité de soutenance de thèse
Laurentian Université/Université Laurentienne
Faculty of Graduate Studies/École des études supérieures

Title of Thesis Titre de la these	PREDICTING BLAST-INDUCED DAMAGE FOR OPEN PIT MINES USING NUMERICAL MODELLING SOFTWARE AND FIELD OBSERVATIONS
Name of Candidate Nom du candidat	Alexander K. Hall
Degree Diplôme	Master of Applied Science

Department/Program Département/Programme	Engineering	Date of Defence Date de la soutenance	December 02, 2014

APPROVED/APPROUVÉ

Thesis Examiners/Examinateurs de thèse:

Dr. Philip Dirige
(Supervisor/Directeur(trice) de thèse)

Dr. Martin Hudyma
(Committee member/Membre du comité)

Dr. Ming Cai
(Committee member/Membre du comité)

Dr. Qian (Ken) Liu
(External Examiner/Examinateur externe)

Approved for the Faculty of Graduate Studies
Approuvé pour l'École des études supérieures
Dr. David Lesbarrères
M. David Lesbarrères
Director, Faculty of Graduate Studies
Directeur, École des études supérieures

ACCESSIBILITY CLAUSE AND PERMISSION TO USE

Abstract

Blasting is the most common method used to fragment rock in the mining industry. However, given the violent nature of explosives and the high variability of results that can occur from blast to blast, there is potential to cause significant damage to the final walls of an open pit, which can lead to slope stability problems, catch bench filling, long-term rock fall hazards and ramp closure. Blasts need to be designed to suit the characteristics of the rock to be broken. Characteristics of the existing rock mass such as natural jointing, joint orientation, joint condition, and the strength of the rock, all need to be accounted for prior to designing a blast.

In general, blasting engineers rely on a combination of empirical analysis and rules of thumb for blast designs. The uncertainty involved with these techniques can lead to significant problems in open pit mining. At the bench scale of an open pit mine, the loss of the bench crest is a concern, however at the full pit scale, bench deterioration can jeopardize worker safety and lead to potential closure of the mine. The results of a blast can be highly variable – a blast design that yields favorable results on one side of a pit can have detrimental effects on another wall of the pit or at different elevations in the pit, based on the characteristics of the rock. It often takes multiple iterations of blast designs to achieve an optimal result, which is costly and time consuming for the company that operates the mine.

The purpose of this thesis is to evaluate the effectiveness of a relatively new software package, Blo-Up, that combines both a finite difference continuum code and a distinct element code in order to model the entire blasting process from start to finish. The main focus of the research will be to examine blast induced damage sustained to final pit walls and provide techniques for minimizing damage. The specific areas of the study are:

1) To confirm the software is able to give results similar to those observed in the field;
2) To model pre-split designs in homogeneous rock;
3) To model pre-split designs in jointed rock masses;
4) To model the effect of a production hole detonation on inclined pre-split holes, as opposed to vertical pre-split holes, and
5) To model effects of large scale production blasts on final wall stability. For the purposes of this review, kimberlite rock was chosen to be the focus of the study due to its ductile characteristics, which makes controlled blasting difficult.

The main findings of the research are as follows:

1) The software is able to replicate blast outcomes observed in the field;
2) The importance of tailoring the pre-split design to the rock mass is critical, and
3) The main production blast must be well balanced if the explosive energy is to be evenly distributed through the system.

Keywords

Blasting, Blast Damage, Open Pit Mining, Pre-split Blasting

Acknowledgments

A number of people must be thanked for their assistance throughout this research. First and foremost, I would like to thank my supervisor Dr. Philip Dirige, who was always available to guide me through this research and keep me on track. Many hours of Phil's personal time were used to help with research and to discuss the direction of the study. Many thanks for your patience and guidance over the two years it took to complete this work.

I would like to express my gratitude to the review committee, Dr. Ming Cai, Dr. Martin Hudyma and Dr. Qian (Ken) Liu for their encouragement and valuable comments during the review process.

I would also like to thank my colleagues at Itasca who have contributed in many ways to this research. Many thanks to Dr. Patrick Andrieux for seeing the potential in me and giving me the opportunity to work on various blasting projects around the world. A special thanks to Dr. Jason Furtney, who spent endless hours reviewing my research and for literally rewriting some of the software code to accommodate my work. Others who provided invaluable support, input and direction are Dr. Richard Brummer, Luigi Cotesta and Chris O'Connor.

Finally, I would like to thank my parents, Don and Donna Hall. Their endless encouragement and support over the years has allowed me to become the person I am today.

Table of Contents

List of Tables

List of Figures

List of Appendices

- Chapter 1: Introduction -

1.1 Introduction

The most common method of excavating rock in the mining industry is by drilling and blasting. However, despite the wide usage of explosives in the industry, there is a lack of understanding of how to achieve a specific result and the factors that control the outcome of a blast. The large initial stress waves created upon detonation, followed by the rapid expansion of gas, are accepted as the main factors that cause fragmentation of rock and blast induced damage to the surrounding rock mass. However, the amount of fragmentation and damage as a result of these factors is poorly understood.

Blast induced damage refers to the extra fracturing or cracking caused by the blast beyond the immediate excavation boundaries or intended area of fragmentation. Although fragmentation and damage are results of blasting, the topic of the effect of blast design and explosive type on the degree of fragmentation is beyond the scope of this thesis. The Kuz-Ram model for prediction of fragmentation from blasting by Cunningham (1983), Cunningham (1987), Drilling of Blasting of Rocks (Jimeno *et al*., 1995), The Modern Technique of Rock Blasting (Langefors and Kihlstrom, 1976), Measurement of Blast Fragmentation (Franklin and Katsabanis, 1996), and Rock Fragmentation Control in Blasting (Cho and Kaneko, 2004), provide good coverage of the subject.

One of the most important aspects of an open pit mine is the stability of the final wall. The final pit wall consists of a series of benches descending to the bottom of the pit, which includes a ramp for accessing the pit. The main purpose of the benches is to provide working platforms for

catching material that may fall from the pit wall, thereby protecting personnel working in the pit. The pit wall is designed to be stable for the life of the mine, however there are certain factors, such as the effect of blasting, that are not accounted for in the design phase of a mine and can affect bench and pit wall stability.

Due to a lack of understanding and control of blasting, pit walls often sustain some level of damage, which can lead to instability of the final wall. Factors such as blast design, type of explosive, strength properties of the rock and presence of natural joints or discontinuities in rocks all play a significant role in the distribution of fragment size and blast induced damage in rock. The research presented in this thesis is intended to give a better understanding of the mechanics of fragmenting rock through blasting, identify various methods of predicting blast induced damage, and present various ways of minimizing blast damage to open pit walls.

1.2 Purpose of Research

The author has provided blasting expertise to several operators in the mining industry with the focus on controlling blast induced damage sustained to final walls. Typically, this is an iterative trial and error process that involves changing small aspects of a blast design until an optimal result is reached, which can be time consuming and costly for the client.

Since 2001, Itasca International Inc. has been a member of the Hybrid Stress Blast Model (HSBM) project (Ruest *et al*., 2006, Ruest, 2008 and Furtney *et al*., 2009), comprised of a consortium of companies, with the common goal of developing a numerical model of the blasting process and fragmentation of rock. The software, called Blo-Up (Ruest, 2008), was created by combining two of Itasca`s numerical modelling codes: FLAC (Fast Lagrangian Analysis of Continua), a finite difference continuum code, and PFC3D (Particle Flow Code), a

three dimensional distinct element code. At the time of writing this thesis, the software was still in the development stage and not commercially available to the public.

The goal of this thesis is to demonstrate the capability of software to predict the amount of damage that can be expected from various blast designs. Data collected while the author provided consulting services to open pit diamond mine operators in Southern Africa will be used to demonstrate that the software can provide results that correlate with field observations.

1.3 Scope of Work

This thesis will use a relatively new software package, Blo-Up, which has been created to model the complete blast process from start to finish. The focus will be to analyse blast-induced damage in rocks incorporating various conditions such as blast design, explosive type, strength properties of the rock mass, and presence and conditions of discontinuities in rocks. The research brings some technical analysis to a process that has traditionally been conducted by trial and error approach, generally performed by engineers with blasting experience gained over many years of practice. This thesis provides some real-world testing and field validation of the capacity of the program.

The main focus of this research will be to examine blast induced damage sustained to final pit walls and present techniques for minimizing damage. The research consists of individual tasks that represent issues that can be encountered in the field and could promote blast-induced damage. The specific areas of the study are:

1) Modelling pre-split designs in homogeneous and competent rock: a basic five hole pre-split model was created for this stage of analysis in models simulating a granite rock. The goal is to demonstrate a pre-split design used in homogeneous and competent rock.

2) Modelling various pre-split designs in soft and jointed kimberlite rock: the basic five hole pre-split model is used with various orientations of joint sets included in the models. The goal is to present a pre-split blast design that minimizes blast-induced damage in kimberlite rock.
3) Modelling the damage and crack propagation at the ends of the pre-split line: a method of controlling the propagation of crack and damage at the ends of the pre-split line will be presented.
4) Modelling inclined pre-split holes: a basic model was created to show the effect of seismic waves generated by a production blast on the pre-split line. Both vertical and inclined pre-split lines were examined to determine if there is any advantage of an inclined pre-slit line for shedding the force of the seismic waves up the pre-split.
5) Modelling large scale production blasts and the effect on the final wall: large scale production blasts are modelled with high and low levels of confinement to determine if the production blast has an effect on the stability of the final wall.
6) Field validation of the optimal blast results obtained from numerical modelling.

1.4 Thesis Outline

This thesis is divided into six chapters and appendices as follows:

- **Chapter 1 – Introduction:** This chapter provides an overview of the problem and discusses the objectives of thesis, approach to the modelling and the thesis outline.
- **Chapter 2 – Background Information:** Reviews background information on the mechanics of blasting and highlights the importance of controlling blast-induced damage in open pit mines. Methods to predict blast damage are also discussed.

- **Chapter 3 – Blo-Up Software:** Provides a description of the software used for the research and gives a brief summary of the physics engine used in the software. In addition, this chapter also details some of the validation work that has been completed to date with the software.
- **Chapter 4 – Numerical Modelling of Pre-Split Blasts:** Presents the findings of the research. Small scale pre-split models are validated in homogeneous rock and in rock with various joint orientations.
- **Chapter 5 – Numerical Modelling of Production Blasts:** Large scale production blast models are also presented in this chapter to compare the amount of damage sustained to final walls with fast and slow timed detonation sequences. Included in this chapter is a brief examination of effect of using buffer rows.
- **Chapter 6 – Conclusions:** Summarizes the conclusions of the thesis. It also gives further suggestions for minimizing blast-induced damage that were not covered in the scope of this thesis. Limitations of the software and models and future work will also be discussed.

- Chapter 2: Background Information -

2.0 Blasting Excavations in Rock

In order to fragment rock, a significant source of energy is required. Blasting is by far the most common and economical method used to fragment rock due to the high energy that explosives produce and the relatively lower cost of drilling and blasting compared with other available techniques of rock excavation. The borehole itself provides confinement and distribution of the explosive along the borehole column, which increases the efficiency of the blast because the explosive energy is confined to the interior of the blasthole. The addition of stemming material to the top of the hole creates a confined system that will further lock the energy generated by the explosive detonation to the interior of the hole. Upon detonation, the high energy stress wave will radiate out into the surrounding rock mass creating a highly fractured zone immediately around the annulus of the hole. These fractures are exploited by the expanding gasses resulting in increased fracturing.

2.1 Mechanics of Blasting Rock

There are two processes that occur when an explosive is detonated in a borehole: 1) stress waves are produced from the detonation and 2) high pressure gasses are created. Stress waves propagation and gas expansion are different processes that take place in rock blasting but they are not independent; both are the result of the same explosive chemical reactions (Trivino, 2012). Stress waves created from the detonation will damage the rock mass immediately surrounding the borehole; however the stress wave quickly attenuates as it travels away from the blasthole. High pressure gas created during the detonation reaction results in extensive secondary breakage

of the rock by exploiting cracks created by the initial stress wave and any natural fabric in the rock mass. The following sections will discuss these processes of breaking rock in more detail.

2.1.1 Stress Wave Propagation

When the explosive chemical reaction occurs, a high-detonation pressure is produced in the borehole. The result is massive compressive forces acting on the walls of the borehole almost instantaneously. This compressive force is known as the stress wave, which radiates outward away from the borehole. At some distance away from the borehole the energy from the explosive decreases to a point at which no further shattering of the rock occurs.

The stress wave is sometimes referred to as the shock wave. Shock waves are a specific physical phenomena occurring in materials in which the speed is a strong function of the material density which causes shocks to occur. In blasting, the strongest shock wave is the detonation front. The shock wave generated in the rock within the vicinity of the blasthole quickly attenuates into stress waves, which propagate at the sonic velocity of the rock mass. In the mining and blasting industry, people casually say shock wave to refer to both the detonation wave and the elasto-plastic stress wave in the rock, but this is not technically correct. The term stress wave will be used in this thesis to refer to the large wave travelling through the rock after explosive detonation.

The stress wave is the initial process that breaks the rock in the immediate vicinity of the blasthole. The immediate area around the borehole is crushed in compression with fracturing of the rock occurring beyond the immediate halo of crushed rock. Due to the small size of a borehole, the high pressure gasses created from the initial detonation is confined and is responsible for producing stress waves. This initial stress wave velocity decreases significantly

as the distance from the blasthole increases (Krehl, 2001). There are three major zones of deformation that will develop around the borehole after an explosion (Figure 1).

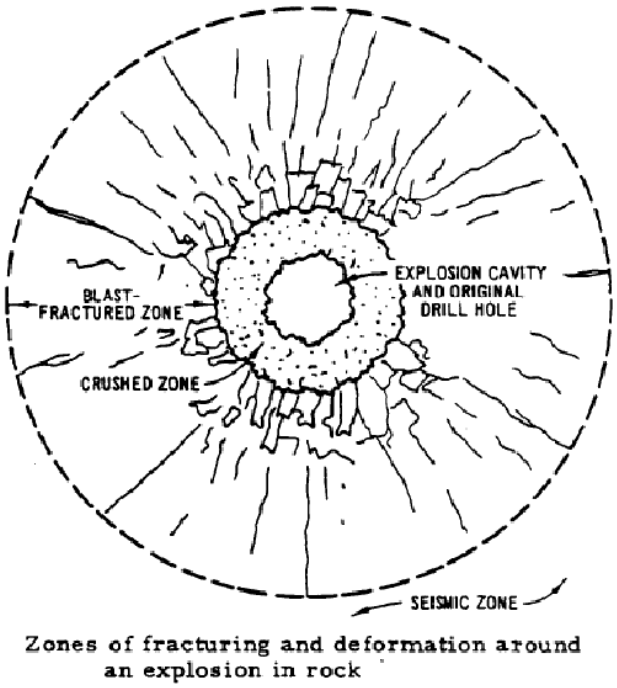

Figure 1 – Illustration showing the three main zones of deformation around a borehole (Sharma, 2011).

The three main deformation zones are:

1. The explosive cavity and crush zone: the epicenter of the blast, this is the area that will experience crushing of rock and the highest compressive forces.
2. Fractured zone: this area will experience some crushing and propagation of cracks radiating out into the rock mass.
3. Seismic zone: the stress wave energy has dissipated or significantly attenuated below the elastic limit of the rock and little or no breaking occurs. The wave front will then propagate as a seismic wave.

The sequence of rock breaking is illustrated in Figure 2.

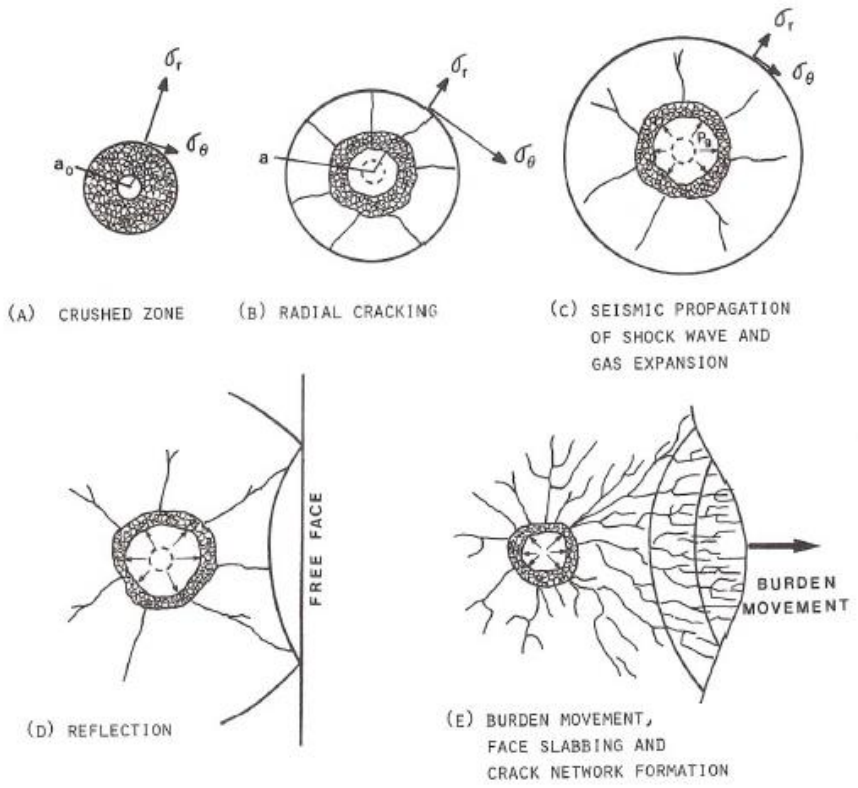

Figure 2 – Clockwise from top left: (A) the crushed zone, (B) radial cracking, (C) seismic propagation of the stress wave and gas expansion into the cavity, (D) reflection of seismic waves, and (E) burden movement, face slabbing and crack network formation (Hartman, 1992).

As the distance away from the borehole is increased, energy decreases and the stress wave amplitude rapidly downgrades to an elastic seismic wave. The seismic waves will travel much further than the initial stress wave, but are not intense enough to initiate damage or further breaking. Figure 3 shows a schematic of a seismic wave prorogation through a rock mass.

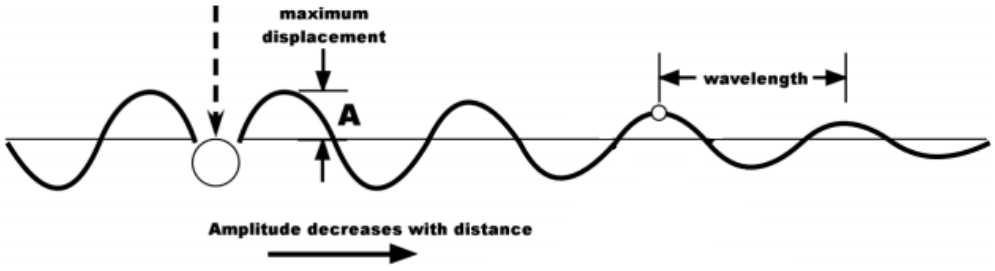

Figure 3 – Schematic showing a stress wave deteriorating into a seismic wave (Richards and Moore, 2013).

There are different types of seismic waves, also known as body waves, which are created from a blast. The first type, P waves or primary waves, also known as longitudinal waves, propagate away from a blast in compression and travel very quickly. The second type, S waves, also known as shear waves, move perpendicular to the P waves and are typically 50-60% slower than the P wave (Richards and Moore, 2013). The speed of these waves depends on the characteristic of the rock they are travelling through, mainly the density of the rock, grain orientation and the water content – for example, waves will travel faster through granite rock as opposed to kimberlite rock. Rayleigh and Love waves are generated by blasting, however, these are surface waves, which move slowly and fade rapidly with depth and have virtually no effect on the fragmentation or damage of the rock mass.

There are correlations, which can be made between Young's modulus (*E*) and shear modulus (*G*) and ground longitudinal v_l and transversal v_t wave velocities. By using these correlations, an estimate of wave velocities can be made based on the properties of the rock the waves will be travelling through. These correlations have been described in detail (Srbulov, 2010). The common equations for these relationships are:

$$E = \rho \cdot v_l^2 \qquad \text{(Equation 2.1)}$$

$$G = \rho \cdot v_t^2 \qquad \text{(Equation 2.2)}$$

$$G = \frac{E}{2 \cdot (1+v)} \qquad \text{(Equation 2.3)}$$

Where, v is Poisson's ratio and ρ is density.

The angle of a reflected wave equals the angle of the incident wave according to Fermat's principle of the least time for wave reflection (Srbulov, 2010). A compressive wave reflects as a

compressive wave from a fixed boundary and as a tensile wave from a free boundary. Rock that has no cohesion or is broken, such as a final wall boundary after a pre-split has been detonated, will not sustain tension and as a result the reflected waves cause loosening. It should also be mentioned that transversal waves reflect from a fixed boundary with the same amplitude as the amplitude of the incoming wave but with opposite sign. At a free boundary, the shear stress will be zero and incoming transversal waves doubles its incoming amplitude (Srbulov, 2010).

2.1.2 High Pressure Gas Expansion

High pressure gas expansion after the initial detonation of explosive is critically important for creating fragmentation or damage of the rock mass. The high pressure gas will exploit the path of least resistance in the rock mass and travel through the new cracks created by the stress wave and through any natural jointing in the rock. Ultimately, the network of cracks and natural joints in the rock are broken into fragments. Once the gas dissipates and pressure drops as it travels along the fractures, its ability to break the rock to fragments is decreased and eventually at some distance, no more rock is fractured. Gas reaching a free face will rapidly vent to atmospheric pressure. Fractures can, however, extend beyond the excavation boundary provided that gas pressures are large enough to expand cracks. Figure 4 shows an example of fracture network created by gas penetration.

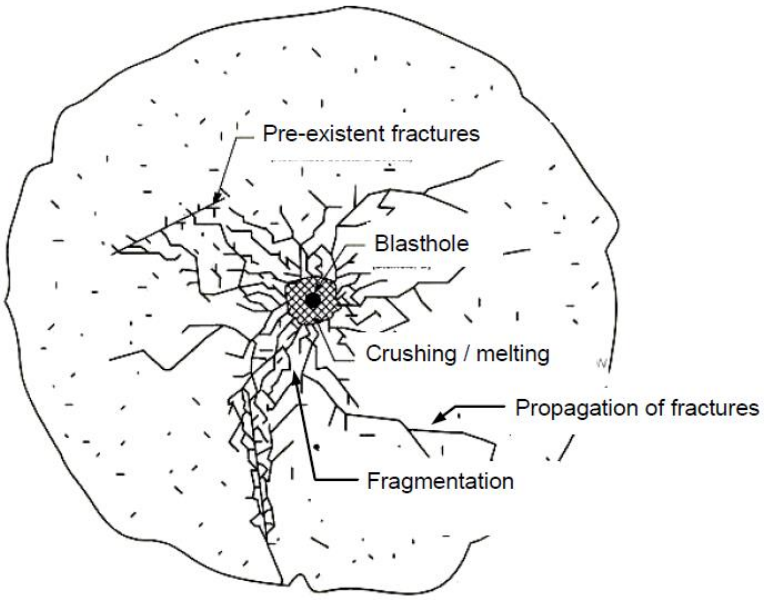

Figure 4 – Fracture network created by gas penetration (Yamin, 2005).

Peak overpressure will occur very quickly after the blast has been initiated, which is followed by a rapid decay of pressure in the system to atmospheric pressure. Due to the rapid decrease in pressure, a vacuum is created in the system for a short duration until atmospheric pressure is achieved. The air-blast overpressure for a fully confined blasthole can be estimated using Equation 2.1 (ICI, 1990).

$$P = 3.3\left(\frac{D}{\sqrt[3]{W}}\right)^{-1.2} \qquad \text{(Equation 2.4)}$$

Where, P is the detonation pressure (GPa), D is the distance from the blast (m) and W is the charge mass per delay (kg).

If the velocity of detonation (VOD) and density of the explosive are known, the detonation pressure can also be estimated using Equation 2.2 (IATG 01.80, 2013).

$$\mathrm{P_{det}} = 2.5 \text{ x VOD x} \frac{\mathrm{D}}{0.000001} \qquad \text{(Equation 2.5)}$$

Where, P_{det} is the detonation pressure (GPa), VOD is the velocity of detonation (m/s), and D is the density of the explosive (g/cm^3).

2.2 Open Pit Blasting

The main part of a blast in surface excavations is referred to as a production blast. The design of the production blast is tailored to the desired outcome of the blast. There are a multitude of factors that should be considered when designing a blast and several examples are listed below:

- *Fragment size*: in cases where coarse fragment size is desired, it may only be necessary to 'bump' the rock to get coarse fragmentation. This means less explosive energy is required – fewer holes and less explosive can be used. However, more often than not, small fragmentation size is required for an operation. Typically, broken rock is taken to a mill so that it can be crushed further in order to extract economic minerals. It is more efficient to achieve smaller fragmentation during blasting than subjecting the rock to various crushing stages in the mill to attain the desired size.
- *Muck pile shape and material throw*: depending on the type of equipment used at the mine site, the shape of the muck pile may be important. For example, if draglines are used it is important to have steep muck piles.
- *Minimizing fly rock, noise and vibration*: some locations close to residential areas or close to large structures will need to minimize the amount of fly rock, air blast and vibrations produced during a blast.
- *Minimizing damage to final walls*: no blast design is intended to cause damage to a final pit wall.

Depending on the desired outcome of a blast, there are several factors that can be modified in the blast design. The most relevant factors that can be modified are:

- *Timing*: a blast with fast timing will typically have finer fragmentation of the rock and a steeper muck pile at the end of the blast.
- *Borehole length and diameter*: more or less explosive can be used.
- *Borehole burden and spacing*: close spacing of holes will result in finer fragmentation.
- *Explosive type*: various explosive products have different energy.
- *Detonation pattern*: allows the engineer to control where the fractured rock goes.

Figure 5 illustrates a bench layout and also provides insight on the nomenclature used for blast design, while Figure 6 shows a typical blast initiation and the subsequent rock breakage.

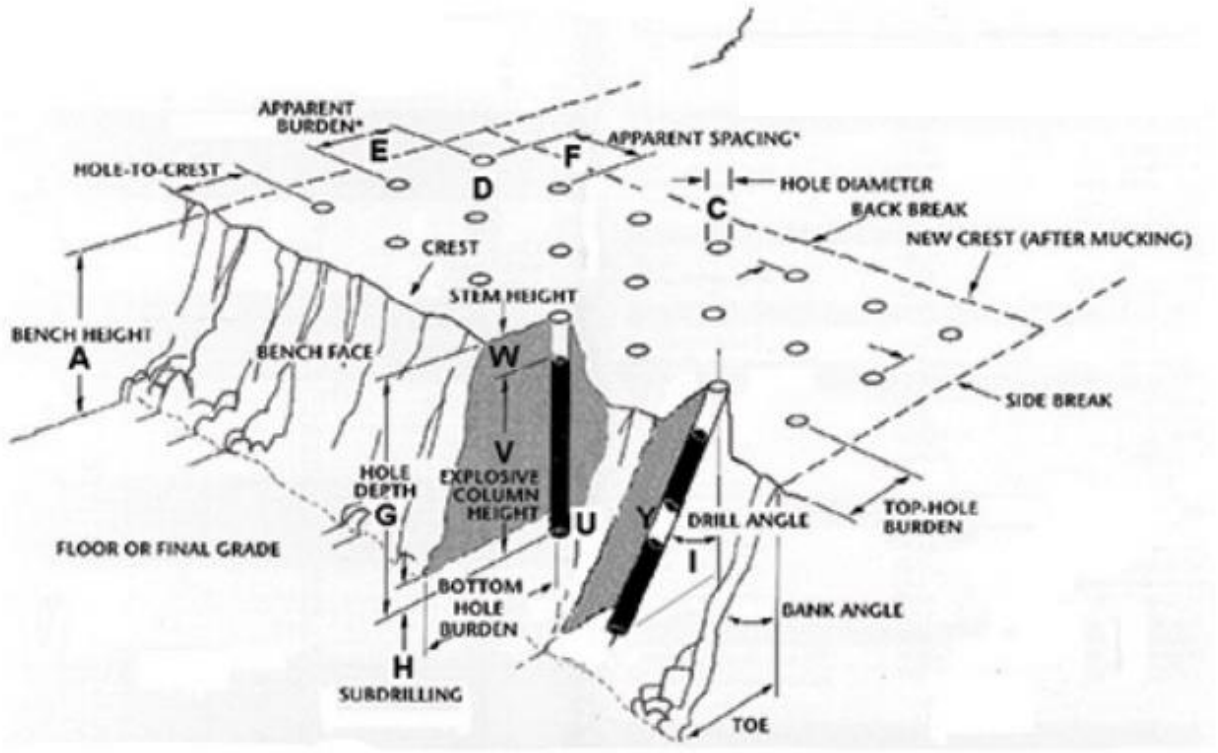

Figure 5 – Schematic showing a bench layout with relevant nomenclature (Therin, 2012).

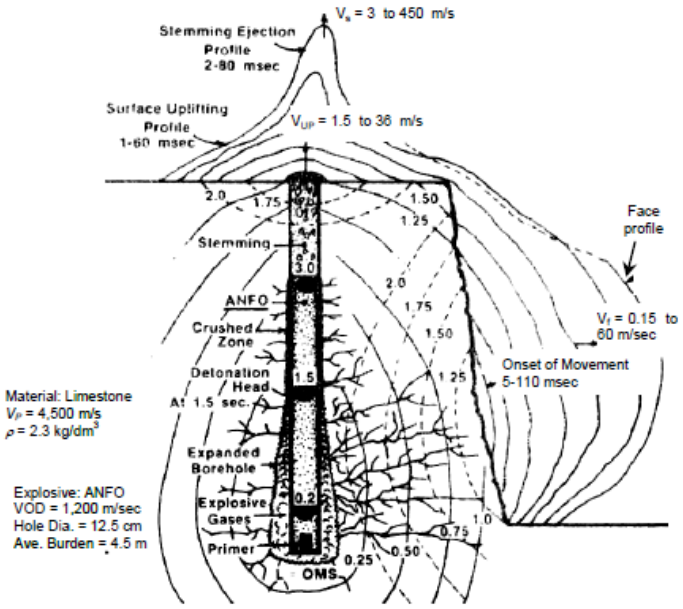

Figure 6 – Typical initiation of a blast with expected movement profile (Morhard, 1987).

2.3 Explosive Selection

Explosives for blasting come in a variety of forms. Some of the predominant forms of explosives used for excavation purposes in mining and civil applications are: a) bulk to be pumped (water gels and emulsions); b) dry as small prills (Ammonium Nitrate and Fuel Oil, commonly known as ANFO), and c) pre-packed in cartridges (water gels and emulsions). Each type of explosive has a unique gas and shock energy generated upon detonation. Therefore, depending on the desired outcome of the blast, the explosive type should be chosen accordingly. For example, if the desired outcome of the blast is to create a highly fractured zone in the rock mass, an explosive with high shock energy, such as an emulsion product, should be selected for use. If the rock mass is highly fractured or jointed already, an explosive with high gas energy, such as ANFO, should be selected.

Figure 7 illustrates the gas and shock energy ratios for ANFO and emulsion explosive products (Rorke and Brummer, 1988). The comparison of energy ratios was developed by ICI

International and models the performance of explosives in rock. Figure 8 illustrates the detonation velocities for various types of explosives (U.S. Dept. of the Interiors Office, 2008). Both figures indicate emulsion products have high shock energy immediately after detonation, while ANFO has more gas energy that begins doing work with a slight delay after detonation.

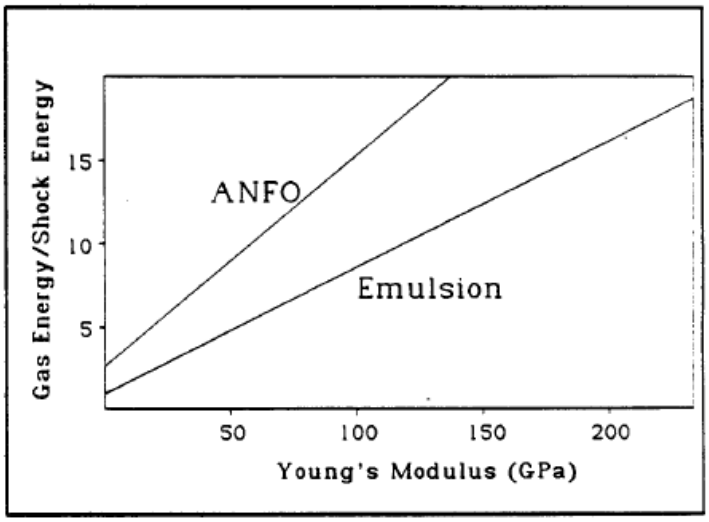

Figure 7 – Graphical representation of the gas and shock energy ratios for different explosive types (Rorke, and Brummer, 1988).

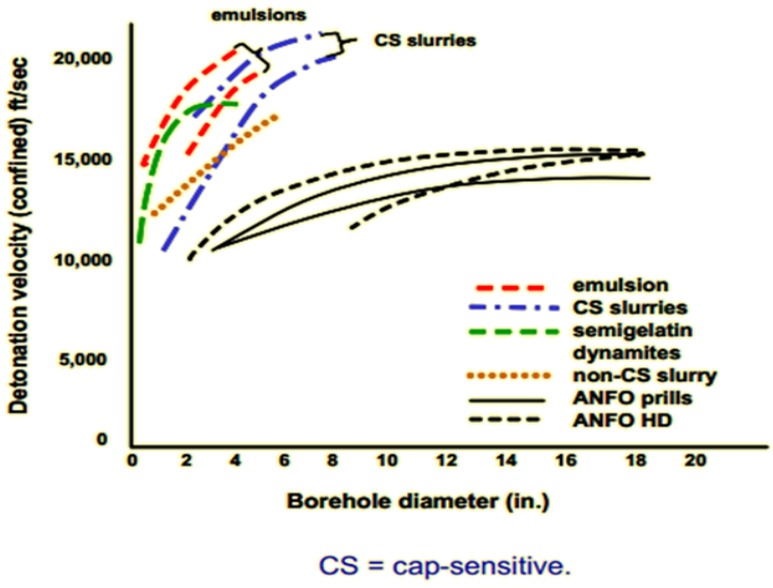

Figure 8 – Graphical representation illustrating the relationships between borehole diameter and the detonation velocity for various types of explosives (U.S. Dept. of the Interiors Office, 2008).

2.4 Basic Guidelines & Rules of Thumb for Blast Design

In general, blasting engineers rely on a combination of empirical analysis and rules of thumb for blast designs. The uncertainty involved with these techniques can lead to significant problems in open pit mining. It often takes multiple iterations of blast designs to achieve an optimal result, which is costly and time consuming for the company that operates the mine. This section will detail some of the generally accepted rules of thumb and guidelines used.

2.4.1 Guidelines for Powder Factor and Splitting Factor

Powder factor is defined as the amount of explosive used to break a volume of rock. It can be calculated by dividing the volume of rock required to break by the weight of explosives used (Equation 2.3). Based on industry experience, Dyno Nobel has suggested ranges of powder factor values that have worked well in practice (Dyno Nobel, 2010). The four ranges were based on the quality of the rock for a production blast and three ranges have been given for pre-split blast (Table 1). Powder factor (PF) can be determined using Equation 2.6.

$$PF = \frac{C}{BH \times B \times S} \qquad \text{(Equation 2.6)}$$

Where, C is the explosive charge mass per hole = explosive density x (π x r^2 x h) (kg); BH is the bench height (m); B is the burden (m); and S is the hole spacing (m).

Table 1 – Summary of expected ranges for powder factor based on industry experience (Dyno Nobel, 2010).

Rock Type	Production Blast Powder Factor (kg/m^3)	Pre-split Blast Powder Factor (kg/m^2)
Hard	0.7-0.8	0.6-0.9
Medium	0.4-0.5	0.4-0.5
Soft	0.25-0.35	0.2-0.3
Very Soft	0.15-0.25	

Splitting factor is another general guideline that can be used to design a pre-split (St. J. Tose, 2006). Although similar to the powder factor equation, splitting factor is calculated by dividing the charge mass per hole by the hole spacing between the pre-split holes (Equation 2.7) instead of dividing the charge mass per hole by the hole spacing, burden and bench height.

$$P = \frac{C}{HS \times BH} \qquad \text{(Equation 2.7)}$$

Where, P is the Split Factor (kg/m^2); C is the explosive linear charge per hole which is determined by multiplying the explosive density x (π x r^2 x h) (kg); HS is the hole spacing (m); and BH is the bench height (m).

The argument for using the splitting factor as opposed to powder factor for the pre-split is due to the cubic metre (m^3) reference in the powder factor equation. Considering burden for a pre-split, calculation is not reasonable because the pre-split is fired prior to the production blast. Burden should be the distance to the nearest free face, however, since the pre-split line is fired prior to the main production blast, the burden then should be the distance of the pre-split holes to the first row of production holes, which could be very high. The Dyno Nobel rule of thumb guidelines suggest that for the pre-split calculation, the burden should be the distance to the closest row of production holes, which is not actually correct, as they are the last holes to be fired in the sequence. The powder factor equation should not be used for designing a pre-split because it is ultimately volumetric and has to take into account the inter-row distance. Splitting factor (kg of explosives per m^2 to split) makes much more sense and will be used throughout this thesis. The suggested range for the splitting factor is between 0.3 to 0.7 kg/m^2 (St. J. Tose, 2006).

It should be reiterated that both the splitting factor and the powder factor guidelines are general rules of thumb that are used for laying out a blast at many operating mines today. Further

tailoring and refinement will undoubtedly be required in the field. These rules of thumb do not take into consideration site specific conditions, which can be detrimental to the outcome of the blast.

Figure 9 shows a photo of a mine site in Southern Africa that designed the pre-split within the acceptable splitting factor range. However, the natural discontinuities existing in the rock resulted in significant damage to the final wall as a result of high pressure gasses exploiting the natural joint sets in the rock mass. Specific characteristics of the rock mass, such as jointing, are not captured in the powder factor calculation, which can lead to shortfalls in the field.

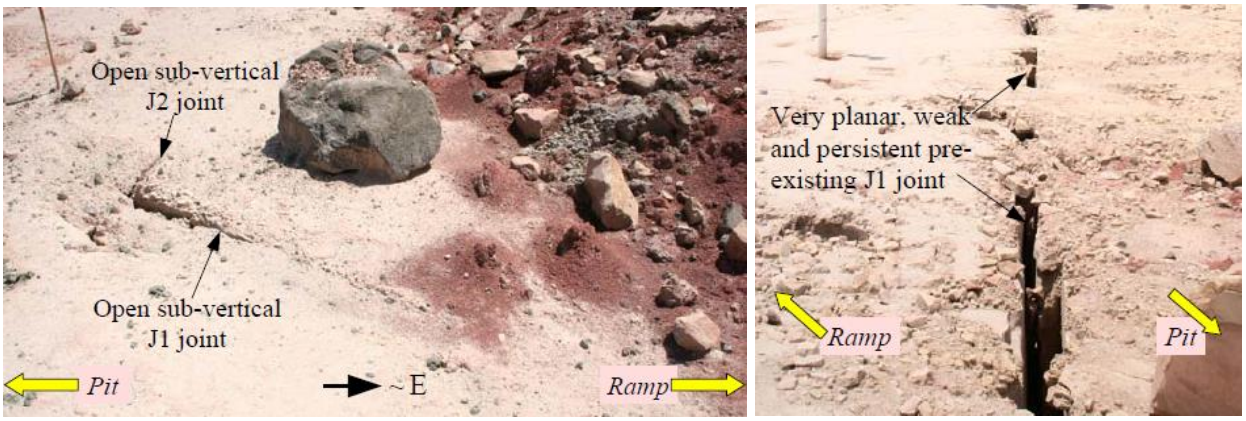

Figure 9 – Location where site specific characteristics resulted in poor blast results (Photo courtesy of Andrieux, 2012).

2.4.2 Blastability Index

Lilly (1986) developed a classification system, called Blastability Index, to be used for designing a blast to conform to a specific fragmentation size. The Blastability Index correlates with the powder factor. Lilly recognized some of the most important parameters that can affect the outcome of a blast are the specific characteristics of the rock mass. Four main parameters were identified that contribute considerably to the outcome of a blast:

1) Structural nature of the rock mass;

2) Spacing and orientation of joints, bedding and foliation;
3) Specific gravity of the material; and
4) Strength of the material.

The index has a maximum value of 100, which would correspond to extremely hard rock masses such as granite, while weaker rock masses, such as shale, would have values around 20. The Blastability Index is used in the Kuz-Ram empirical model for predicting fragmentation size. To date, it has not been used to predict the extent of damage or fracturing.

The Blastability Index equation is as follows (Lilly, 1986):

$$A = 0.06 * (RMD + JF + RDI + HF) \quad \text{(Equation 2.8)}$$

Each of these components represents a separate equation based on other factors. RMD or Rock Mass Description is calculated by:

$$RMD = 10 + 10 * X_i \quad \text{(Equation 2.9)}$$

Where, X_i is the block size of the in-situ rock and is a function of the number of joint sets, joint spacing and the orientation of the joint sets. JF is classified as the Joint Factor:

$$JF = JF_s + JF_o \quad \text{(Equation 2.10)}$$

Where, JF_s is the Joint Spacing Factor and JF_o is the Joint Orientation Factor. Both are defined by ranges summarized in Table 2.

Table 2 – Joint Spacing Factor and Joint Orientation Factor Ranges (Lilly, 1986).

Condition	JFs	Condition	JFo
Spacing < 0.1m	10	dr < 10	10
0.1 < Spacing < Oversize	20	dr < 30	20
Spacing > Oversize	50	dr < 60	30
		dr < 90	40
dr = Joint Dip Direction - Free Face Dip Direction			

RDI is the Rock Density Index, and is defined as:

$$RDI = 25 * (\rho_r - 2) \quad \text{(Equation 2.11)}$$

Where, ρ_r is the specific gravity of the rock. The final component of the Blastability Index is the Hardness Factor (HF) and is defined as:

$$HF = \frac{E}{3} \quad \text{(Equation 2.12)}$$

Where, E is the Young's modulus of the rock in GPa.

2.4.3 Rules of Thumb for Blast Design

Based on powder factor ranges, Dyno Nobel has come up with basic rules of thumb for laying out production and pre-split holes for a surface production blast (Dyno Nobel, 2010). Typically the diameter of the blasthole will be known based on the specifications of the equipment selected for drilling. With this information, general design parameters for the blast can be determined using the rules of thumb shown in Table 3 and Table 4.

Table 3 – Basic rules of thumb for determining design parameters for a production blast layout (Dyno Nobel, 2010).

Rules of Thumb for Production Blast Layouts	
Design Parameter	**Rule of Thumb for Calculating Design Parameter**
Blast hole diameter (D)	Known Value
Bench height (BH)	hole diameter / 15 (ignore units)
Burden (B)	25 to 40 x D
Spacing (S)	1.15 x B
Sub-drill	3 to 15 x D
Charge length (C)	> 20 x D
Stemming	20 x D or 0.7 - 1.2 x B
Burden Stiffness Ratio	BH/B 1-3.5 is good fragmentation and over 3.5 is great fragmentation
Stemming Size	D/10

Table 4 – Basic rules of thumb for determining design parameters for a pre-split blast layout (Dyno Nobel, 2010).

Rules of Thumb for Pre-split Blast Layouts	
Design Parameter	**Rule of Thumb for Calculating Design Parameter**
Spacing	D x 12
Burden (B)	0.5 x production blast burden
Uncharged length	10 x D

Often, when a pre-split blast is completed, buffer rows of holes are drilled between the final production hole and the pre-split line and loaded with less explosive in order to minimize blast-induced damage from occurring. As with most aspects of blast design, there are only broad guidelines and rules of thumb available for designing a buffer blast. The typical base point to begin designing the buffer blast is with the burden and spacing of the holes. The following equations are general rules of thumb used to design the buffer rows:

$$B_p = (0.45\ to\ 0.5) \times B \qquad \text{(Equation 2.13)}$$

$$B_b = (0.75\ to\ 1.0) \times B \qquad \text{(Equation 2.14)}$$

$$S_b = (0.75) \times S \qquad \text{(Equation 2.15)}$$

Where, B_p is the burden between pre-split and the buffer row, $B_b$is the burden between the buffer row and first production row, S_b is the buffer row hole spacing, *S* is standard hole spacing and *B* is the standard hole burden (Morhard, 1987).

Because less explosive is used in the buffer row holes compared with the main production blast holes, careful attention needs to be taken to ensure projections are not left sticking out of the bench between holes and there is not a toe left at the foot of the final wall face. In addition, proper fragmentation must be attained by the buffer rows. Due to the explosive column being smaller, the center of gravity of the explosive is lower in the hole. Therefore, the buffer row explosive can be considered to be a spherical charge and cube root scaling can be applied (Morhard, 1987). Spherical cratering tests have indicated the onset of fracturing occurs at a critical depth to the center of gravity of the charge given by:

$$d_c = (A \times W)^{1/3} \qquad \text{(Equation 2.16)}$$

Where, d_c is the distance from the center of gravity of the charge to the collar of the blasthole (m), W is the weight of the explosive charge (kg) and A is the factor dependant on the ground characteristics. The A factor will range from 1.11 in high strength brittle rocks to 1.79 in softer more ductile rocks. This equation will provide a guideline for determining the minimum buffer charge that will result in adequate fragmentation to surface (Morhard, 1987).

2.5 Methods to Predict Blasting Damage

There have been many different attempts by various authors to predict the amount of blast induced damage in rock. Some of the more popular methods include measurement of peak particle velocity (PPV), gas pressure measurements and physical measurements of cracks. The following sections will discuss these methods.

2.5.1 Peak Particle Velocity

Probably the most recognized method for determining blast induced damage is the PPV of the blast. PPV is a relatively simple method compared to others and has been found not only theoretically proportional to blast-induced stress, but also well correlated to actual damage (Trivino, 2012). The disadvantages of this method are that it does not provide actual determination of blast-induced damage, and it is generally used in combination with some form of scaling law, disregarding directionality and distinction between different types of waves.

The commonly accepted method to predict blast-induced damage in nearby structures is the standard charge weight scaling law (Hopler, 1998 and Dowding, 1996), given by Equation 2.13:

$$PPV = Kw^{\alpha}r^{-\beta} \qquad \text{(Equation 2.17)}$$

Where, PPV is the peak particle velocity at a given point (m/s); w is the explosive weight (generally taken as the total explosive weight per delay, in kg); r is the direct distance from source to the point (m); and the parameters K, α and β are specific site constants. This method can be seen as a simple fitting method in which the PPV at a given point is assumed to be only a function of the total explosive charge per delay and the distance from the source.

United States Bureau of Mines has also determined an empirical propagation equation relating particle velocity to charge mass and distance. The PPV at some point away from the detonation can be estimated using the following formula:

$$V = K\left[\frac{d}{Q^{0.5}}\right]^{B} \qquad \text{(Equation 2.18)}$$

Where, V is the peak particle velocity (mm/s); K is the site and rock factor constant; Q is the maximum instantaneous charge (kg); B is the constant related to the rock and site (usually -1.6); and d is the distance from the charge (m).

In the absence of field measurements with which to fit Eq. [2.14], preliminary values of K = 1,725 and B = 1.6 can be used to estimate 'upper bound' (90% confidence) vibrational amplitudes (ISEE, 1998). Note that the square root attenuation implemented in the PPV equation applies to cylindrical charges, which are defined as explosive charges that are longer than about seven times their diameter. For shorter charges, a cube root attenuation is more appropriate.

Particle velocity can also be related to stress and is expressed as:

$$\Delta\sigma = \rho \frac{\Delta x}{\Delta t} \Delta\dot{u} \qquad \text{(Equation 2.19)}$$

$$\Delta\sigma = \rho\, c_c\, \dot{u} \qquad \text{(Equation 2.20)}$$

Where, $\frac{\Delta x}{\Delta t}$ is the propagation velocity of the longitudinal wave front c_c. The maximum stress then occurs at the maximum particle velocity, $\dot{u}_{max}$ (Dowding, 1985). This relationship is important because of the dynamic loading on the rock, as a result of the explosive detonation, can be related to PPV.

Several guidelines exist to relate PPV to damage in various structures, including excavations in rock (Table 5 and 6). Note in both tables, the work suggested that no fracturing of intact rock should occur at velocity levels below 250 mm/s. The work of Yu and Croxall (1985) suggests that only minor slabbing failure will be observed at PPV levels of 500 mm/s. Therefore, based on this criterion, the PPV behind the limits of the blast should be below 500 mm/s to avoid significant damage from occurring.

Table 5 – PPV and their effects on structures.

Peak particle velocity (mm/s)	Effects on structures and "typical" (hard) rock masses	Reference
>2,500	Complete break-up of rock masses	(1)
635 to 2,500	Strong tensile and some radial cracking of rock	(1)
305	Falls of ground in tunnels	(2)
250 to 635	Minor tensile slabbing in rock	(1)
<250	No fracturing of intact rock	(1)
200	Initiation of cracks in concrete blocks	(2)
195	50% probability of serious damage to plaster	(3)
135	50% probability of light damage to plaster	(3)
70	Minimum level for damage to civil structures	(3)
50	Safe limit for residential structures (houses)	(3)
15	95% of people can feel this level	(3)
0.5	Typical perception threshold for humans	(3)

References: (1) Bauer and Calder (1978); (2) Bauer and Calder (1977); (3) Siskind et al. (1980). Note: all threshold values rounded to the nearest 5 mm/s.

Table 6 – Damage criteria (Yu and Croxall, 1985).

Yu and Croxall (1985) Damage Criteria Discovered Following Kidd Mine Investigation	
Nature of Damage	**Threshold PPV**
No Visible Damage	250
Minor Scabbing Failure	500
Possible Formation of Cracks Along Weakness Planes	1,000
Moderate Scabbing Failure	1,200
Major Scabbing Failure	1,800

2.5.2 Explosive Gas Pressure

Gas pressure generated by explosives can be determined by field measurements. Observation holes are drilled adjacent to one or more charged holes where pressure sensors are installed. Once the explosive in the blasthole is detonated, high pressure gas will travel through discontinuities in the rock mass. The sensors will record the gas pressure as discontinuities

connecting the charged hole with the sensor hole are wedged open. This permits direct determination of the distances of fracture development. This type of measurement is detailed in works conducted by Brinkmann *et al*. (1987), Brent and Smith (1996), and Yamin (2005).

The downside of using this method to determine the amount of blast-induced damage is that the results are highly influenced by the local conditions of the rock mass. A rock with a strong foliation present will exhibit significant damage in the orientation of the foliation, which can be misleading for damage indication and prediction unless the fabric of the rock is recognized.

2.5.3 Physical Measurement of Cracks

This method has been conducted in blocks of relatively intact rock (Olsson *et al*., 2002; Mohanty and Dehghan Banadaki 2009; Dehghan Banadaki, 2010) and also in controlled bench blasting (Ouchterlony *et al*., 1999 & 2001). A blast is detonated in a homogeneous rock and the blasted rock is sliced perpendicularly to the blasthole axis, and the length and quantity of blast-induced fractures are measured. The method has been applied to single holes in blocks with no significant displacement of material, and also to bench blasting with fragmentation at the front of a series of blastholes. This method is the least practical method to use as rock masses are highly variable and any axis cut along the borehole will likely give a unique answer. In addition, the logistics of preparing a block for the test and cutting it is inherently costly and problematic. It is, however, probably the most direct and reliable method to measure blast-induced damage and it allows the distinction of fractures induced only by stress waves from those created and enhanced by gas penetration, by casing the blastholes.

2.6 Techniques to Minimize Blast-Induced Damage

Controlled blasting refers to different practices used in a blast to minimize the damage sustained to critical areas, such as the final rock wall. In open pit mining operations, excessive over break at the perimeter areas of the blast can be costly and put employees working in the pit in danger (Workman and Calder, 1992). Over break will result in steeper pit wall angles, which results in increased waste removal and potentially unstable walls. Catch benches, designed to halt the fall of loose material, will be reduced in width and potentially be rendered ineffective.

There are several main techniques used to control the damage exposure to the final wall:

- *Pre-splitting*: used extensively in surface operations to control damage sustained to the final wall. A row of lightly charged holes are fired along the boundary of the final wall prior to the main production blast. The idea is to create a fracture plane along the final wall face, which prevents stress waves and detonation gasses from propagating across from the main production to the final wall.
- *Trim or cushion blasting*: similar to the pre-split method, the trim technique uses a row of lightly loaded holes that are drilled along the planned excavation limit and are designed to create a continuous crack.
- *Buffer blasting*: usually used in conjunction with pre-splitting and trim blasting. A buffer row of holes are drilled at the back of the production blast and are lightly loaded to prevent the effect of excessive energy at the back of the production blast.
- *Line blasting*: holes are drilled close together at the perimeter of the excavation limits. These holes are not loaded with high explosives but rather with deflagration explosives such as black powder or pressurized water cartridges to form the excavation limit.

- *Air deck blasting*: basically an empty space with no explosive is left in the borehole. The air deck can be at the bottom or in the middle of the column and is a method for decoupling the explosive and more evenly distributing explosive energy throughout the rock mass. Decoupling or the use of decoupling ratio is designed to reduce the charge concentration in the blasthole and minimize stresses exerted on the walls of the blasthole. Decoupling ratio is defined as the ratio of diameter of the hole to the diameter of the charge or the amount of explosive in the hole compared to void space in the hole.

Regardless of what is being used to control damage sustained to the final wall, the main blast can still cause significant damage. In addition, a poorly engineered control practice can also lead to significant damage to the final wall. There are three main factors that will dictate the outcome of a blast. These are the blast design, the rock mass properties and the geology of the area. Of these factors, only blast design can be altered to minimize blast-induced damage. The following are a list of blast design parameters that can be altered to minimize damage.

- *Blasthole size*: the size of the blasthole determines the amount of explosive that can be put into the hole. Explosive performance is a function of the blasthole diameter with fully coupled charges. A lower VOD usually results in a lower reaction extent for the same type of explosive.
- *Explosive type*: there are many different types of explosive that all have their own characteristics and properties. Explosives with a high VOD will release high pressure energy quickly, which causes more fracturing of rock in the initial stages of detonation. Explosives with a relatively low VOD but high weight strength with generate more detonation gasses that can cause extended damage to fractured ground.

- *Spacing of holes*: large spacing between blastholes means more energy is required to fragment the rock, which will inevitably lead to more damage in the rock mass. One of the mandates in the mining industry is to cut costs. In an effort to cut costs and increase efficiency, fewer holes are drilled, which means the distance between holes is larger. In order to achieve fragmentation, holes are often loaded 'heavily' in order to compensate for the required energy to break the rock to a desired fragmentation size. This will have negative effects on the final wall stability.
- *Timing and sequence*: timing and sequence can have a significant impact on the outcome of the blast. Typically a slower timed sequence is favorable for wall stability. Blasts with longer detonation timing between holes and rows allow the broken rock to move away (creating a new free face). When timing between holes and rows is faster or closer, the rock blasted in each row will not have enough time to move away to create a free face for the next row of broken rock to move towards. As a result the blast will get backed up and energy from the blast will begin to be forced up and back toward the final wall because there is no other place to go. Fast timing is a major contributor to wall instability in production blasts.
- *Detonator accuracy*: the type of detonator used in the blast can have a significant effect on the outcome of the blast. Using electronic detonators gives the blasting engineer more freedom to design the blast compared with non-electric detonators. Electronic detonators have better accuracy than non-electric detonators and delay times can be programmed as opposed to non-electric detonators, which come with pre-determined delays. The electric detonators can also be checked prior to blasting to ensure they are all online. Once the

detonation sequence is initiated all electronic detonators will fire, whereas if a cable is cut or damaged non-electric detonators will not detonate.

  - In pre-split blasting, it is important that several holes or even all holes are fired with the same firing time in order to allow stress waves and detonation gasses to act simultaneously. The accuracy of delay timing is critical to achieve this effect. This is why pre-split blastholes are usually fired with "zero" delay electric detonators in order to minimize cap scatter and improve accuracy.

- *Burden*: the amount of burden (distance of the blasthole to a free face) is as important as timing and blasthole spacing. If a hole is too far away from a free face, the blast will be considered to be over-confined. Over-confinement can lead to substantial damage sustained to the rock mass.

- Chapter 3: Hybrid Stress Blast Model Software -

3.1 Existing Numerical Codes

Many groups in the mining industry are working on developing numerical modelling codes for blasting. The work includes: CPEX and SABREX by Imperial Chemical Industries (ICI, now AkzoNobel), BLASTEC by Nitro Nobel, DYNOVIEW by Dyno Nobel Explosives, the distinct modeling code (DMC) by Preece (1993), the ELFEN/MBM/SoH by Minchinton & Lynch (1996) and the work of the Hybrid Stress Blast Model (HSBM) project, to name a few (Sellers *et al*., 2012). The main goal of all of these efforts and studies is for predicting the outcome of a blast at the planning stage of the blast design. This chapter will detail the HSBM software being developed. For a more comprehensive description of the ICI and Dyno Nobel software packages, a detailed description can be found on their individual websites (www.akzonobel.com, and www.dynonobel.com).

3.2 Introduction to Blo-Up Numerical Modelling Software

Blo-Up is a numerical modelling tool used to provide results for blast design. The software has been developed through an international collaborative project called Hybrid Stress Blasting Model (HSBM). The aim of the HSBM project is to combine a detonation model (VIXEN) with a rock breakage model (Blo-Up). The project has been funded by a consortium of companies focussed on research and technology exchange. Blo-Up was developed to numerically model the entire blasting process, including the high pressure gas expansion, the near field explosive and rock interaction, damage development, fragmentation, and heave of broken material.

The driving factors for developing the software are to:

- Better prediction of fragmentation in order to increase productivity for equipment and to prevent extensive crushing at the milling stage.
- Reduce damage to material being blasted, such as coal and diamonds.
- Minimize pit wall damage so that steeper pit walls can be excavated.
- Minimize dilution for thin vein deposits.

Additional benefits of the model would be to assist mine personnel with less experience in blasting to make better decisions, reduce costs, minimize dilution and provide a better safe working environment. The physics behind the Blo-Up model and individual programs that were combined to create the software are discussed in the following section.

3.3 The Blo-Up Model Physics

This section will discuss the physics behind the Blo-Up software and the individual programs that were combined to create Blo-Up. The following sections are summarized from the *Itasca Blo-Up User's Guide Release Version 2.7* (2012). The primary physics engine used in Blo-Up is based on Itasca Consulting Groups FLAC and PFC3D codes. The programs use both a combination of continuous and discontinuous numerical models in order to predict detonation pressures, dynamic wave propagation and material throw.

3.3.1 Explosive Model

The explosive model is represented within the FLAC zones and is confined to the borehole. The VIXEN detonation software gives the velocity of detonation (VOD), the Williamsburg equation of state (EoS) parameters and the final reaction extent, is described in detail by Braithwaite & Sharpe (2009). After the blast has been initiated, energy is released into the FLAC zones and is controlled by a programmed burn algorithm (Kapila *et al*., 2006). The reaction in the FLAC

zones representing the explosive is controlled by a steady detonation wave propagating up the borehole at a pre-determined VOD of the explosive.

The near-field rock is modeled as a Mohr-Coulomb material that is in contact with the explosive zones which are represented by the Williamsburg EoS. Explosive energy increases the isotropic stress in the explosive zones and expands the confining material. The explosive gas volume increase is conveyed to the Williamsburg EoS, which gives a new pressure. Figure 10 illustrates the components of the near-field model coupled to the large scale model. Figure 11 presents an example of various characteristics monitored in the near-field model.

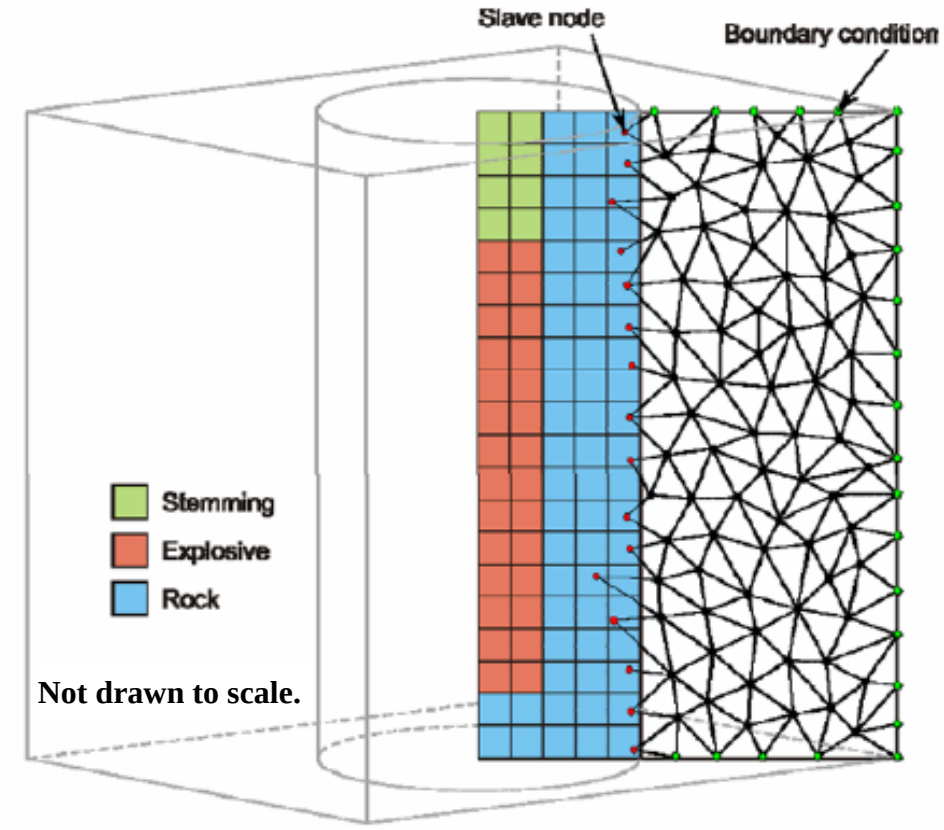

Figure 10 – Illustration depicting the components of the near-field continuum model (represented by FLAC zones) coupled to the far-field model (represented by PFC3D point masses) (Itasca, 2012).

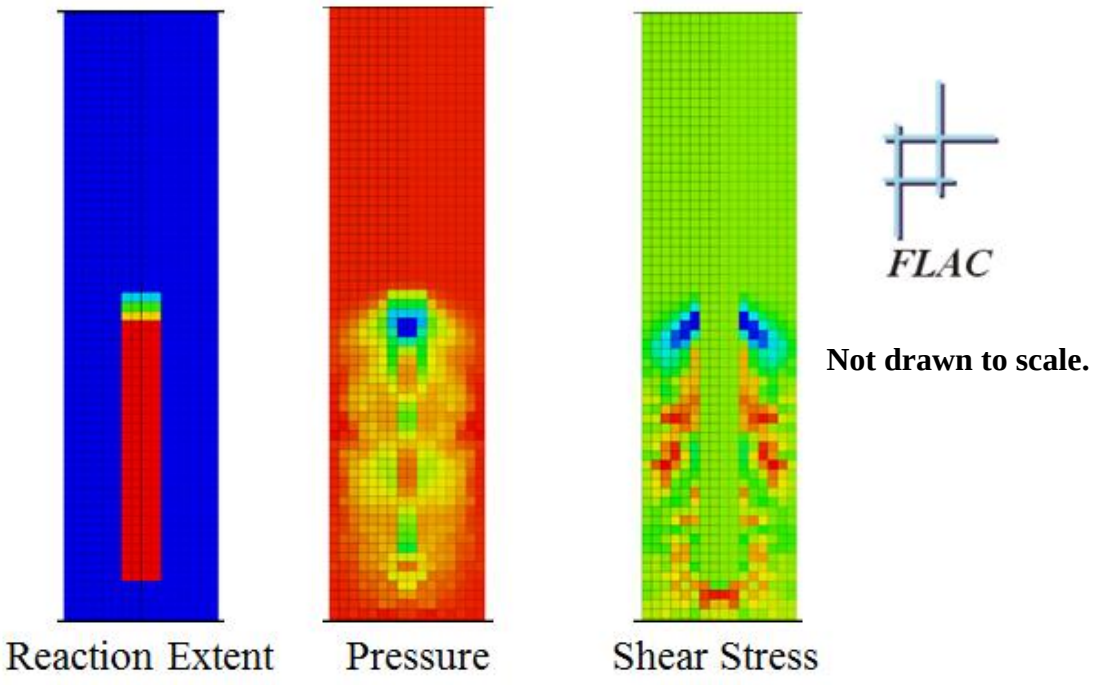

Figure 11 – Example of a model monitoring various characteristics in the near field FLAC model (Itasca, 2012).

3.3.2 Near-Field Model

The near-field model consists of the borehole, the explosive and the region of rock that extends two diameters (of the hole) from the center of the borehole. The two and a half diameter extension of the near-field model into the surrounding rock mass is a default setting in the program and is implemented on the basis that FLAC continuum code is better suited to simulate shear stresses and crushing of the rock than a discontinuous code. The near-field continuum runs with the core routines of Itasca's FLAC code as it is ideal for modelling the compression and shear failure that will occur in this region. The far-field model is, in essence, stitched to this near-field model and allows energy from the blast to propagate from the blasthole location into the surrounding rock. Due to the axisymmetric loading that takes place on the annulus of the borehole after detonation of explosives, an equal force is applied to the PFC3D point masses on the boundary of the FLAC zones (Itasca, 2012).

3.3.3 Far-Field Model (Main Rock Mass Representation)

The main rock mass is represented with a lattice-type discrete element method, which is a simplification of the full DEM calculation cycle performed by PFC3D. Discrete element codes like PFC3D explicitly integrate the equations of motion of discrete particles using force-displacement-laws, bonding models and dampening to describe particle interaction. With this simplified model, an emergent rock-like behaviour is observed. Two important features of the model are the ability to propagate stress waved and fracture behaviour.

In PFC3D, a force and bending moment are applied at the contacts between bonded spherical particles with translational and rotational degrees of freedom. The lattice method applies forces to point masses, which have only translational degrees of freedom. The point masses are initially connected by springs, which have a tensile breaking strength. The radial fracturing occurring away from the borehole is primarily tensile-mode failure, which is still represented well with the lattice-model simplifications. The model geometry is built up of point masses distributed in a non-repeating pattern with a user specified spacing between nodes. Figure 12 illustrates the far-field lattice represented by PFC3D code. Lattice nodes that overlap the near-field model are controlled by the movement in the FLAC zones. The lattice nodes then contribute a force back to the FLAC zones. This mechanism provides a direct coupling between the lattice region and the borehole representation (Itasca, 2012).

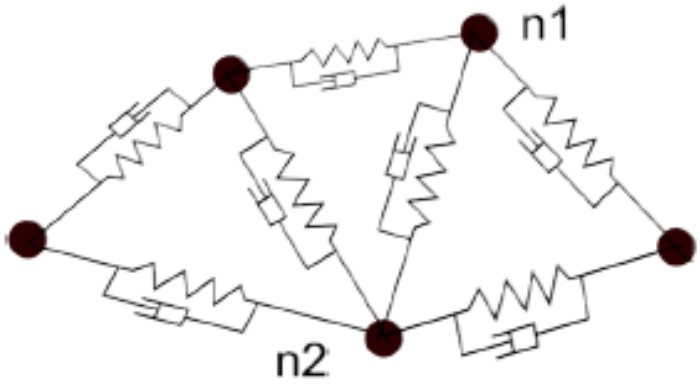

Figure 12 – Far field model made up of point masses connected by springs (Modified after Itasca, 2012).

The equation of motion for a point mass or node in the lattice model is given as (Itasca, 2012):

$$\sum \vec{f} = m(\ddot{x} - \vec{g}) \qquad \text{(Equation 3.1)}$$

Where, $\Sigma\vec{f}$ is the sum or the unbalanced forces acting on a specific node, *m* is the mass of the node and $\vec{g}$ is the acceleration due to gravity and $\ddot{x}$ is the acceleration at the position of the node in 3D space (dots over x imply derivatives with respect to time).

The sum of the forces is given by (Itasca, 2012):

$$\sum \vec{f} = \vec{f_c} + \vec{f_d} + \vec{f_g} \qquad \text{(Equation 3.2)}$$

Where, $\vec{f_c}$ is the force from lattice springs, $\vec{f_d}$ is a viscous damping force and $\vec{f_g}$ is the gravitational force.

As in regular PFC models, the force from the lattice springs is proportional to the distance between the nodes. The equation for this is (Itasca, 2012):

$$\Delta\vec{f_c} = k_n\,(\dot{x}^{n1} - \dot{x}^{n2})\Delta t \qquad \text{(Equation 3.3)}$$

Where, k_n is the contact normal stiffness, and Δt is the integration time-step. This assumes that the normal and shear contact stiffnesses are the same. The normal contact stiffness, k_n is taken as the average of the nodes attached to a spring (Itasca, 2012):

$$k_n = \frac{k_n^{n1} + k_n^{n2}}{2} \quad \text{(Equation 3.4)}$$

The force in the direction of a given spring is (Itasca, 2012):

$$f_{ns} = \frac{x^{n1} - x^{n2}}{|x^{n1} - x^{n2}|} \cdot \vec{f_c} \quad \text{(Equation 3.5)}$$

Each spring has a tensile strength, which is the average of the tensile strengths of the attached nodes. If the force on a given spring, f_{ns}, exceeds this tensile strength, the spring breaks and is removed from the lattice. Removing springs from the lattice removes the strain energy that was contained in the spring. Viscous damping is added to the lattice springs to account for the attenuation observed in real rock. The spring damping force is defined as (Itasca, 2012):

$$\vec{f_d} = \propto \sqrt{m k_n} (\dot{x}^{n1} - \dot{x}^{n2}) \quad \text{(Equation 3.6)}$$

Where, $\propto$ is a damping coefficient that may be set from zero to unity. Damping is the ability of the numerical model to dissipate energy through the system. A value of zero results in no damping used, while a value of unity corresponds to critical damping. The actual damping coefficient for a rock mass must be calibrated based on results observed in the field. The acceleration of a node can be written using a central difference approximation as (Itasca, 2012):

$$\ddot{x}^t = \frac{1}{\Delta t} \left(\dot{x}^{t + \frac{\Delta t}{2}} - \dot{x}^{t - \frac{\Delta t}{2}} \right) \quad \text{(Equation 3.7)}$$

Where, $\dot{x}^{t+\frac{\Delta t}{2}}$ is the node velocity a half-time-step in the future and $\dot{x}^{t-\frac{\Delta t}{2}}$ is a half-time-step in the past. Substituting this into the equation of motion (3.1) gives (Itasca, 2012):

$$\dot{x}^{t+\frac{\Delta t}{2}} = \dot{x}^{t+\frac{\Delta t}{2}} + \left(\frac{\sum \vec{f}^{t}}{m} + \vec{g}\right)\Delta t \qquad \text{(Equation 3.8)}$$

The node position, x, is updated by (Itasca, 2012):

$$x^{t+\Delta t} = x^{t} + \left(\dot{x}^{t+\frac{\Delta t}{2}}\right)\Delta t \qquad \text{(Equation 3.9)}$$

There are two types of springs that connect lattice nodes in a Blo-Up model. When the model is built, intact springs connect all the nodes representing a fully intact rock. The intact springs can support tension up to the local tensile strength at which point the springs break. Temporary contact springs form between the nodes which come into contact during movement. Contact between the fragments occurs during the model run time. Figure 13 illustrates the temporary contact in the lattice material. The contacts are treated physically the same as the intact springs, however, no tensile strength is associated with these contacts. Only frictional sliding is considered.

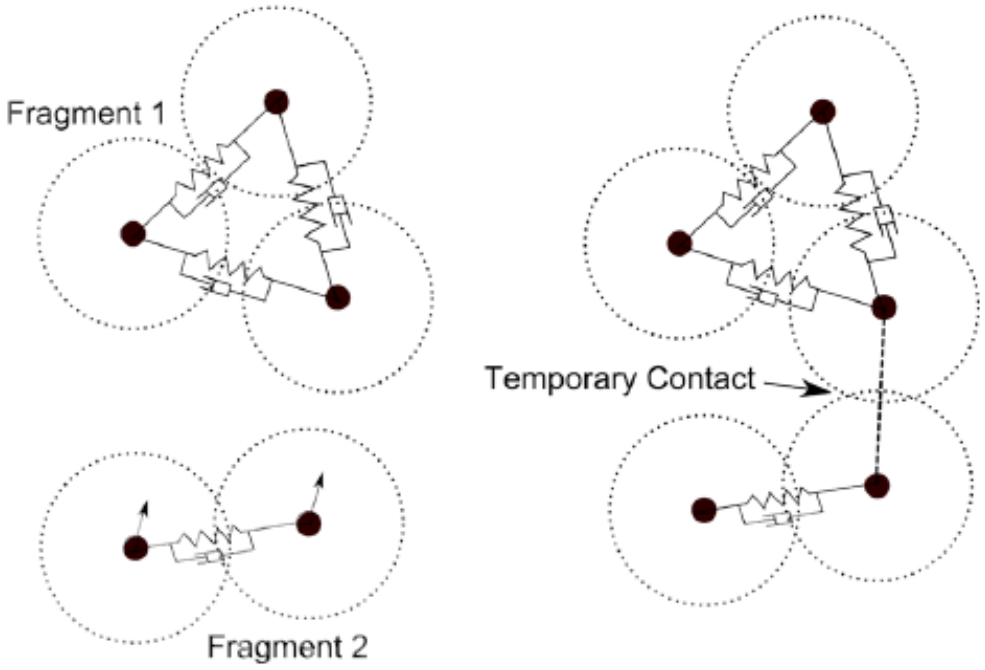

Figure 13 – Illustration showing the lattice after springs are broken and when the fragments come back into contact (Itasca, 2012).

The contact force $\vec{F}_c$ can be decomposed into normal and shear components $\vec{F}_{cn}$ and $\vec{F}_{cs}$ (Itasca, 2012):

$$\vec{F}_{cn} = \vec{F}_c \cdot \vec{n} \quad \text{(Equation 3.10)}$$

$$\vec{F}_{cs} = \vec{F}_c - \vec{F}_{cn} \quad \text{(Equation 3.11)}$$

Where, $\vec{n}$ is the normal direction between the lattice nodes making up the contact (Itasca, 2012):

$$\vec{n} = \frac{x^{n1} - x^{n2}}{|x^{n1} - x^{n2}|} \quad \text{(Equation 3.12)}$$

A ratio is defined as (Ruest, 2008):

$$f_{ratio} = \frac{|\vec{f}_{cs}|}{f_{coff}\,|\vec{f}_c|} \quad \text{(Equation 3.13)}$$

Is calculated for each contact where $f_{cof\,f}$ = 0:75. When $f_{ratio} > 1$ frictional sliding is defined to occur and the shear component of the contact force becomes (Itasca, 2012):

$$\vec{f}_{cs} = \frac{\vec{f}_{cs}}{f_{ratio}} \quad \text{(Equation 3.14)}$$

The decrease in shear stiffness removes energy from the system and as a result, no damping force is added to contacts undergoing frictional sliding. New contacts are formed when two lattice node centroids move to within two resolutions of one and other (specified by the diameter of the node). The contact is removed when the nodes move a distance greater than two resolutions apart. The intact springs (which represent undamaged rock) are initially over-connected. As a result of this over-connection and of the frictional sliding the mechanical and wave propagation behavior of intact springs and contacts are different. The temporary contacts are more dissipative of energy as they are intended to represent broken rock.

3.3.4 Rock Properties

The user specifies the rock properties such as Young's modulus, Poisson's ratio, density, uniaxial compressive strength (UCS), tensile strength, friction angle and the damping coefficient. Mohr-Coulomb constitutive parameters can all be derived from these inputs with the standard formulae. The lattice normal contact stiffness and spring tensile strength are dependent on the lattice resolution, which is defined by the user.

It should be noted that rock is stronger when subjected to rapid (or dynamic) loading. Dynamic tensile strength of rock is known to be a function of strain rate. In the Blo-Up model, the tensile strength of the rock is dependent on the strain rate the rock experiences locally. This is currently implemented as a simplified model where the spring tensile strength is scaled as a power law function of the distance away from the nearest borehole. Figure 14 shows a graph of the tensile

strength multiplier, t*, for several values of strength curves on the horizontal, b. The tensile strength multiplier is largest in close proximity to the hole and decreases with distance.

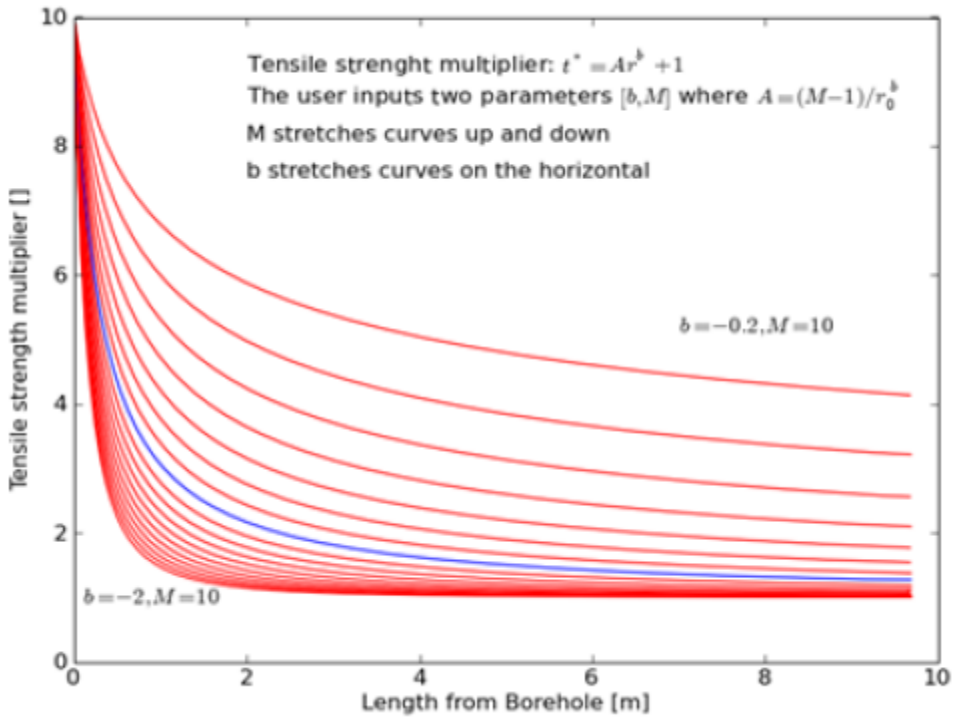

Figure 14 – Tensile strength multiplier for M = 10 and several values of b (Itasca, 2012).

Joints in the Blo-Up model are represented as planes with weaker tensile strength than the surrounding host material. The lattice spring breakage criterion considers the tensile stress in the direction of joint opening. Typically, joint sets will have little or no tensile strength in the field, depending on the stress conditions, therefore modelling joints in Blo-Up is a limitation of the software. Ideally, the joints sets should be represented with Coulomb sliding model (DEM smooth joint model), however this procedure has not been applied in the code at this stage. When a joint lattice spring is broken, a temporary contact with frictional resistance to sliding is inserted.

3.3.5 Gas Cavity Model

The continuum model component of the Blo-Up software examines the rock behaviour from detonation to equilibrium pressure state. At equilibrium pressure state, the rock in close proximity to the blasthole will be crushed. Before gas can escape, it reaches a quasi-steady balance with the plastic and elastic deformation of the rock. From this point forward, the reaction gas products are represented in Blo-Up as an expanding three-dimensional cavity. This gas balloon representation is coupled to the lattice nodes, which represent the rock mass. Lattice nodes in contact with the gas cavity, termed gas slave nodes, are used to enforce the coupling. These nodes have force applied in the outward radial direction from the blasthole center-line corresponding to the gas pressure. As the burden moves, the volume of gas increases, the pressure of the gas is adjusted according to the EoS. The volume of the gas cavity is determined from the location of the gas slave nodes.

In the current Blo-Up version, the full behaviour of the reaction gas products is simplified. The gas expansion is treated as a single contiguous body undergoing constant adiabatic expansion (axial flow not explicitly represented) (Itasca, 2012):

$$p = \frac{e}{V_j^{1.65}} \qquad \text{(Equation 3.15)}$$

Where, p is pressure, e is an internal energy and V is volume of the gas cavity. The volume of the j^{th} gas cavity is taken as a cylinder with a height and radius determined by the average location of the gas slave nodes (nodes which define the gas cavity) as (Itasca, 2012):

$$V_j = h_j \pi \frac{1}{N} \sum_i |\vec{r}_i|^2 \qquad \text{(Equation 3.16)}$$

Where, the sum is over the gas slave nodes, N is the number of gas slave nodes, h_j is the blasthole height, r_i is the radial distance of a given gas slave node from the blasthole center-line. The radial distance $\vec{r}_i$ is defined as (Itasca, 2012):

$$\vec{r}_i = (p_i - o_j) - \vec{n}_j\,((p_i - o_j) \cdot \vec{n}_j) \qquad \text{(Equation 3.17)}$$

Where, p_i is the local vector of the ith gas slave node, o_j is the toe location of the jth hole and n_j is the normal direction of the blasthole defined to point from the hole toe to collar.

3.4 Validation Work Completed

Significant work has been completed to validate this new technology. Initial testing was conducted on concrete cubes in order to provide a uniform material for comparison (Sellers *et al*., 2009). A 33 mm diameter hole was drilled 1.3 m into each of the concrete blocks and was filled with 600 g of emulsion with a density of 1.18 g/cm^3. The charge length was 60 cm and the stemming was 70 cm (Sellers *et al*., 2009). The idea was to cause significant damage to the cubes but not completely destroy them so that the damage could be compared with models. In general, the Blo-Up results were very close to what was measured in the field, such as breakout angles, gas pressure and velocities. Figure 15 illustrates a small scale blast that was carried out on a block of concrete (Onederra *et al*., 2012).

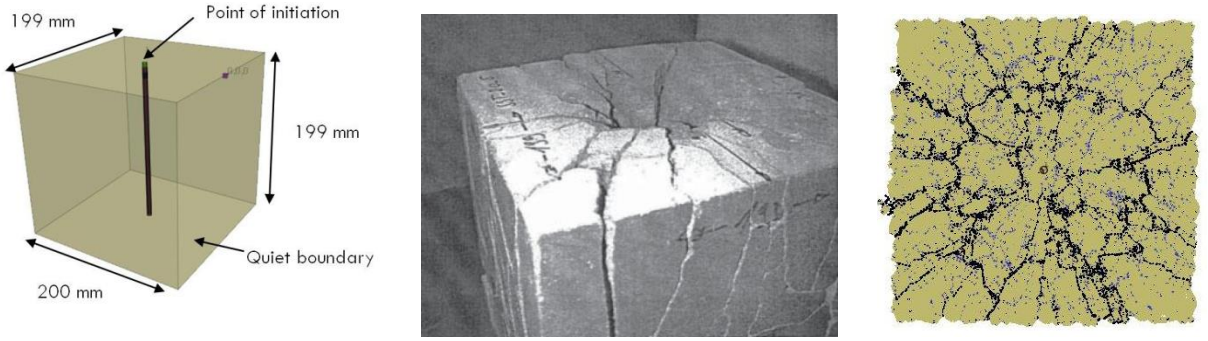

Figure 15 – From left to right, a small scale model built to replicate a small scale blast in a block of concrete, the physical block of concrete after the blast and the Blo-Up numerical model after modelling the blast (Onederra *et al.*, 2012).

Once the model was calibrated to match small scale blasts in concrete cubes, larger scale models could be constructed. The idea was to be able to show blasters how changing specific factors in the blast could alter the outcome. One of the easiest changes to make in the Blo-Up program and in the field is altering the powder factor of the blast by modifying the spacing and diameter of the holes. The result is significantly different throw of muck and trough dimensions of the settled material. In addition, smaller fragmentation can be achieved with higher powder factors, which can also be tracked in the program.

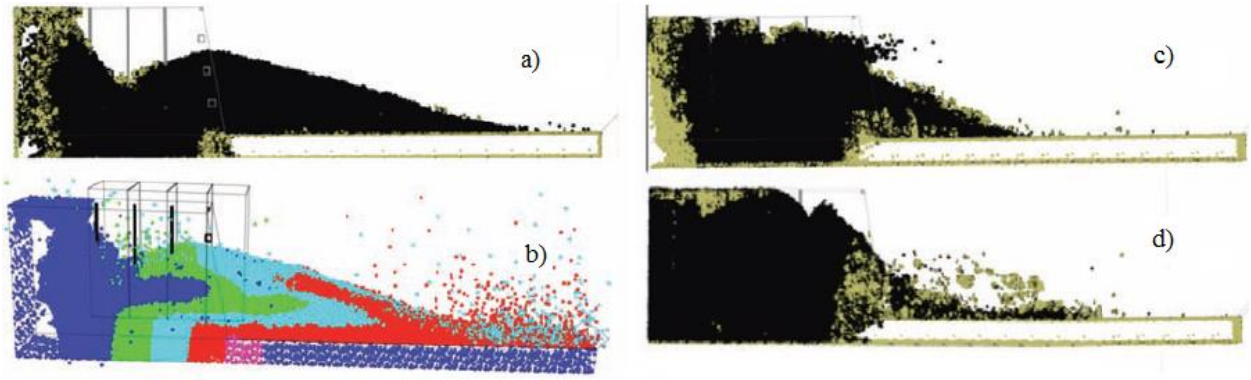

Figure 16 – Results of blasting with various powder factors: a) 1.2kg/m^3 powder factor, b) image showing mixing of burdens, c) 0.72 kg/m^3 powder factor and d) 0.44 kg/m^3 powder factor (modified after Sellers *et al.*, 2009).

These are a few examples of the work that has been completed to date with the HSBM software. Many other examples of validation work can be found in technical papers presented at various conferences, such as FragBlast or the International Society of Explosives Engineers conference.

- Chapter 4: Numerical Modelling of Pre-Split Blasts -

As outlined in Chapter 1, the scope of this thesis is to demonstrate that Blo-Up software can model a blast and give results similar to what is observed in the field, and use the result of modeling to improve blast results. The main focus of this thesis is related to blasting in kimberlite rock. Due to the soft and ductile characteristics of kimberlite, blasting is often challenging.

The blasting simulation was broken down into three parts: (1) the pre-split blast; (2) the main production blast without buffer holes; and (3) the main production blast with buffer holes. It was important to ensure satisfactory results were achieved for the pre-split blast before larger scale modelling was attempted. Basic pre-split models were initially run in order to observe the potential damage caused by the pre-split blast itself. Once a good correlation was observed, larger scale models were created.

This chapter is divided into individual tasks that represent issues that can be encountered in the field and could promote blast induced damage. The specific areas examined in this chapter are:

1) Modelling pre-split designs in homogeneous rock: a basic five hole pre-split model was created for this stage of analysis. The goal is to demonstrate a pre-split design used in granite will not give the same results in kimberlite and to present a pre-split design that minimizes damage in kimberlite.
2) Modelling various pre-split designs in jointed kimberlite rock: the basic five hole pre-split model is used with various orientations of joint sets included in the models. The goal is to present a pre-split blast design that minimizes blast induced damage.

3) Controlling damage and cracking at the ends of the presplit line: a method of controlling the propagation of cracking and damage at the ends of the pre-split line will be presented.
4) Modelling inclined pre-split holes: a basic model was created to show the effect of seismic waves generated by a production blast on the pre-split line. Both vertical and inclined pre-split lines were examined to determine if there is any advantage to having an inclined pre-slit line for shedding the force of the seismic waves up the pre-split.
5) Modelling large scale production blasts with no buffer holes and the effect they have on the final wall: large scale production blasts are modelled with high and low levels of confinement to determine if the production blast has an effect on the stability of the final wall.
6) Modelling large scale production blasts with buffer holes and the effect they have on the final wall.

4.1 Basic Numerical Model for Pre-split

The basic pre-split model was constructed with five holes as illustrated in Figure 17. Only five holes were modeled in order to minimize the size of the model and run time to complete the analysis. Further analysis was completed with additional holes, however the results were not sensitive to change, and therefore the smaller model was used for preliminary model testing purposes. The plane through the model represents the cut plane used in all future plan view slices (unless otherwise specified).

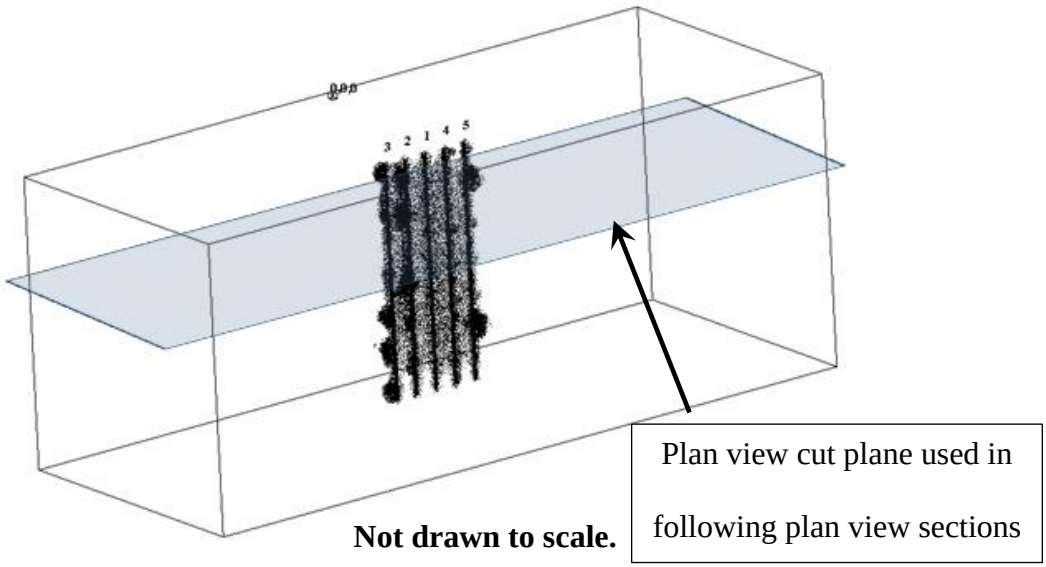

Figure 17 – Basic model geometry used in the pre-split analysis.

In order to prevent too many variables from changing between models, several variables remained constant:

- *Rock properties*: the rock properties, detailed Table 7, did not change.
- *Blasthole diameter*: the pre-split hole diameter was set to 100 mm.
- *Blasthole geometry*: pre-split hole and charge length remained 8 metres in all models.
- *Detonation timing*: all charges are fired simultaneously.
- *Explosive properties*: An emulsion product was used with a velocity of detonation (VOD) of 5,900 m/s and a density of 1,200 kg/m^3. The only change made to the explosive was the decoupling ratio, which is defined as the ratio of diameter of the hole to the diameter of the charge. The emulsion product is in cartridge form that varies in diameter based on operator requirements.

Based on the explosive properties for the emulsion product, the splitting factor can be calculated using the equation below, with the charge radius and the blasthole spacing being the only factors subject to change.

$$Split\ Factor = \frac{Charge\ mass\ per\ hole}{Hole\ spacing} = \frac{(\pi \times Charge\ radius)^2 \times 1200\,{}^{kg}/_{m^3} \times 8m}{Hole\ spacing}$$ (Equation 4.1)

Emulsion products are generally used for pre-split application because: 1) emulsions generate more of a shock pressure and less gas pressure than ammonium nitrate with fuel oil (ANFO), which is better for a pre-split mechanism of creating a fracture line at the final wall limits, 2) the packaging of cartridges come in specific diameters and can be selected based on the desired decoupling ratio and, 3) decoupled emulsions are less likely to be subjected to dead-pressing than ANFO. Dead-pressing occurs when the stress wave from an adjacent hole compresses the undetonated explosive, which can result in a misfire. The shock front cannot be ahead of the detonation reaction front because the reaction drives the stress wave. This can de-sensitize the explosive, resulting in misfires. Explosives can be superdriven, which is where the detonation occurs faster than the steady state detonation by using a large initiation charge (booster). This is also called the booster effect, in this case the shock and detonation are coincident.

4.2 Pre-split Blasting in Hard Rock and Soft Rock

One of the goals of this study is to demonstrate that a pre-split blast design that yields favorable results on one side of a pit but can have detrimental effects on another wall of the pit or at different elevations in the pit, based on changes in geology or the fabric of the rock mass. To demonstrate this concept, an identical pre-split design was applied in a soft rock (kimberlite) and a hard rock (granite). The properties of the rock types used in the models are summarized in Table 7. The properties for kimberlite were based on those documented by Sellers *et al*., (2012) and the granite rock properties were based on the strongest granite documented by Rummel *et al*, (1989).

Table 7 – Summary of the rock properties used in the pre-split analysis.

	Kimberlite	Granite
Density (kg/m³)	2,757	2,828
Young's Modulus (GPa)	52.9	86.0
Poisson's Ratio	0.31	0.23
UCS (MPa)	110	200
Tensile Strength (MPa)	11.5	20.0

A decoupled emulsion product, with properties listed above, was used with a decoupling ratio of 2:1 (50 mm diameter charge in a 100 mm hole). The spacing between the pre-split holes was set to 1.5 metres, resulting in a splitting factor of 0.50 kg/m^2, which is within the guidelines for pre-split design of 0.3 to 0.6 kg/m^2 (St. J. Tose, 2006).

Figure 18 shows the results of modelling a pre-split blast in granite with the properties listed in Table 7. The black represents the fractures and micro cracking developed after the explosive in the pre-split was detonated. The simulated blast successfully creates a pre-split fracture; however there is approximately 0.5 to 1 metre of damage around the annulus of the blastholes.

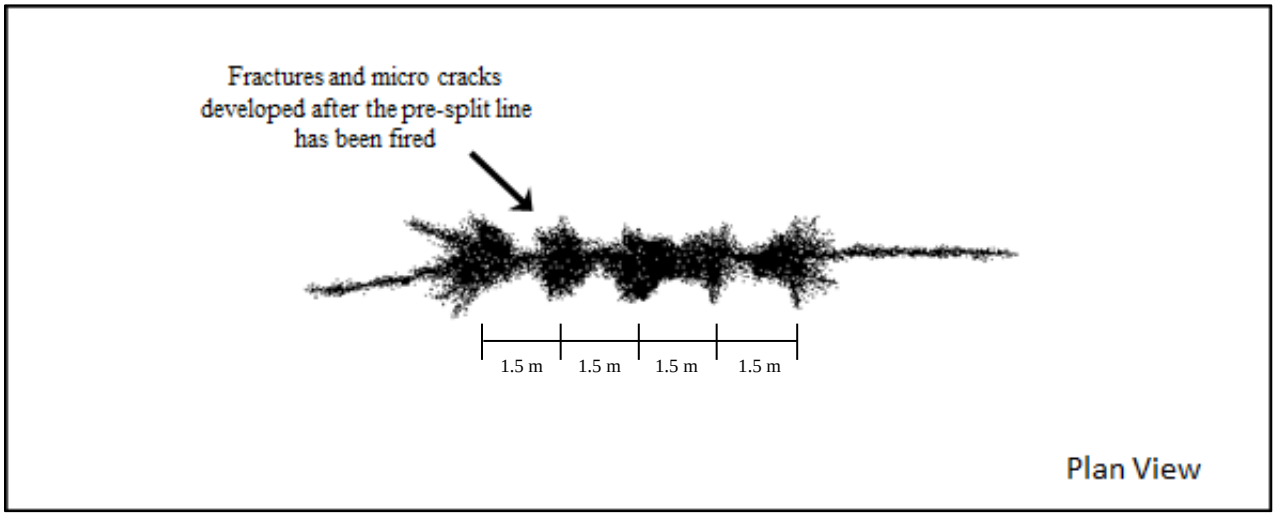

Figure 18 – Results of a simulated pre-split blast in granite with a decoupled ratio of two.

Figure 19 shows the exact same blast layout applied in kimberlite instead of granite. The extent of damage is more severe and extends to approximately 1.5 to 2 metres into the final wall. In addition, cracking extends out at approximately 30 degree angles of the pre-split line. One would expect to see ragged walls, no half barrels, and up to 2 metres of slough from the final wall.

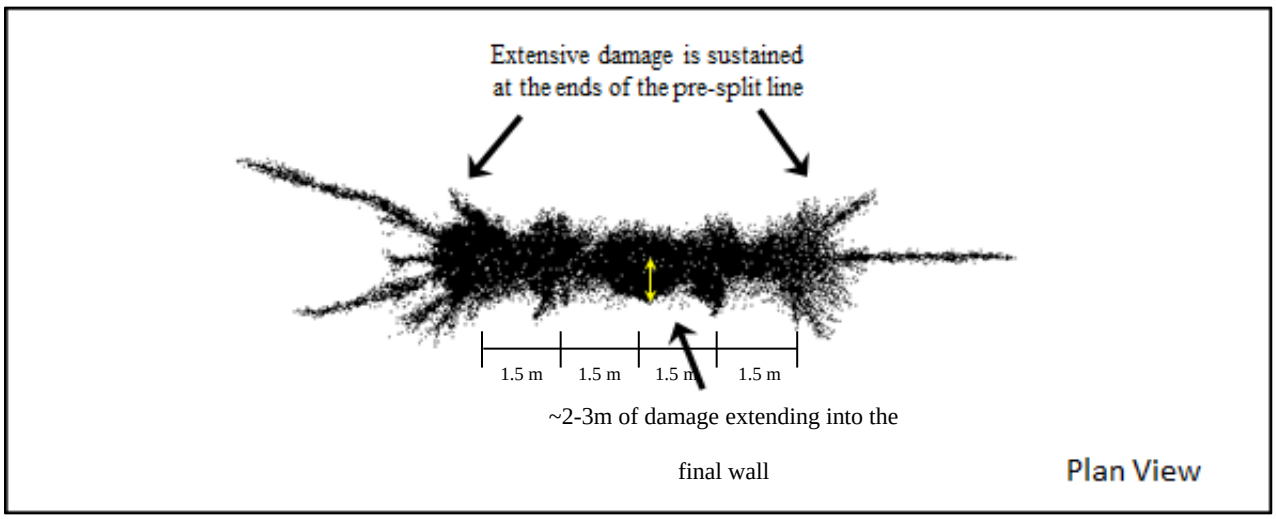

Figure 19 – Results of a simulated pre-split blast in kimberlite with a decoupled ratio of two.

Due to the stiff characteristics of a hard rock, like granite, a pre-split shear can be propagated along the line of holes with relative ease. The rapid expansion of gasses after explosive detonation will compress the rock around the blasthole. A hard rock will undergo minimal compression before it fractures and allows the high pressure gasses to travel through the system. Softer rock, like kimberlite with ductile characteristics and lower acoustic impedance, will absorb much more of the initial compression force before the rock cracks. The result is a larger zone of crushing and damage around the blasthole in soft rock. Therefore, when pre-split blasting is conducted in softer rock, the explosive energy should be more evenly distributed.

This can be achieved by reducing the spacing between holes and reducing the amount of explosives used in each hole.

Based on the results from these two models, one pre-split design should not be used for all rock types, but should be tailored based on the rock properties. The design presented above would work for a harder rock, such as granite, however it would result in significant damage in a more ductile rock, like kimberlite.

4.2.1 Examining Various Types of Explosive with Varying Rock Strengths

In order to examine the distribution of explosive energy on rock with different strengths, a series of models were created (Furtney *et al*., 2012). Three rock strengths were considered in the analysis: weak rock with a Young's modulus of 35 GPa and UCS of 100 MPa, medium strength rock with a Young's modulus of 50 GPa and UCS of 200 MPa and a strong rock with a Young's modulus of 70 GPa and UCS of 300 MPa. The density, Poisson's ratio and the friction angle of the rock remained constant at 2,800 kg/m^3, 0.3 and 50˚ respectively. Four explosives were compared: an 800 kg/m^3 ANFO, a 1,150 kg/m^3 emulsion, a 1,000 kg/m^3 heavy ANFO, and a 1,200 kg/m^3 doped emulsion. The mass of explosive used in each of the models was kept constant by varying the charge length and keeping the burden, bench height and breakout angle constant. Figure 20 summarizes the results of the study (Furtney *et al*., 2012).

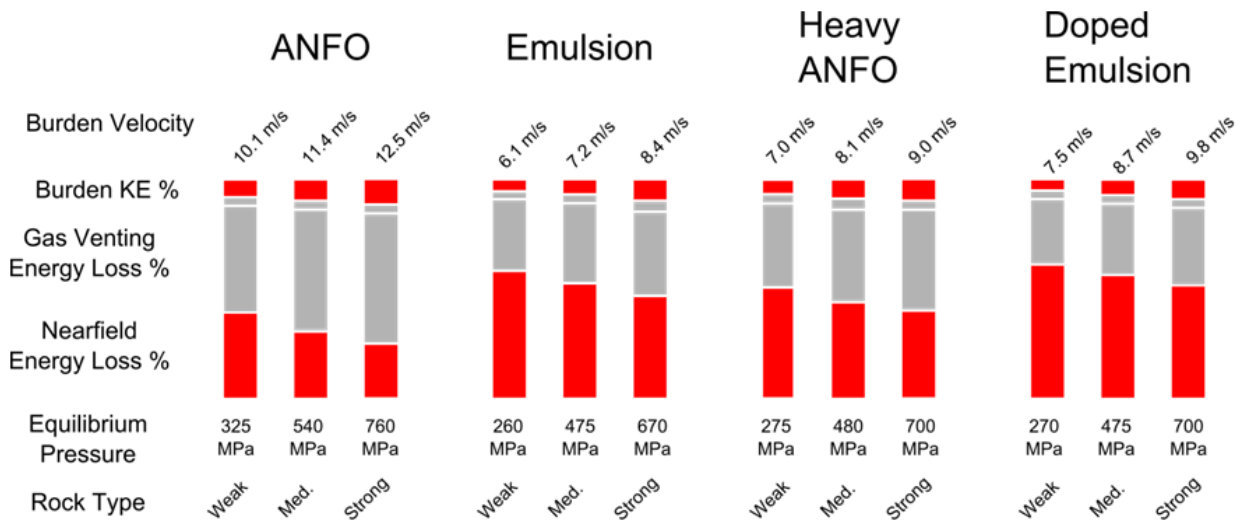

Figure 20 – Summary of energy distribution predictions for four types of explosives used in three different rock strengths (Furtney *et al.*, 2012).

There are two main conclusions that can be drawn from this work:

1) ANFO and emulsion products generate different amounts of gas energy. Emulsions rely more on higher shock energy to fracture rock as opposed to ANFO, which relies more on gas energy to break rock.
2) The weaker that a rock is, the more energy is consumed at the beginning of the blast process. This is due to the ductile characteristics of weak rock types, which will undergo more compression than harder rock types before fracturing occurs. Therefore, an emulsion product that generates more near-field energy would be well suited for softer rock types.

4.3 Optimized Pre-split Blasting in Kimberlite Using Blo-Up

As discussed, in order to achieve favorable results for a pre-split, the blast must be tailored to the characteristics of the rock mass. The pre-split design modeled in kimberlite (Figure 19) results

in significant damage sustained to the final wall. In order to prevent this damage, the explosive energy must be better balanced in the system.

Figure 21 illustrates the same pre-split model in kimberlite rock as detailed above. However, the decoupling ratio has been increased from two to three, which means that the explosive cartridge diameter is decreased from 50 mm to 33 mm thereby reducing the amount of explosive used. With a decoupling ratio of 3:1 (33.3 mm charge diameter), the splitting factor is reduced from 0.50 kg/m^2 to 0.33 kg/m^2, which is still within the generally accepted splitting factor design criteria (splitting factor guidelines is 0.3 to 0.7 kg/m^2). The result of this analysis indicates a successful pre-split blast with minimal damage sustained to the final wall (Figure 21). The model resulted in approximately 0.25 metres of blast-induced damage into the final wall.

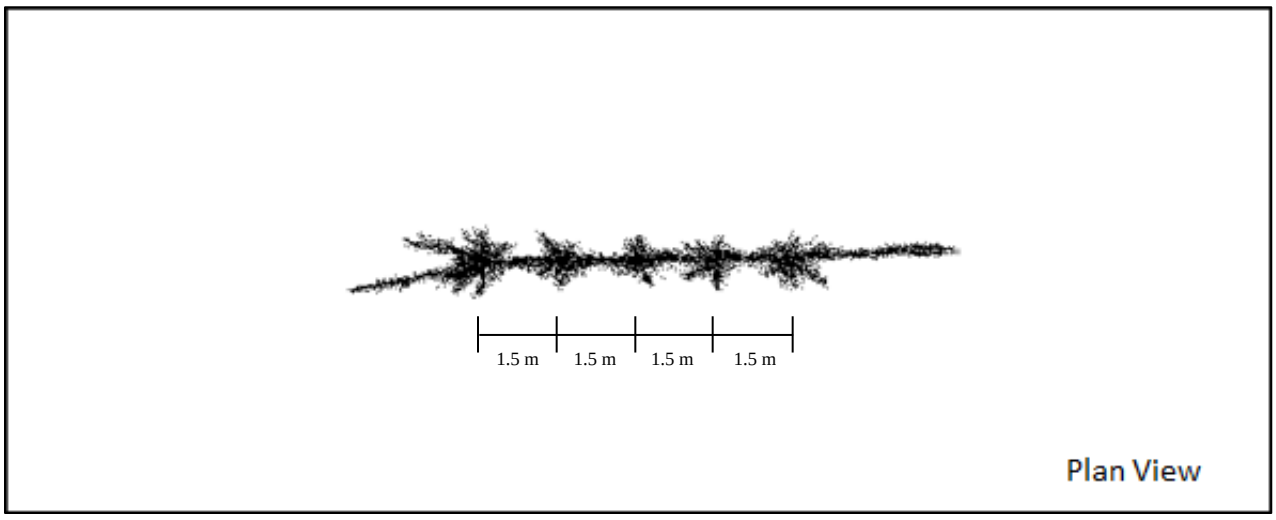

Figure 21 – Results of a simulated pre-split blast in kimberlite with a decoupled ratio of three.

There were several iterations of modelling that occurred before this successful pre-split design was found. Other factors such as reducing the diameter of the hole, reducing hole spacing and decreasing the amount of explosive, were all investigated with mixed results (a brief summary of the iterations are presented in Appendix I). The results presented in Figure 21 are favorable

because the components of the operation do not need to change. Drilling additional holes or changing the diameter of the holes is generally considered to be a last resort for operators. The longer cycle time associated with drilling additional holes and having to re-tool equipment to accommodate smaller diameter holes will cause disruption to the operation. Therefore, the option for increasing the decoupling ratio of the explosive is more appropriate because explosives product manufacturers can accommodate these requests.

4.3.1 Controlling Damage at the End of Pre-Split Lines

Damage, is however, erratic at the ends of the pre-split line, which is apparent in the Blo-Up model (Figure 23a) and was also observed in the field as shown in Figure 22b. This damage is caused by over confinement of the system at the end of the pre-split line. Explosive energy has no place to go at the end of the line and causes cracking to propagate out at shallow angles from the pre-split line.

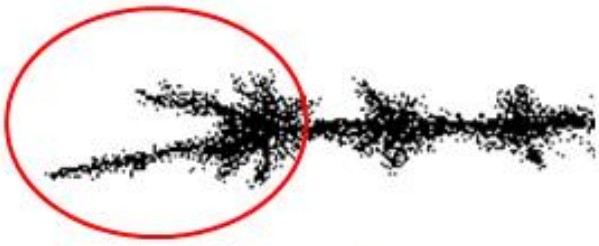

Blo-Up model showing fracturing at the end of the presplit line

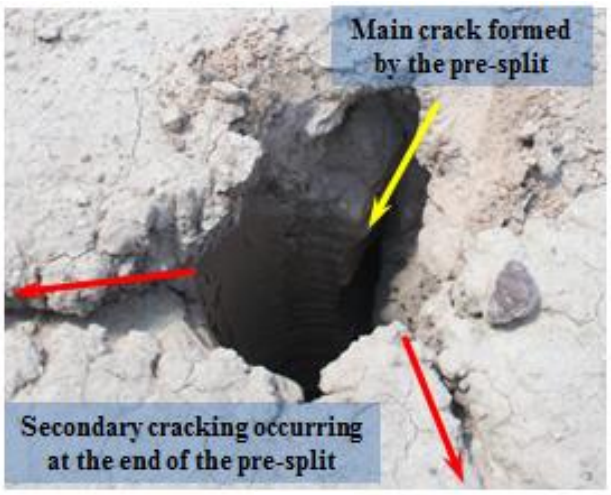

(a) **(b)**

Figure 22 – Image showing erratic damage sustained at the edges of the pre-split line. (a) Blo-Up model showing fracturing at the end of the presplit line; (b) field observed cracks at the end of the pre-split line.

In practice, this over confinement can be avoided by drilling additional holes at the end of the pre-split line and leaving these holes uncharged. Having empty holes provides some relief for the explosive energy to propagate towards and vent out. The empty hole must be drilled closer (than the normal pre-split hole spacing) to the final charged hole on the pre-split line in order for the charged hole to propagate the pre-split crack to this uncharged hole before fracturing is able to deviate from the main pre-split line.

In order to demonstrate the effect of relief holes, the same Blo-Up model was run with uncharged holes placed near the final charged holes on both ends of the pre-split line. The model used one empty hole placed 0.5 metres away from the final charged hole at both ends of the pre-split line. The results from this model are shown in Figure 23. Cracking from the pre-split blast propagates to the empty hole thereby allowing the final crack and damage to be controlled.

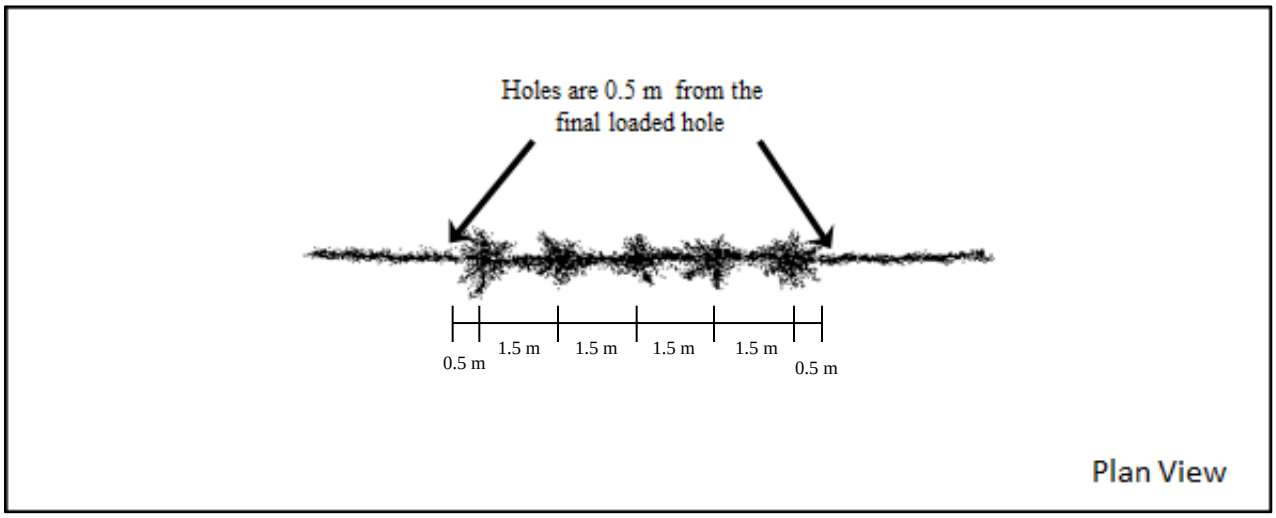

Figure 23 – Results of a pre-split with one empty hole drilled at each end of the pre-split line.

The author has observed a similar situation in the field, where excessive damage was sustained to the final walls and at the ends of the pre-split line. Recommendations were made to increase the

decoupling ratio and to drill uncharged holes at the ends of the pre-split line. Figure 24 illustrates the final wall that was created after the recommendations were implemented. The results of this model and the photo presented below show the model is able to simulate a blast and give results that are comparable with what is observed in the field.

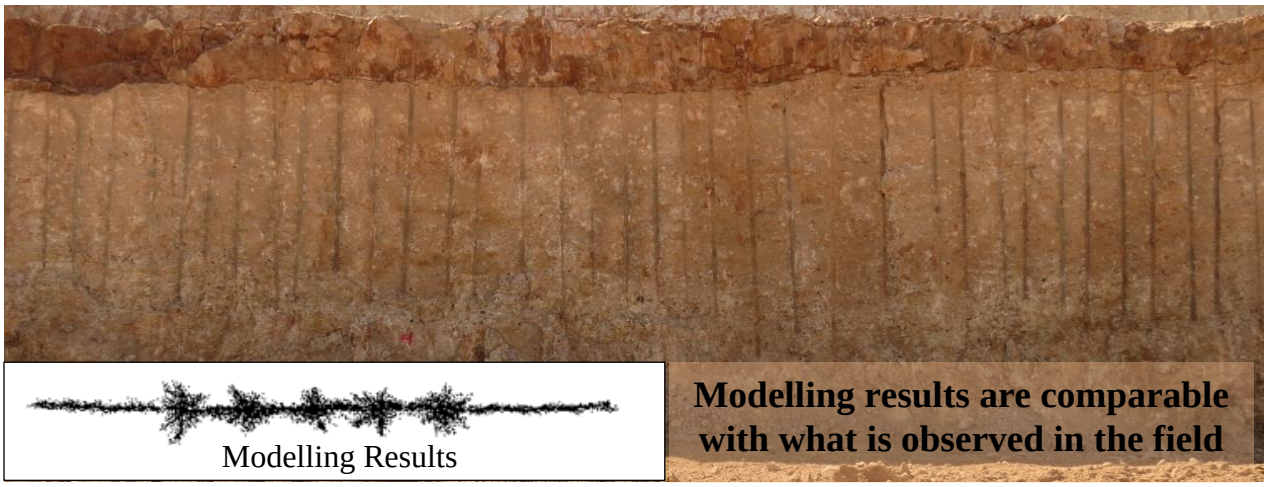

Figure 24 – Example of a successful pre-split blast in soft ground with uncharged holes placed at both ends of the pre-split line. The Blo-Up model results are also presented to show the modelling results are comparable with what is observed in the field.

Up to this point the Blo-Up modelling results, by and large, have generally been consistent with observations trialed in the field. By increasing the decoupling ratio, the total amount of energy of the explosive is reduced. Essentially, the explosive energy is more evenly distributed, resulting in a well-defined pre-split line and minimal damage to the final wall. The addition of uncharged holes provided relief for the pre-split fracture to propagate towards and prevents erratic damage from occurring on the ends of the split line.

4.4 Pre-split Blasting in Jointed Rock

Modelling completed thus far assumes the rock mass is homogeneous, which is highly conservative because rock masses typically have some kind of natural geological structures present, such as: jointing, foliations or some other type of discontinuity. This is especially true

for kimberlite deposits and the host rock for the kimberlite pipe. Kimberlite emplacement is extremely violent, which undoubtedly causes significant damage to the country rock. Figure 25 shows the sharp contact between a kimberlite pipe and the surrounding shale host rock. The kimberlite appears to be relatively massive; however the shale is significantly broken and jointed in comparison. The image is an example of why one blast design cannot be applied in all locations. Even at a pit scale, the blast design must be tailored to the characteristics of the rock mass.

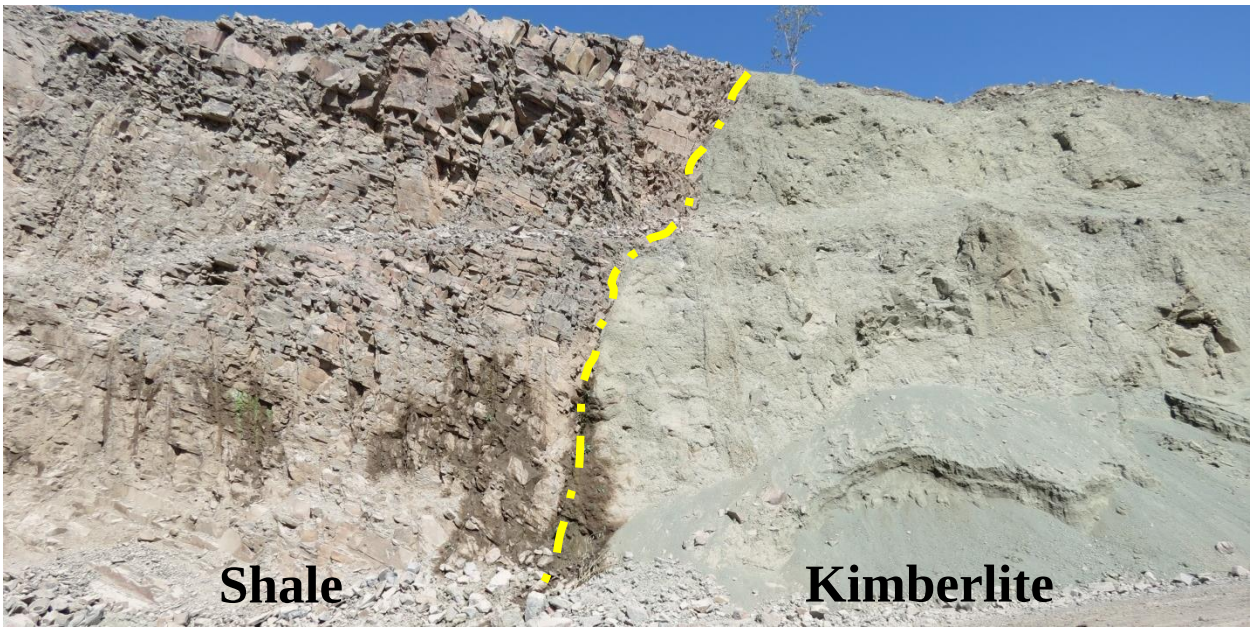

Figure 25 – Image showing the sharp contact between a kimberlite pipe and shale host rock.

High pressure gas, generated from the detonation of explosives, will exploit any natural weak features in the rock mass and wedge these discontinuities open. At some distance away from the borehole, the gas pressures will begin to weaken and the temperature will begin to cool. Once the gas reaches a free face, all of the gas in the system will rapidly vent to atmospheric pressure and no more fracturing occurs. Depending on the orientation and persistence of the joint set, extensive damage can be sustained to the final wall. Take for example Figure 26; two dominant

vertical joint sets exist in the rock mass with a 90 degree difference in strike to one another. Another flat-lying horizontal joint set also exists, however it was not a significant controlling factor in the outcome of the blast. Detonation and gas pressures from the pre-split blast wedges the sub-vertical joints open and passes through, exploiting the path of least resistance, which causes extensive over break on the final wall.

Figure 26 – Strong vertical jointing present in the rock has resulted in ragged final walls.

The Blo-Up model that was discussed in Section 4.3 was re-run with the two dominant vertical joint sets incorporated in the model having similar orientations observed in the field as shown Figure 26. As discussed in Chapter 3, adding joints into the model provides directional weakness to the rock, which can result in significantly different outcomes. The joint sets are represented as planes of weakness in the model and were given a 20 percent reduction in strength compared with the surrounding rock. Figure 27 presents the results of the model with jointing included. The results of the previous run, with homogeneous kimberlite rock properties, indicated the desired formation of a pre-split line with 0.1 – 0.2 metres of damage sustained to final wall. This damage was limited to the immediate annulus of the borehole. The same blast

design applied in the jointed rock mass resulted in approximately 1 metre of damage extending into the final wall. The results of this jointed model are similar with the field observations. Joints were spaced at 0.5 metres, which means there could be 2 to 3 joints between each of the pre-split holes.

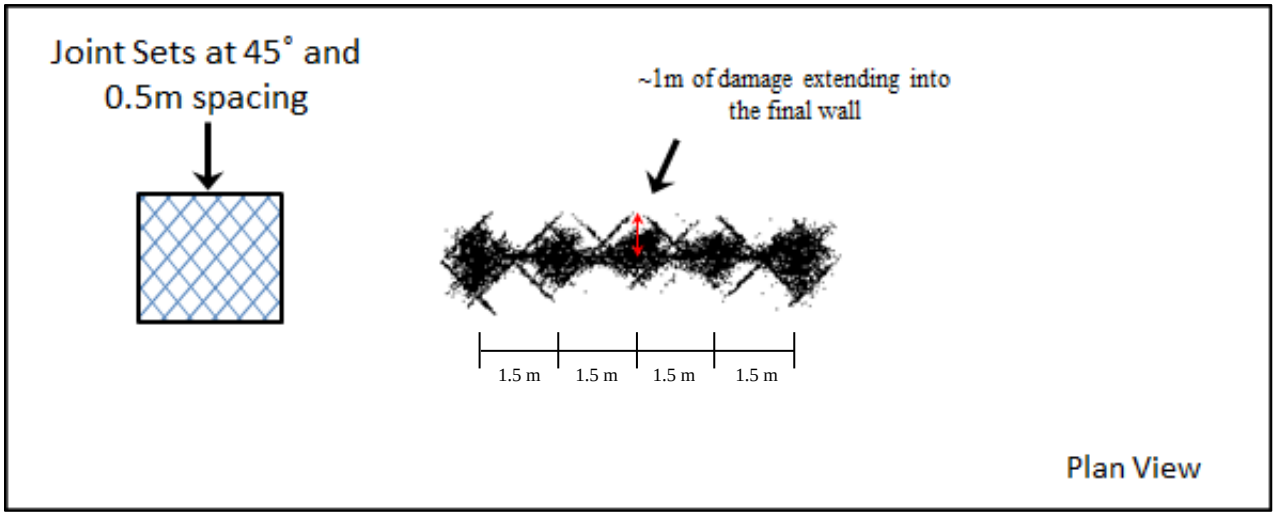

Figure 27 – Results of model with jointing included.

When the results of a blast are strongly influenced by weak geological features, it is more critical to evenly distribute the energy of the blast. This can be achieved by using smaller diameter holes, drilled closer together and using less explosive in the hole. Larger holes spaced further apart can result in excessive localized energy which will force weak discontinuities to open over long distances.

Drilling smaller holes or spacing holes closer together will also reduce the significance of the geological features in the rock mass. As shown in Figure 28 a and b, when intersecting geological discontinuities are present and the spacing of the holes is farther apart (Figure 28a) more damage will occur in the final wall compared to smaller spacing of holes is used (Figure 28b).

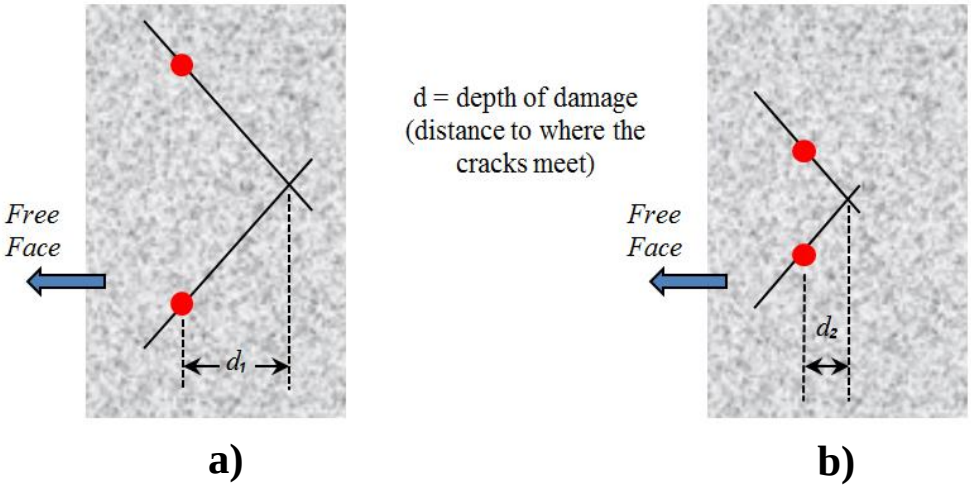

Figure 28 – Illustration showing the effect of intersecting geological discontinuities on blast-induced damage. (a) wide spacing shows more damage indicated by the distance to where the cracks meet and (b) tighter spaced holes will reduce the amount of damage (Andrieux and Hall, 2013).

In order to limit the amount of damage sustained to the final wall, the spacing of the holes was reduced to 0.8 metres. With a spacing of 0.8 metres, less damage could occur on the final wall. In addition, the decoupling ratio was increased from 3:1 to 5:1 (20 mm diameter charge). This increase in the decoupling ratio and decrease in hole spacing results in a splitting factor of 0.38 kg/m^2, which is still within the splitting factor guidelines of 0.3 to 0.6 kg/m^2. The results of the analysis are shown in Figure 29. Although there is still damage occurring to the final wall, it is far less than the previous model due to better distribution of explosive energy.

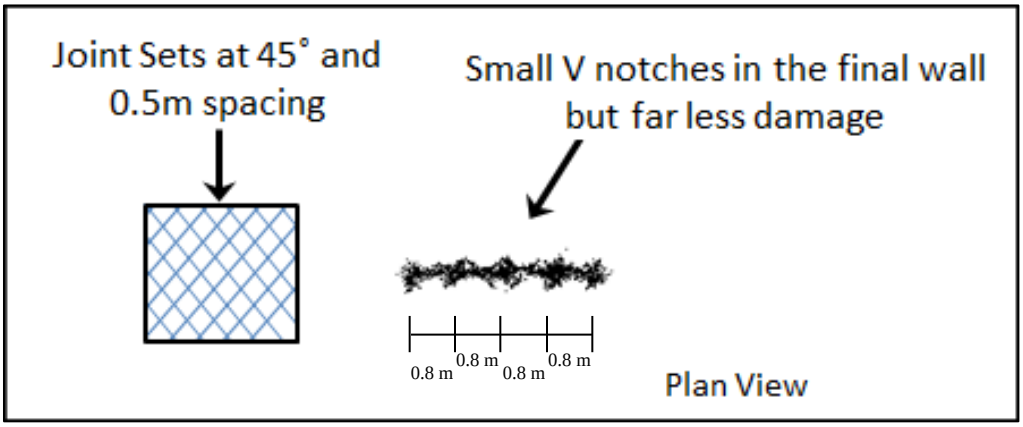

Figure 29 – Results showing a decrease in the hole spacing and an increase in the decoupling ratio in the jointed model.

To illustrate the significance of trial and error blasting, Figure 30 presents a site that conducted trial and error blasting until an optimal pre-split design was achieved. A full four benches were excavated before a proper result was found (not including the benches above). The problem with this approach is the long-term issues that the mine must deal with on an ongoing basis. The benches where trial and error blasting took place sustained significant damage and are not of sufficient size to arrest material falling from higher on the pit wall. Ongoing monitoring of this area and possibly secondary support may be required to ensure the safety of personnel working below.

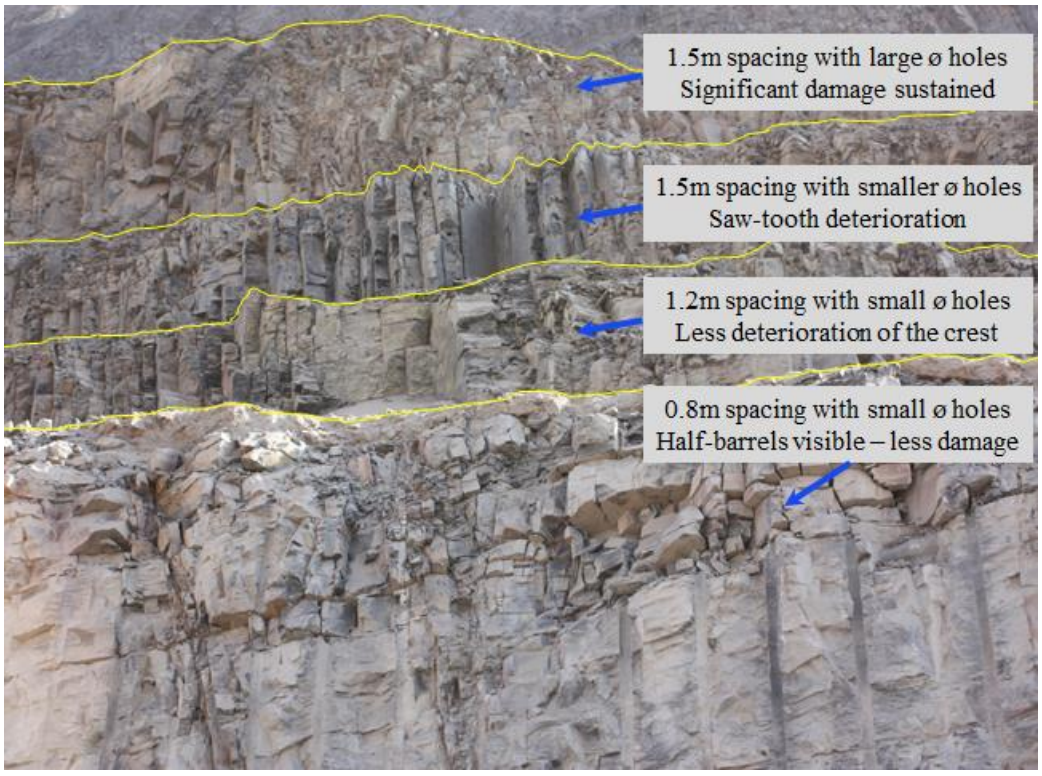

Figure 30 – A series of benches detailing the progression of trials to obtain an optimal pre-split blast design with acceptable results on the bottom bench.

The visual observations made on the benches presented in the figure above were used as a case study for the modelling work that has been completed. Figure 31 illustrates the actual observations made on the benches in the pit and the modelling simulations used to predict

damage. Using Blo-Up for determining the best possible pre-split blast design would be highly advantageous based on these results. The blasting engineer could have modelled various design parameters and had a greater level of confidence in the outcome of the blast before conducting field trials.

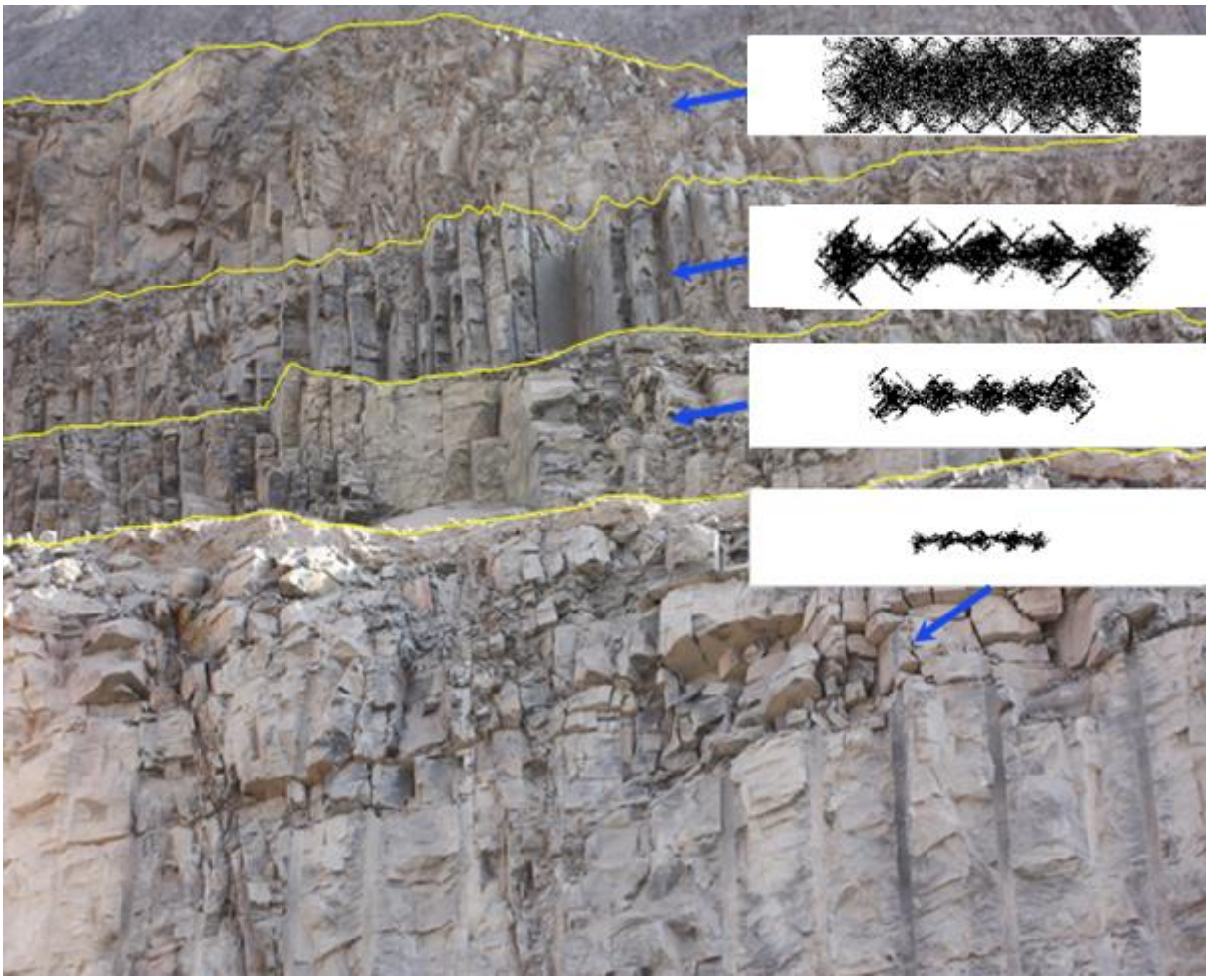

Figure 31 – Image showing the observations made in the field along with model results used to simulate damage.

Figure 32 illustrates another joint set orientation that can be detrimental to the overall stability of a pit wall. Long persistent joint sets dipping out of a pit wall at approximately 30 to 50 degree angles are challenging because the risk of failure increases due to increased kinetic freedom for the rock mass to unravel. High pressure gasses exploit these joint sets, wedging them open,

resulting to delamination from surrounding rock. Due to the dip and orientation of the joint set, any wedges that may form will likely be unstable over the long term. This joint set orientation can potentially lead to large scale instability on the final pit wall. Even small deterioration of the crest of a bench will decrease the width of the catch bench, putting personnel and equipment at risk from falling material.

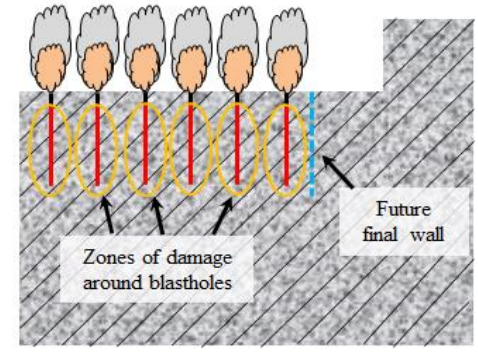

(a) High pressure gas will exploit the natural joint sets present in the rock

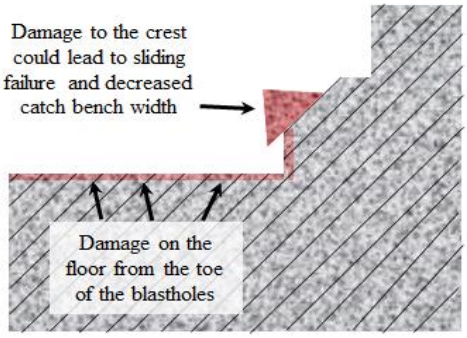

(b) Damage is sustained to the to the crest of the bench and the floor

(c) Real world example of slope failure due to adverse jointing

Figure 32 – Joint sets dipping out of the pit wall will likely lead to small scale crest failure and potentially large scale instability.

The pre-split model, discussed in Section 4.2, with a splitting factor of 0.50 kg/m^2 was modelled with the joint set orientation shown in Figure 32. Figure 33 presents the modelling results, which are similar to those observed in the field. As the full explosive column is detonated, gas flows back through the joint sets, causing damage on the final wall. Once a free face is reached,

all of the gas in the system will vent to the path of least resistance. By including weak joint sets, the model agrees with this concept and shows up to 4 metres of damage extending into the final wall. Damage will be most severe at the top of the hole where gasses vent. Based on the results, this catch bench would fail. This is a costly problem for an open pit mine as extra waste material must be handled resulting in a loss in potential production and increased stripping ratio. Personnel and equipment are put at risk from falling material because there is no catch bench to arrest debris falling from above.

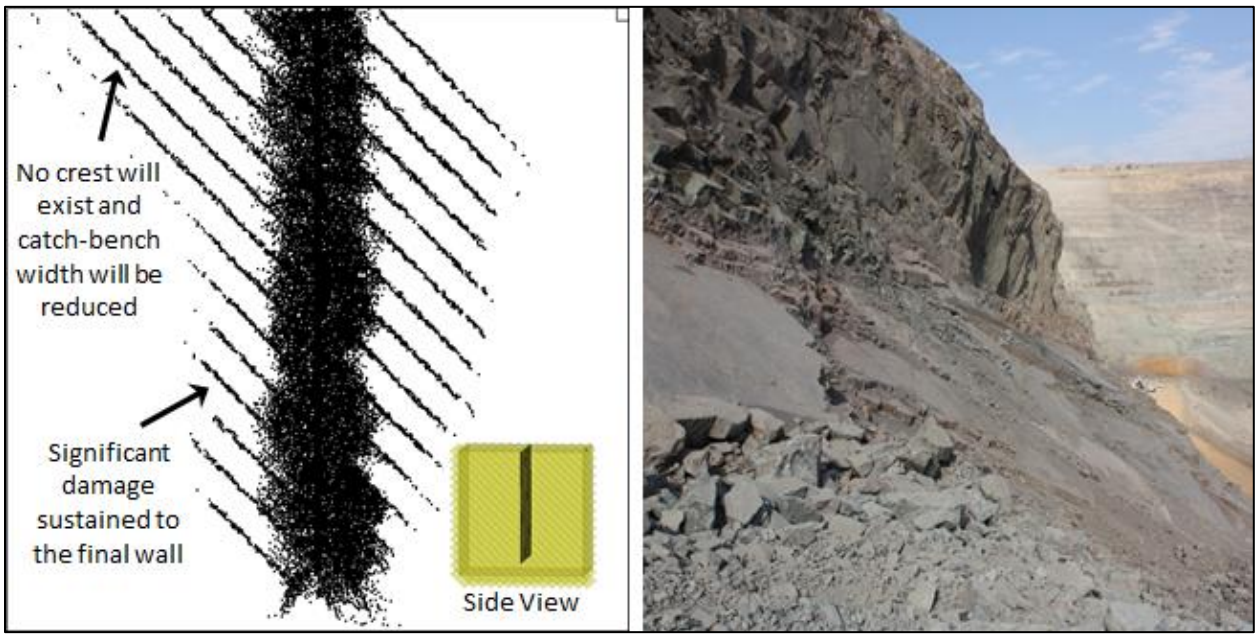

Figure 33 – On the left, the Blo-Up model showing significant damage sustained to the final wall as a result of the presence of weak joints in unfavorable orientations. The image on the right shows that the model is producing results comparable with what is observed in the field.

In order to prevent or limit the blast-induced damage sustained to the final pit wall, the explosive energy should be more evenly and better distributed in the rock mass. To test this hypothesis, a model was run with the hole spacing reduced to 0.8 metres and the decoupling ratio was increased from three to five, providing a splitting factor of 0.38 kg/m^2. The results of this new model are shown in Figure 34. Although there is still damage occurring to the final wall, there is

far less blast-induced damage that can be observed, compared to the previous model (Figure 33), due to better distribution of explosive energy.

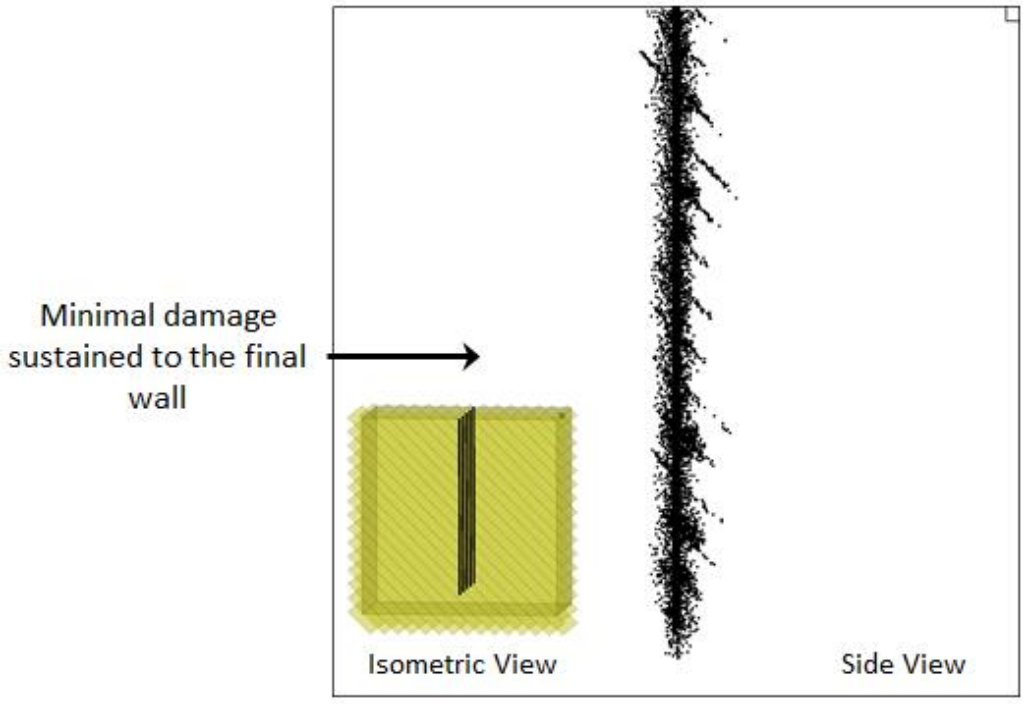

Figure 34 – Minimal damage sustained to the final wall when hole spacing and amount of explosive is reduced.

In general, the models have produced results that would be expected in the field, which was one of the goals of this project. The purpose of a pre-split is to protect the final wall of a pit; however, if not designed properly the pre-split itself can cause extensive damage to the final wall. One general pre-split blast design cannot be applied to all rock types. The pre-split design must be tailored to the rock type and the geological characteristics of the rock itself in order to achieve optimal results. When adverse geology is present, smaller holes, with less explosive, drilled closer together should be utilized to better distribute the blast energy throughout the rock mass. Although this will result in longer cycle times and decreased production rates due to drilling additional holes, the process will promote the stability of the final pit wall, avoid costly

pit wall maintenance and safeguard the personnel working in the mine. Furthermore, a wall deemed to be unstable could require a pushback of the existing pit walls, which could be enough to close the mine due to excessive costs associated with pushbacks.

4.5 Inclined Pre-split Holes

Pre-split holes are often drilled as vertical as possible in order to minimize the amount of waste mined, keep walls steep and simplify the drilling layout. From a wall stability perspective, having an inclined pre-split line makes the pit walls shallower, thereby making the walls inherently more stable. From a blasting perspective, having an inclined pre-split line is advantageous, especially if a production blast is particularly violent and generates significant seismic waves.

After the pre-split blast has occurred the characteristics of the interface generated from the pre-split blast is somewhere between a closed fracture and a fracture with a finite aperture with a small zone of surrounding damage or micro-fracturing. When a stress wave reaches the damaged area around the pre-split, it encounters an acoustic impedance boundary represented by the micro-fractures. When the stress wave hits the pre-split fracture, some of the stress wave energy is reflected back into the burden and some propagates into the final wall. A portion of the initial aperture of the pre-split fracture may be pushed tight to the final wall by the incident wave and possibly reopen when the wave reflects off the surface.

If the stress wave intersects a vertical pre-split line, the detonation stress wave will be reflected back into the burden and into the final wall. If the magnitude of this initial stress wave is large enough and the aperture of the pre-split fracture closes, a portion of the stress wave can continue

travelling through the pre-split line and into the wall behind. This can lead to damage of the final wall.

If the stress wave intersects an inclined pre-split line, the incident wave front will be reflected upward or back into the burden and downwards into the final wall. The inclined pre-split line allows the stress wave to deflect off the pre-split line, thereby reducing the effective magnitude of the wave. Figure 35 a and b illustrate the concept of vertical and inclined pre-splits.

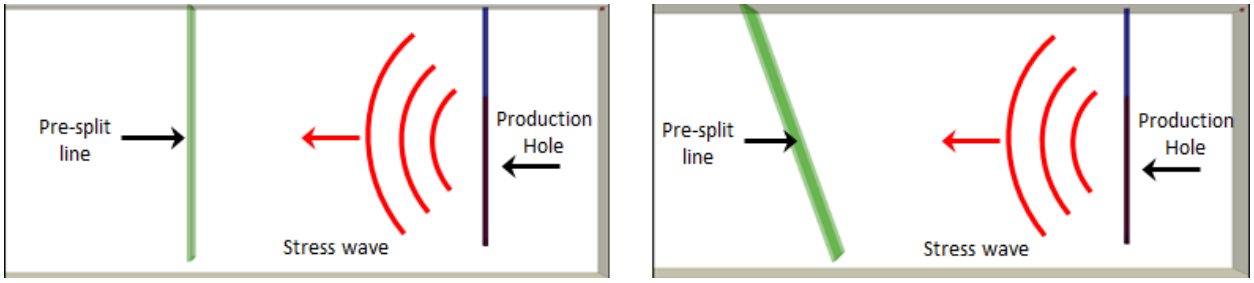

a) **b)**

Figure 35 – Basic schematic showing the concept a) vertical versus b) inclined pre-split holes.

A Blo-Up model with homogeneous kimberlite properties was created to examine the PPV after a production hole is fired for both a vertical pre-split line and a pre-split line inclined at 75˚ (Figure 36). This was examined by writing an algorithm that determined the PPV of each of the point masses in the model and contoured each one with the defined color scale. The algorithm to contour the PPV in each lattice is presented in Appendix II. A single 200 mm hole was used in the model loaded with 5 m of explosive and 3 m of stemming. This hole is over-confined as there is no free face for rock to break towards, therefore the energy from the blast radiates evenly outward in all directions. It is important to note that this model was built only to examine the interaction of the production stress wave with each of the pre-split interfaces. The pre-split interface in both models is represented by a 0.05 metre thick air gap artificially inserted in the model to simulate a pre-split line. This sized gap would be similar to what would be expected in

the field with an ideal pre-split blast. The pre-split is not modelled explicitly because it generates high levels of PPV, which can complicate the data that is supposed to be assessed; therefore the thin air gap (or crack) was used to simulate the existence of an ideal pre-split interface so that the main production blast could be examined in better detail without other influences.

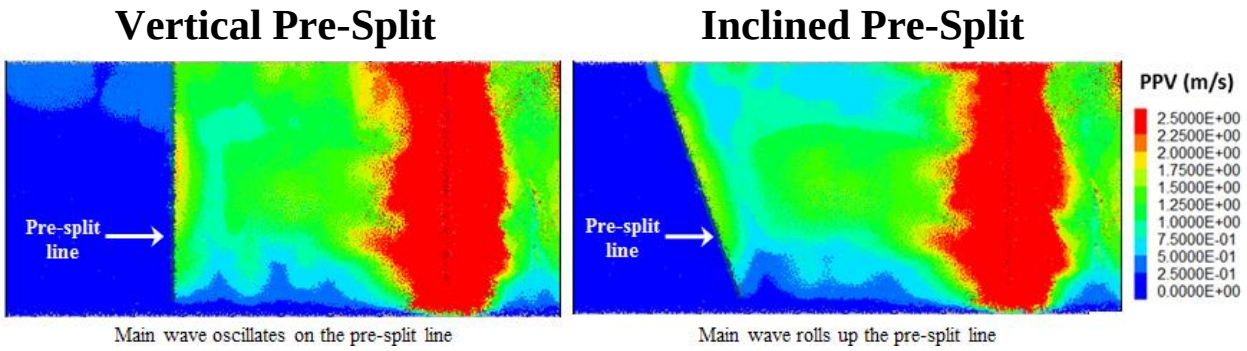

Figure 36 – PPV comparison of a stress wave hitting a vertical inclined and vertical pre-split line.

For the vertical pre-split model (Figure 36a), the full force of the incident wave is applied to the midpoint of the pre-split fracture and is followed by smaller waves. The result is a PPV of approximately 1,750 – 2,000 mm/s applied at mid-point of the pre-split boundary. The inclined pre-split model (Figure 36b) has less dynamic load applied to the midpoint of the pre-split fracture because the incident wave deflects up the pre-split fracture. The highest PPV levels are recorded at the collar of the pre-split line where the blast energy dissipates and can do little damage to the final wall. The maximum PPV recorded midpoint on the inclined pre-split model is approximately 1,000 – 1,750 mm/s.

The Blo-Up software is also able to track various changes in the rock after an explosive is detonated. Ideally strain or stress should be measured to predict damage in rock, however these parameters were not available in the Blo-Up code at the time of writing this thesis. Instead,

strain rate was measured at the pre-split line because it allows the determination of the dynamic rock mass deformation where the rock is actively being strained. Strain rate is measured directional to the change in length of an object, therefore the strain rate is measured perpendicular to the charged column. Strain does not have any units because it is the ratio of the change in length of an object divided by the original length of the object as the result of stress applied to it. However, strain rate is the change in length of an object divided by the original length of the object over time; therefore the units of strain rate are 1/time, given as:

$$Strain\ Rate = \frac{Change\ in\ length\ of\ an\ object\ (m)}{Original\ length\ (m)} \times \frac{1}{Time} \quad \text{(Equation 4.2)}$$

Strain rate history points were placed 0.1 metres behind the pre-split line at different elevations to track the change over time. The results of tracking strain rate for an inclined and vertical pre-split line are summarized in Figure 37 and Figure 38. Strain rates at the midpoint of the vertical hole are much higher than the inclined hole. This is a result of the main stress wave intersecting the mid-point of the hole first with no means of dissipating. The inclined pre-split line does not have a significant change in the strain rate at any elevation because the stress wave hits the center of the pre-split and is able to dissipate as the wave is deflected up to the free face (or surface). The difference between the maximum strain rate experienced on the vertical and inclined pre-split lines is approximately 70 percent. The results show an advantage, from a stability perspective, of having an inclined pre-split.

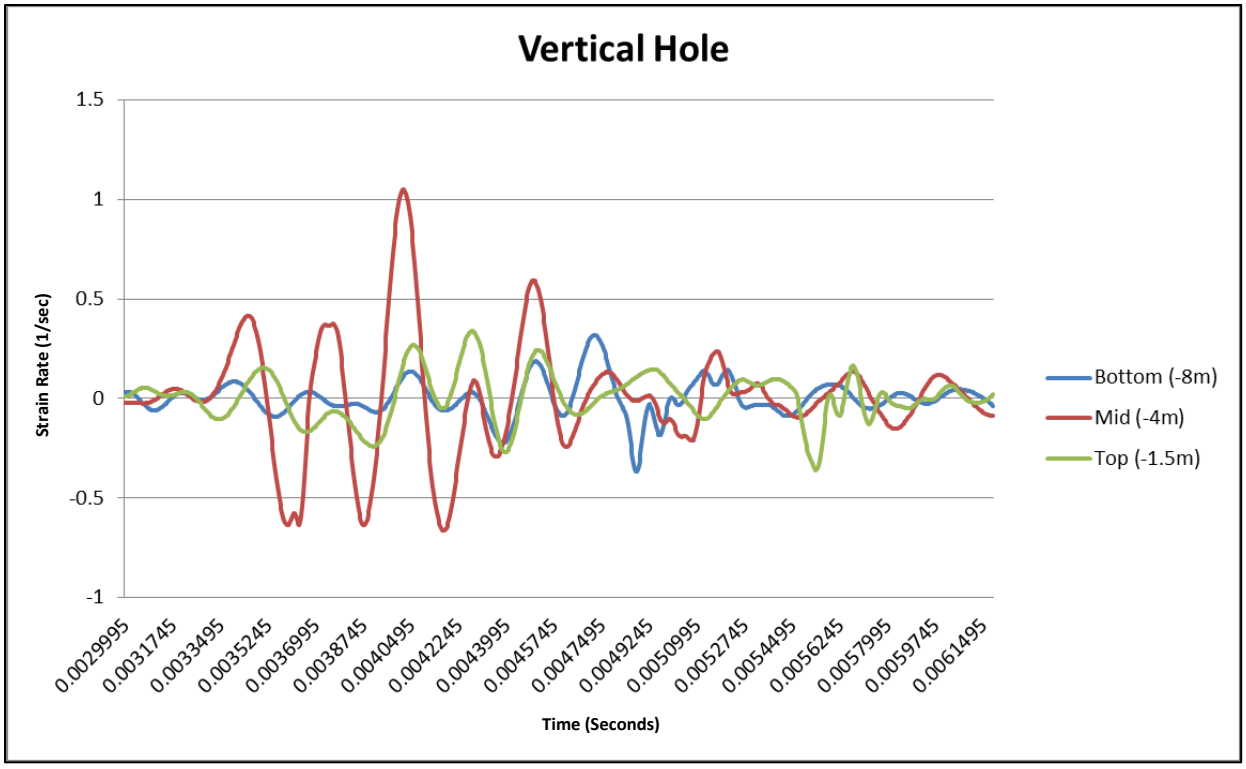

Figure 37 – Strain rate change at different elevations behind a vertical pre-split line.

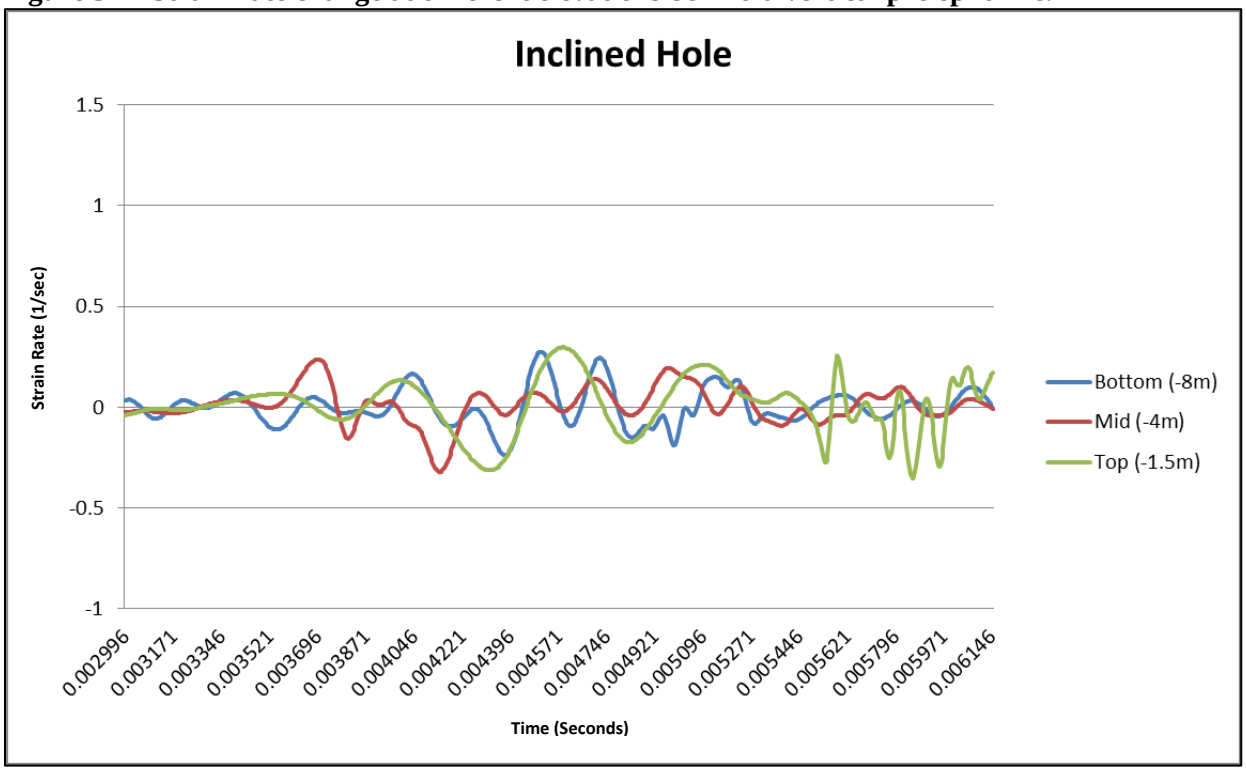

Figure 38 – Strain rate change at different elevations behind an inclined pre-split line.

- Chapter 5: Numerical Modelling of Production Blasts -

Production blasting can have a significant effect on the stability of the final pit wall even if a proper shear has been created by the pre-split blast. In particular, if a production blast is over-confined, the stress wave generated could intercept the pre-split fracture interface with enough force that the aperture of the fracture could close and allow the stress wave to continue travelling into the final wall, possibly leading to damage. Several factors that can lead to an over-confined blast are listed below:

- *Timing*: in an attempt to achieve steeper muck pile and finer fragmentation, faster timing between detonations is often employed. However, with faster timing, the broken material has insufficient time to migrate away from the blast, which can lead to over-confinement.
- *Misfires and out of sequence detonations*: any detonation that does not have sufficient burden will have excessive localized energy resulting in an over-confined situation.
- *Complex blast sequence or geometry*: box cuts and V-shaped blast patterns are inherently over-confined due to the pattern of the blast layout.

When a detonation occurs, energy radiates out into the surround rock mass. When a blast is over-confined, a large amount of energy will be forced backward into the rock mass instead of toward the nearest free face. The confinement of the explosive is a critical parameter, as it has a large effect on the utilisation of the available energy and the amount of useful work the energy will provide.

In an over-confined situation, most of the gas energy generated by explosive detonation is dissipated inside the rock mass prior to venting, which leaves little energy once a free face is

found to heave the broken muck (Figure 39a). This situation is typically associated with high ground vibrations, a tight and steep muck pile, local vertical rock projections (cratering), back-break and low air over-pressures. In a more balanced situation, the high pressure gases drive open discontinuities in the rock mass and then find a free face with enough remaining energy to heave the blasted material. This "proper" situation results in a balanced distribution between ground vibrations and air over-pressures, and yields optimum overall blasting results (Figure 39b). An under-confined situation results in the detonation gases performing little useful work in the rock mass before finding a free face and venting to atmospheric pressure (Figure 39c). This results in excessive gas energy being available at venting time, often causing fly rock and high air over-pressure problems.

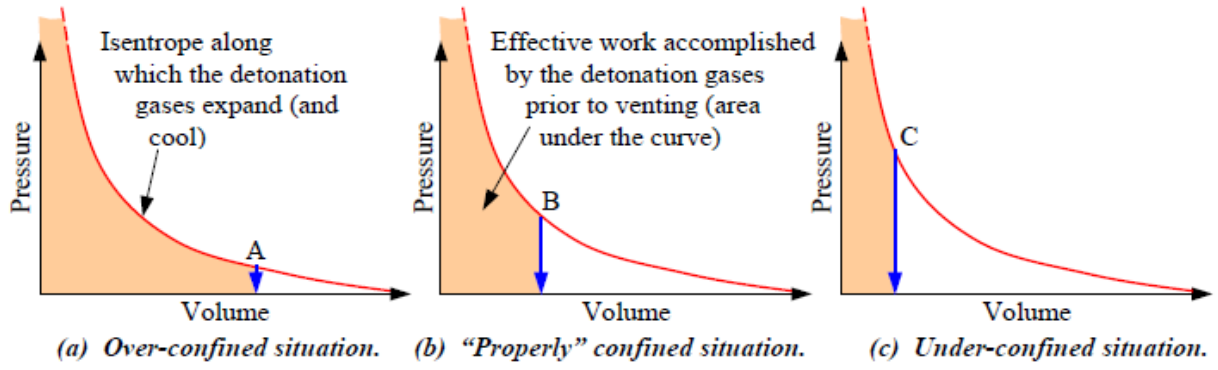

Figure 39 – Possible states of charge confinement, and the resulting amount of effective work performed by the detonation gases (modified after Andrieux and Hall, 2013).

Some production blasts are fired quickly in order to 'freeze' the blasted rock in place, which makes mucking and loading easier. This is especially true for diamond mines where dilution can cause significant problems. The energy generated from these over-confined blasts can damage the final wall, particularly in a deposit with adverse geological conditions. Figure 40 shows two examples of blasts from a diamond mine in Southern Africa that had "out of sequence" detonations and fast blasting. In both cases the blasting was over-confined as broken material

did not have enough time to clear the area before subsequent rows of holes were detonated. This resulted in over-confinement of the system, which forces energy from the blast up and back instead of forward to the free face. Figure 41 shows a blast that is properly confined. Broken material is able to move away from the area prior to subsequent detonations. This is a more balanced production blast that will not cause significant damage to the final walls of the pit.

a) **b)**

Figure 40 – Image showing out of sequence detonations (a) and fast blasting (b).

Figure 41 – More balanced blast that allows broken material to migrate away before subsequent rows are detonated.

5.1 Large Scale Blast Model

In order to replicate observations made in the field, a large scale model with homogenous kimberlite rock properties was built using the Blo-Up software. No jointing is included in the

large scale models because it is beyond the scope of this research; however the same principles that were applied in Section 4.4 can be applied on a larger scale to prevent excessive blast-induced damage when adverse joints are present.

Slow and fast production blasts were modelled in order to determine the effect on the final pit wall stability. The model with fast timing is meant to simulate a production blast that is over-confined, while the slower blast is meant to simulate a more balanced situation. Figure 42 shows the large scale model that was created. The model includes 15 holes representing the pre-split line and 12 production holes. The model is bounded on the back, the sides, and the bottom, meaning no broken material can migrate to these areas. The top and the front are the only free faces that provide relief for material to move towards.

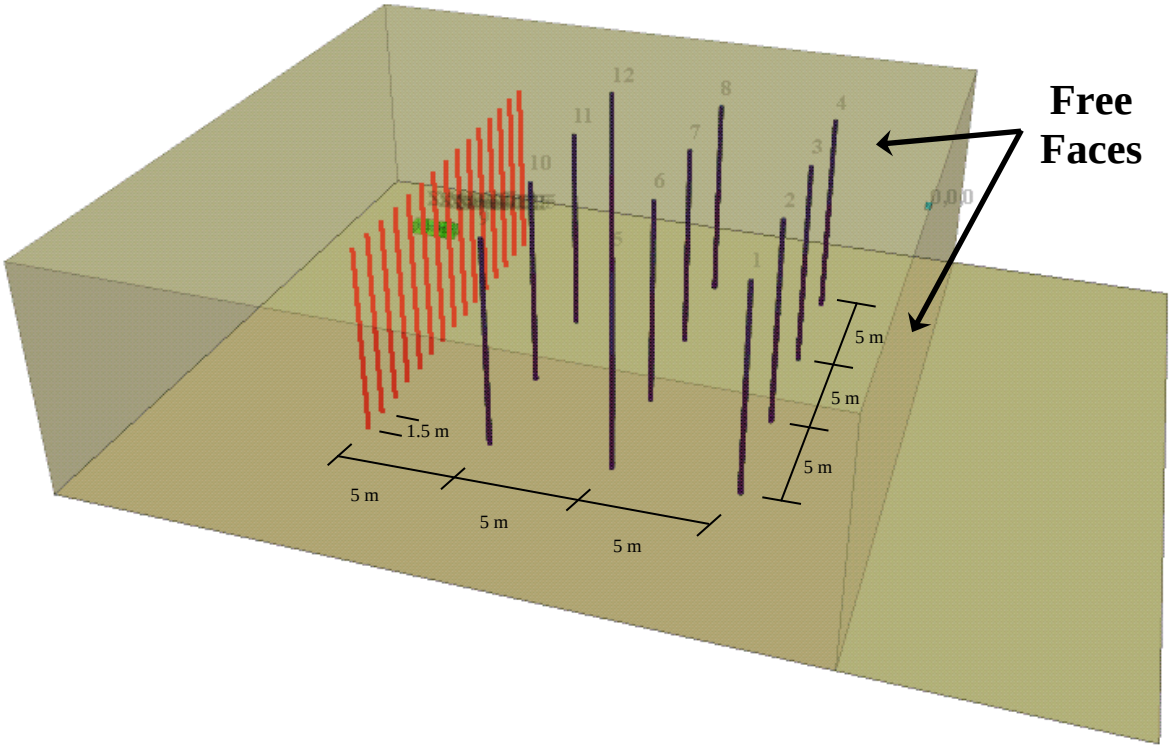

Figure 42 – Image of the Blo-Up model created to monitor the strain rate behind the pre-split line.

Aside from the timing of the detonation sequence, no variables were changed in the models. The pre-split design is based on the ideal results achieved using a 1.5 metre hole spacing, a decoupling ratio of three, for a splitting factor of 0.33 kg/m^2 (described in Section 4.3). Table 8 summarizes the parameters used in the slow and fast blasting large scale blast models. The production holes have a powder factor of 0.82 kg/m^3, which is on the high end of the recommended rules-of-thumb guidelines presented by Dyno Nobel, which is between 0.3 – 0.8 kg/m^3 (Dyno Nobel, 2010).

Table 8 – Summary of the parameters used in the slow and fast blast models.

Model Parameters for Fast and Slow Blast Models		
Parameter	**Fast Blast**	**Slow Blast**
Production Blastholes	-	-
Hole diameter (mm)	165	165
Hole spacing (m)	5	5
Burden (m)	5	5
Timing between holes in the same row (ms)	2	8
Timing between final detonation in row and beginning of next row (ms)	2	20
Explosive type	ANFO	ANFO
Explosive density (kg/m³)	800	800
VOD (km/s)	4.84	4.84
Powder factor (kg/m³)	0.82	0.82
Pre-split Blastholes	-	-
Hole diameter (mm)	100	100
Hole spacing (m)	1.5	1.5
Explosive type	Emulsion	Emulsion
Explosive density (kg/m³)	1200	1200
VOD (km/s)	5.92	5.92
Decoupling ratio	3	3
Splitting factor (kg/m²)	0.33	0.33

The fast model has a 2 millisecond (ms) time delay of detonation between holes and between rows. This timing is very fast, however the objective of the diamond mine that used this timing

was to freeze the broken rock in place, which prevents dilution. The slow model had 8 ms time delay between holes and a 20 ms delay of detonation between rows. History points were inserted behind the pre-split line to determine the strain rate experienced at varying distances. The history points were located at various distances behind the pre-split line. In order to prevent significant strain applied to the history points from the pre-split detonation, the points were placed halfway between two middle pre-split holes at 4 metres depth (half way down the hole) and at 0.1, 0.25, 0.5, 1.0 and 1.5 m behind the pre-split line (Figure 43).

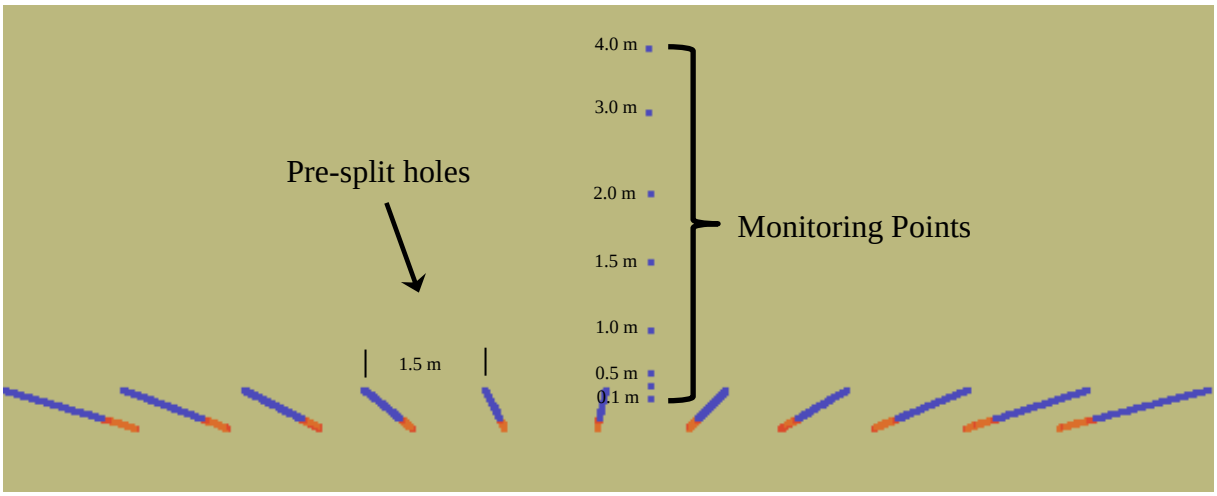

Figure 43 – Image showing the location of the monitoring points in the model (plan view).

5.2 Large Scale Over-Confined Blast

Figure 44 illustrates the strain rate results for the blast model with fast timing between detonations resulting in an over-confined system. The history marker located 0.1 metre behind the pre-split line has much higher oscillation amplitude than the other history points, which is expected as it is closest to the pre-split fracture and will be subject to some form of damage. As discussed, the Blo-Up far-field model is made up of spheres that are connected by springs. When one of the springs break, the sphere connected to the broken spring becomes a fragment in the model. This results in higher strain rate oscillation amplitude due to numerical instability,

which is similar to what is observed in the results. The sphere located 0.1 metre behind the pre-split line has been subjected to a significant disturbance due to seismic waves and has sustained damage. The other history points exhibit large amplitude oscillations, however due to their depth into the final wall, they most likely would not be completely destroyed by the blast.

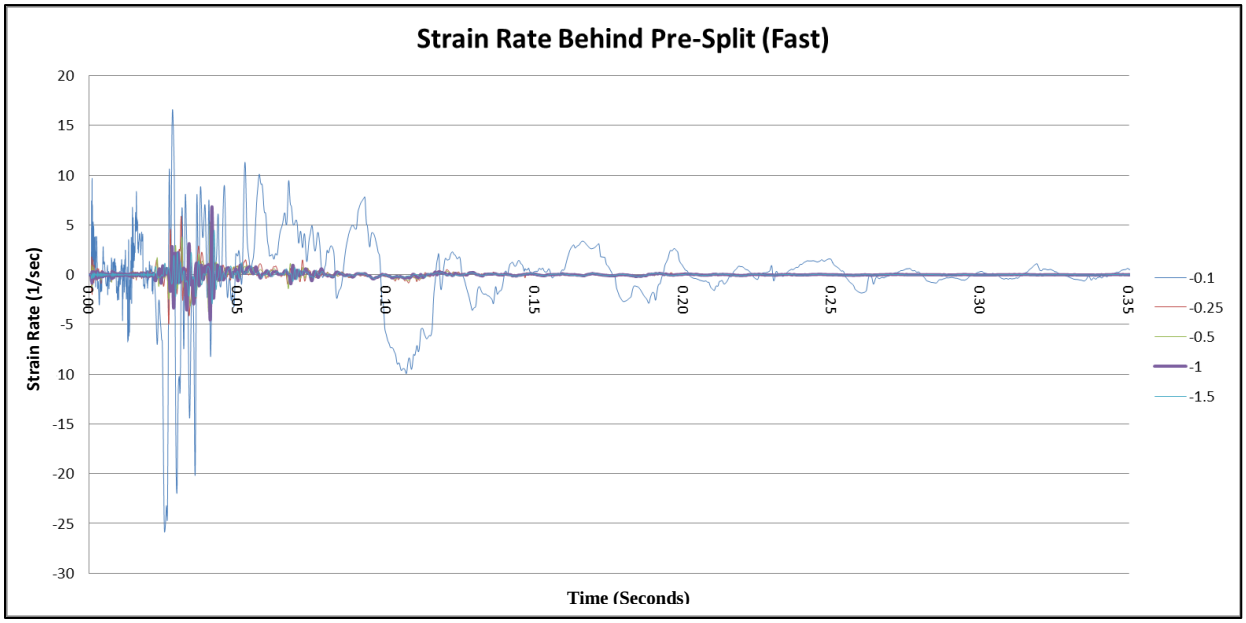

Figure 44 – Results of a fast production blast on the final wall stability.

The remaining history markers located 0.25, 0.5, 1.0 and 1.5 metres behind the pre-split are examined more closely in Figure 45. The overall length of time along the x-axis has also been decreased in the chart to focus on the interval of interest. The first oscillations occurring at 0 ms are a result of the pre-split detonation. These oscillations are significantly smaller in magnitude than the following oscillations generated by the production blast. As successive rows are detonated, the energy in the system continues to back up. The oscillations in strain rate generated by detonating the first row of production holes dissipates prior to detonation of the second row, however there is no dissipation between the second and third rows. The stress wave generated from the second row of production holes passes by the third row of holes at the same

time as the stress wave from the third row is generated, which means the stress wave is magnified by harmonic reinforcement.

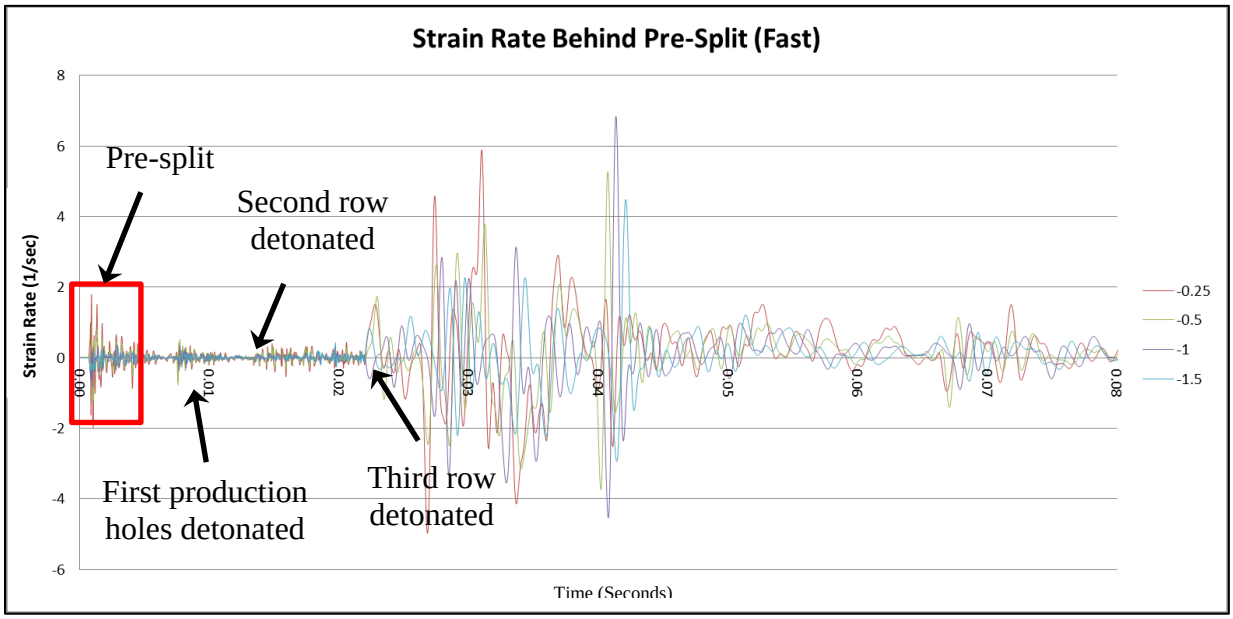

Figure 45 – Fast blast results with the first history marker removed and model time decreased.

Although the graphs show significant oscillation in strain rate, there is no clear method for relating damage to strain rate. As discussed in Chapter 2, Peak Particle Velocity (PPV) can be used to correlate potential damage. An algorithm was written to determine the maximum PPV experienced at designated points in the model (Appendix III). Based on the PPV level experienced at a given point, the amount of damage can be estimated based on the work by Bauer and Calder (1978). Table 9 presents the expected damage with associated PPV levels.

Table 9 – Effects on structures and typical hard rock masses (Bauer and Calder, 1978).

Peak Particle Velocity (mm/s)	Effects on Structures and typical (hard) rock masses
>2,500	Complete break-up of rock masses
635 to 2,500	Strong tensile and some radial cracking of rock
250 to 635	Minor tensile slabbing
<250	No Fracturing of intact rock

The effect of the pre-split blast, by itself, must be considered when examining the amount of damage sustained to the final wall. A basic pre-split model was run with PPV indicators located at various distances behind the pre-split line (0.1, 0.25, 0.5, 1.0, 2.0, 3.0, 4.0 and 5.0 metres). The results are summarized in Table 10. The point 0.1 metre behind the pre-split line suggests there will be moderate damage sustained to the rock. This damage should be expected as the rock around the blastholes is subjected to compression during the pre-split detonation. Beyond 0.1 metre, there is minimal disturbance to the rock mass.

Table 10 – Basic pre-split model tracking PPV behind the pre-split line.

Split Factor	**Distance Behind Pre-split (m) and Corresponding Maximum PPV (mm/s)**							
0.33 kg/m³	*0.1m*	*0.25m*	*0.5m*	*1m*	*2m*	*3m*	*4m*	*5m*
0.33	653	513	335	298	268	238	207	176

Table 11 presents the maximum PPV experienced at different distances behind the pre-split line for the production blast with fast timing. Based on the results from the model, at least 0.25 metre of the final wall would be heavily damaged. In addition, strong tensile cracking would extend 5 metres into the final wall. Due to the high level of confinement of this blast, the stress wave generated from the detonation is able to close the aperture of the pre-split fracture and continue into the final wall, resulting in significant damage.

Table 11 – Results of tracking PPV behind the over-confined blast.

Timing (ms)		**Distance Behind Pre-split (m) and Corresponding Maximum PPV (mm/s)**							
Hole-Hole	*Row-Row*	*0.1m*	*0.25m*	*0.5m*	*1m*	*2m*	*3m*	*4m*	*5m*
2	2	2,533	1,837	1,735	1,444	1,267	1,089	861	708

5.3 Large Scale Evenly Balanced Blast

An alternate model was run with slower timing between holes and rows to simulate a blast that better distributes energy. The timing was increased between holes from 2 ms to 8 ms and the

timing between rows was increased from 2 ms to 20 ms. As a result of the slower timing between detonations, the rock has time to fragment and migrate away from the blast area before successive detonations occur. As a comparison, the final hole in the fast blast model detonated at 34 ms, while the final hole in the slow blast detonated at 146 ms. Figure 46 presents the results of the slow blast. The strain rate, measured on the y-axis, is bounded with the same minimum and maximum values as the over-confined blast model for comparison purposes.

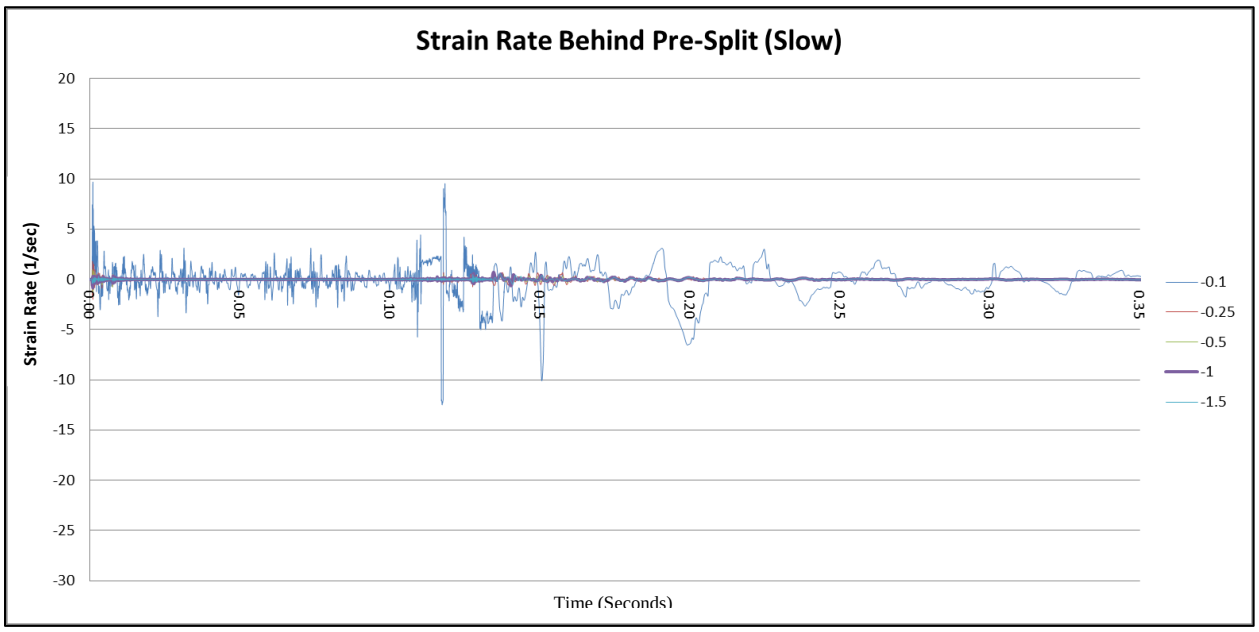

Figure 46 – Results of a blast with evenly distributed energy.

The overall strain rate magnitude observed in the slow blast model is approximately 50 % less than what is observed in the fast blast measured at the history point 0.1 m behind the pre-split line. The smaller amplitude in strain rate indicates less dynamic loading occurring on the final wall. Stress waves generated from detonation of the production holes in a slow blast will travel through the rock and dissipate before successive detonations occur. The marker located 0.1 metre behind the pre-split, indicates some damage has occurred. However, the markers located

further into the wall do not show the same high amplitude oscillations and therefore less dynamic loading (Figure 46).

Unlike the fast blast, the stress waves generated from the slow blast are able to dissipate into the rock mass prior to successive detonations. Given the increase in time between detonations, cracks and fractures are able to develop and extend further away from the blasthole. The cracks and fractures will effectively dissipate the energy of the stress wave travelling through the rock mass because the rock mass will no longer be completely intact. In addition, the longer delay time will prevent harmonic reinforcement from other production stress waves from occurring.

Figure 47 presents the results of the slow blast at history markers 0.25, 0.5, 1.0, and 1.5 metres behind the pre-split line. The results indicate far less dynamic loading occurring in the final wall. The aperture of the pre-split fracture has likely closed and allowed some amount of the stress wave to pass into the final wall; however the overall strain rate is lower than the fast blast model. The maximum amplitude of strain rate, measured 0.25 metre behind the pre-spit line, is approximately 80 % less than the fast blast model. Due to the increase in time between detonations, the stress waves generated from individual production holes are able to dissipate prior to successive detonations occurring, therefore harmonic reinforcement of stress waves between production rows does not occur in this model. The increase in time allows fractures and cracks to develop and extend further into the rock mass, which is also likely to be a contributing factor in the decrease in the strain rate magnitude because the stress wave will be impeded by these discontinuities.

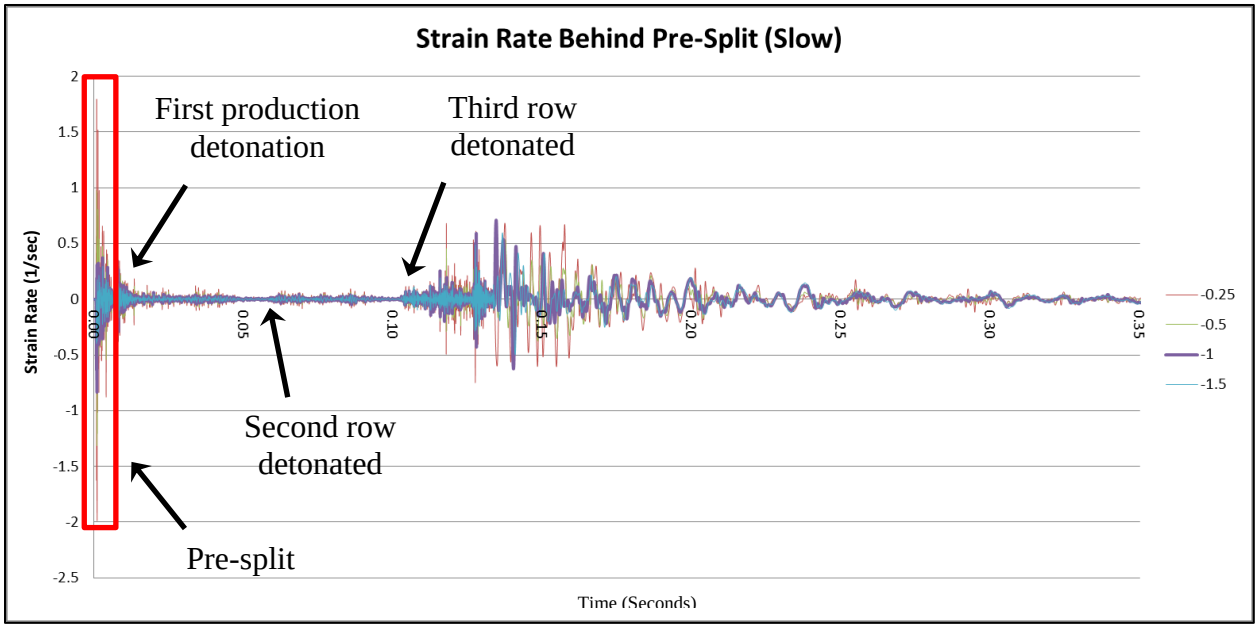

Figure 47 – Slow blast results with the first history marker removed and model time decreased.

The PPV was tracked behind the pre-split in order to determine the amount of blast-induced damage experienced in the final wall. Table 12 summarizes of the PPV experienced behind the pre-split line. Strong tensile and some radial cracking of the rock is experienced 0.1 metre behind the pre-split line but dissipates quickly as distance increases away from the pre-split line.

Table 12 – Summary of the PPV behind the pre-split line for a slow blast.

Timing (ms)		**Distance Behind Pre-split (m) and Corresponding Maximum PPV (mm/s)**							
Hole-Hole	*Row-Row*	*0.1m*	*0.25m*	*0.5m*	*1m*	*2m*	*3m*	*4m*	*5m*
8	20	1,007	511	417	350	292	261	223	187

Based on the results from these two models, a blast with slower timing between detonations or a well-balanced blast will allow more time for material to migrate away from the blast area before subsequent holes and rows are detonated. This will significantly reduce the amount of potential blast-induced damage sustained to the final wall. For the purpose of comparison, the PPV measured in both models is summarized in Table 13 and the strain rates are presented in Figure 48.

Table 13 – Summary of the PPV for the fast and slow blasts.

Timing (ms)		Distance Behind Pre-split (m) and Corresponding Maximum PPV (mm/s)							
Hole-Hole	*Row-Row*	*0.1m*	*0.25m*	*0.5m*	*1m*	*2m*	*3m*	*4m*	*5m*
2	2	2,533	1,837	1,735	1,444	1,267	1,089	861	708
8	20	1,007	511	417	350	292	261	223	187

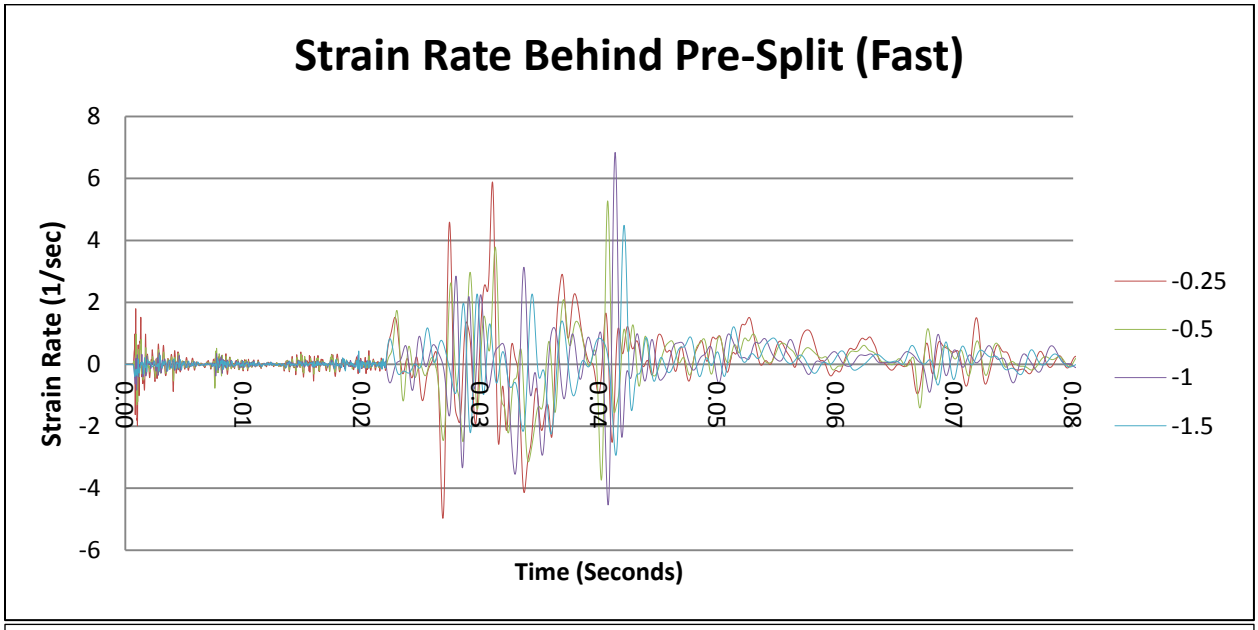

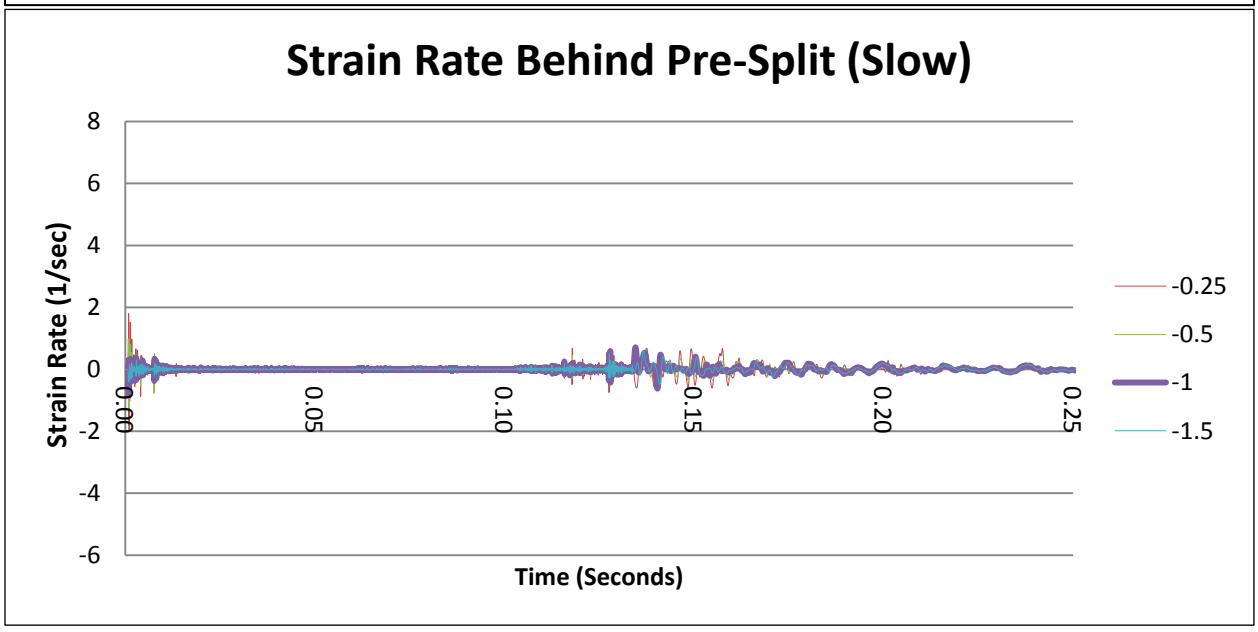

Figure 48 – Comparison of the two blast models.

5.4 Production Blast with Buffer Row Holes

Using one or more rows of buffer holes is another method used to control blast-induced damage sustained to final walls. The buffer row is an extension of the production blast and is located between the final production row and the pre-split. These holes are charged lighter than the main production holes, which essentially creates a buffer region between the main production blast and the pre-split that will limit the amount of blast energy applied to the final wall. Compared to the main production blast holes, the buffer rows may have a smaller hole diameter, reduced burden spacing, reduced hole spacing, less explosive used and increased timing between detonations. The buffer row of holes is necessary when a pre-split blast is being used to control blast-induced damage.

The key factors in designing and optimizing a buffer blast are:

- Dynamic burden relief: any predisposition for the blast to become over-confined is likely to cause damage beyond the pre-split and result in an unstable final wall.
- Buffer row charge distribution: explosive concentration must be low enough to avoid crushing damage, however it also must be evenly distributed enough to ensure adequate breakage of material from the pre-split.

In order to examine the benefits of using buffer rows to protect the final wall of the open pit, the well balanced blast model, detailed in Section 5.3, was altered to include buffer rows. The pre-split blast was not included in this analysis because it generates higher PPV and strain rates localized to the final wall. Therefore, the main production blast was essentially modelled independently and markers tracked the strain rate and PPV at the final wall boundary.

Three models were run to examine the effect of including buffer rows. The first model did not include any buffer row holes and was used as a base case, the second model used one row of buffer holes and the third model used two rows of buffer holes. For the purposes of this analysis, the production borehole size does not change from 165 mm and the ANFO properties described in Section 5.1 are used as the explosive. The buffer hole diameter used in the models was 127 mm. The timing between production holes is 8 ms, while the timing delay between buffer holes is 12 ms. The stemming in all buffer holes is 2 metres. No subgrade drilling is included in the buffer row holes. Table 14 summarizes the parameters used in the buffer hole models. Figure 49 illustrates plan views of the models that include the buffer rows of holes. The modelling parameters are consistent with the rules of thumb detailed in Section 2.4.3.

Table 14 – Summary of modelling parameters used in the buffer hole models.

	Model 1: No Buffer Holes Used	**Model 2: One Buffer Row**	**Model 3: Two Buffer Rows**
No. of Production Rows	4	3	2
No. of Buffer Rows	0	1	2
Production Hole Spacing (m)	5	5	5
Production Burden Spacing (m)	5	5	5
Last Production Row to Pre-Split (m)	5	6.25	10.25
Buffer Hole Spacing (m)	-	3.75	Row 1 = 3.75m / Row 2 = 3.75m
Buffer Burden Spacing (m)	-	3.75	Row 1 = 4m / Row 2 = 3.75m
Last Buffer Row to Pre-Split (m)	-	2.5	Row 1 = 6.25m / Row 2 = 2.5m
Buffer Hole Charge Height (m)	-	3	Row 1 = 3m / Row 2 = 2.6m

Note: with two buffer holes, row 1 refers to the row closest to the last production row, while row 2 refers to the row closest to the pre-split or final wall.

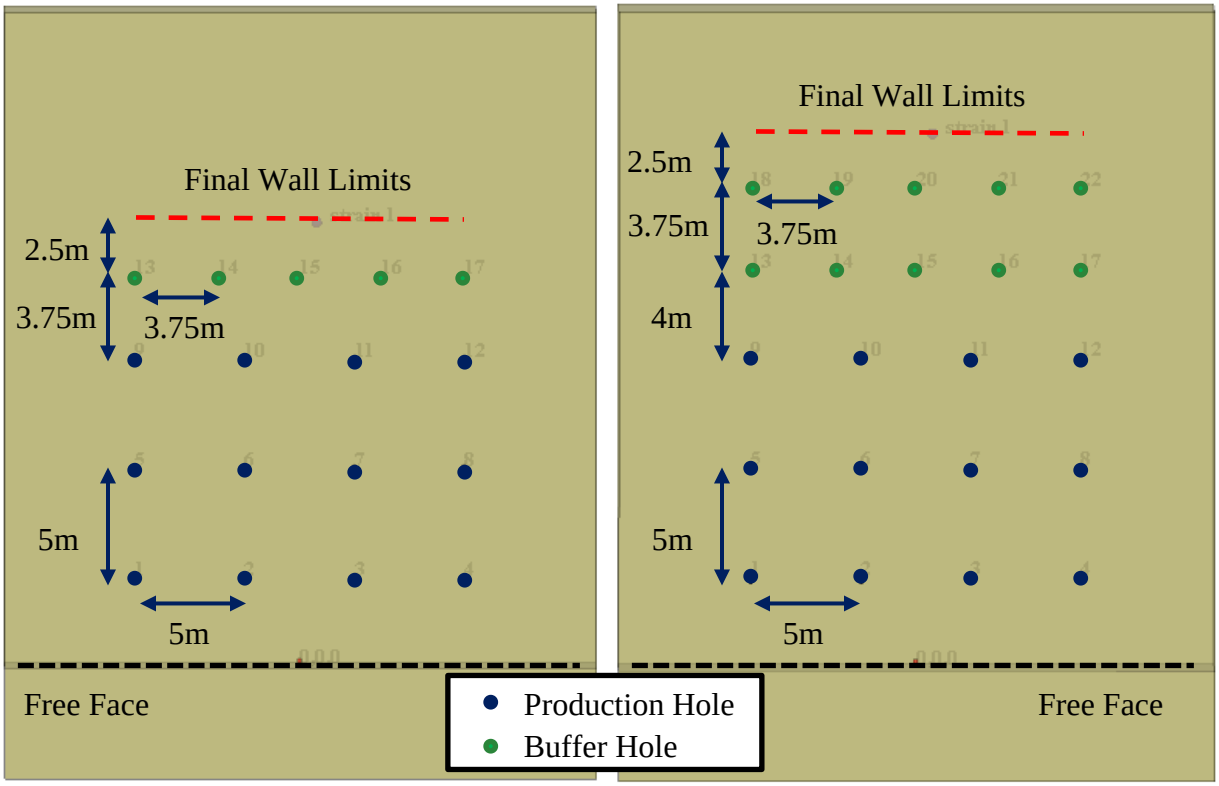

(a) Single Buffer Row *(b) Two Buffer Rows*

Figure 49 – Plan views illustrating the buffer hole models: (a) model layout with single row of buffer holes and (b) model layout with two rows of buffer holes.

The results of the modelling shows a reduction in the amount of blast-induced energy applied to the final wall when buffer rows are used. Figure 50 presents the strain rate measured at the boundary of the final wall when no buffer holes are included. The four spikes in strain rate represent the four rows of production holes detonating. The maximum PPV measured at the final wall boundary in this no buffer row model is 1,638 mm/s. Figure 51 presents the strain rate measured at the boundary of the final wall with three production rows and one row of buffer holes included in the model. The maximum PPV measured at the final wall boundary with one row of buffer holes is 765 mm/s. Figure 52 presents the strain rate measured at the final wall boundary with two rows of buffer holes used. The maximum PPV measured at the final wall boundary is 746 mm/s.

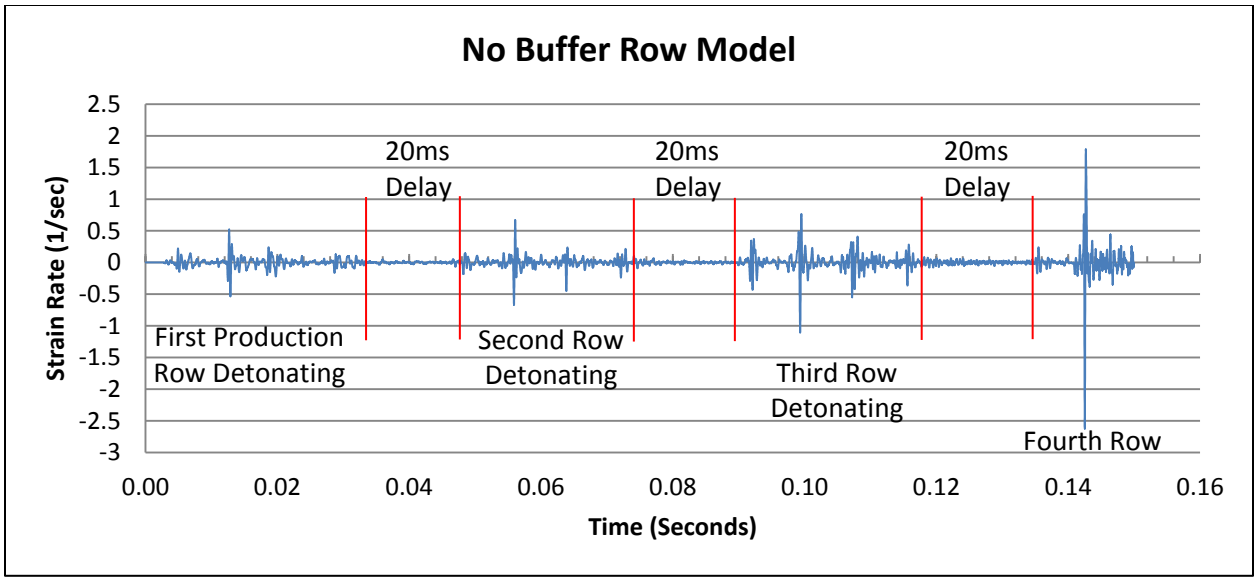

Figure 50 – Model results showing the strain rate measured at the final wall boundary with no buffer rows included in the model.

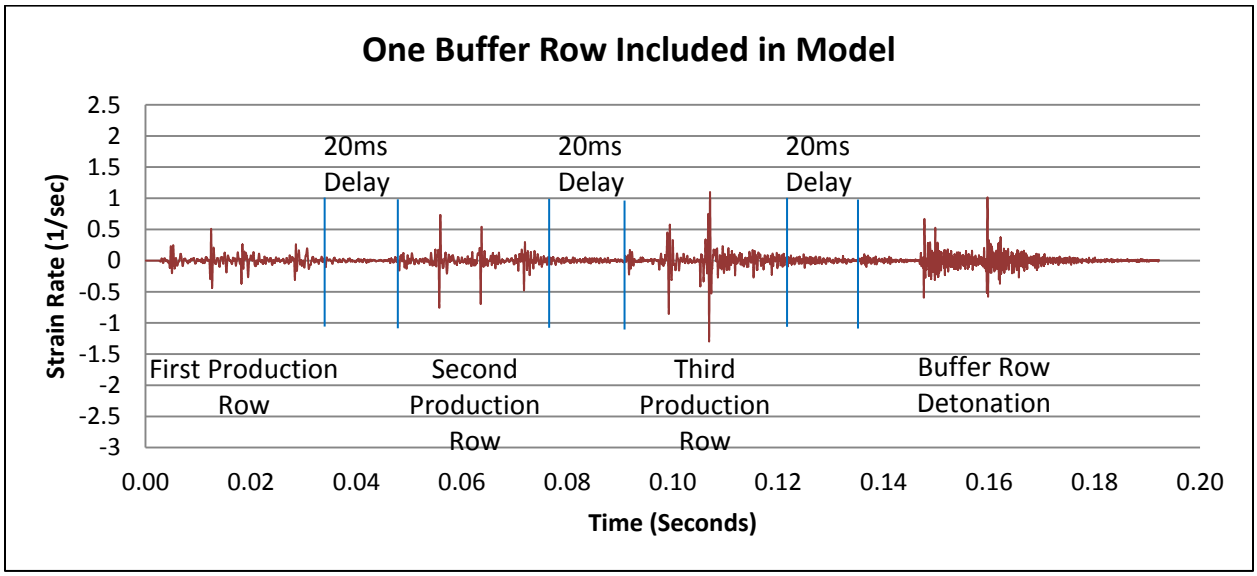

Figure 51 – Model results showing the strain rate measured at the final wall boundary with one buffer row included in the simulation. Note: the two large strain rate oscillations recorded during the buffer row detonation are the buffer holes located closest to the history point.

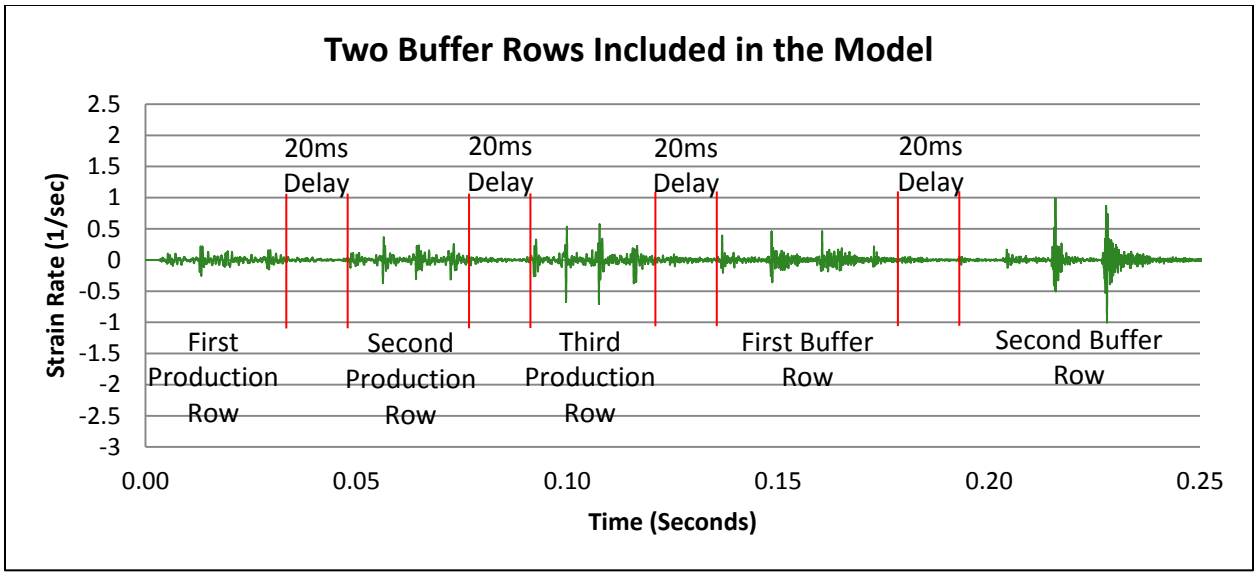

Figure 52 – Model results showing the strain rate measured at the final wall boundary with two buffer rows included in the simulation.

The modelling results presented above indicate that by increasing the distance from the final production row of holes to the pre-split line, there is less dynamic loading applied to the final wall from the main production blast. Buffer rows are necessary to break the rock between the final production row and the pre-split line. The buffer holes also promote final wall stability by reducing the blast induced damage. By using less explosive and spacing the buffer holes closer together, the blast energy is more evenly distributed resulting in less energy generated in close proximity to the final wall.

When the pre-split is included in the model with two buffer rows, the maximum PPV recorded 0.1 metres behind the pre-split is 668 mm/s, which is in the same range as the PPV recorded from the pre-split detonation itself. Figure 53 illustrates the strain rate measured behind the pre-split when the full blast model is simulated and Table 15 summarises the PPV levels measured at various distances behind the pre-split. Therefore, based on the modelling results, if a production blast is well balanced and buffer rows are included to further reduce energy buildup at the end of

the blast, the stress waves generated from the production hole detonations dissipate as they reach the pre-split and do not continue into the final wall. This would be considered an ideal blast that would not result in blast-induced damage sustained to the final wall.

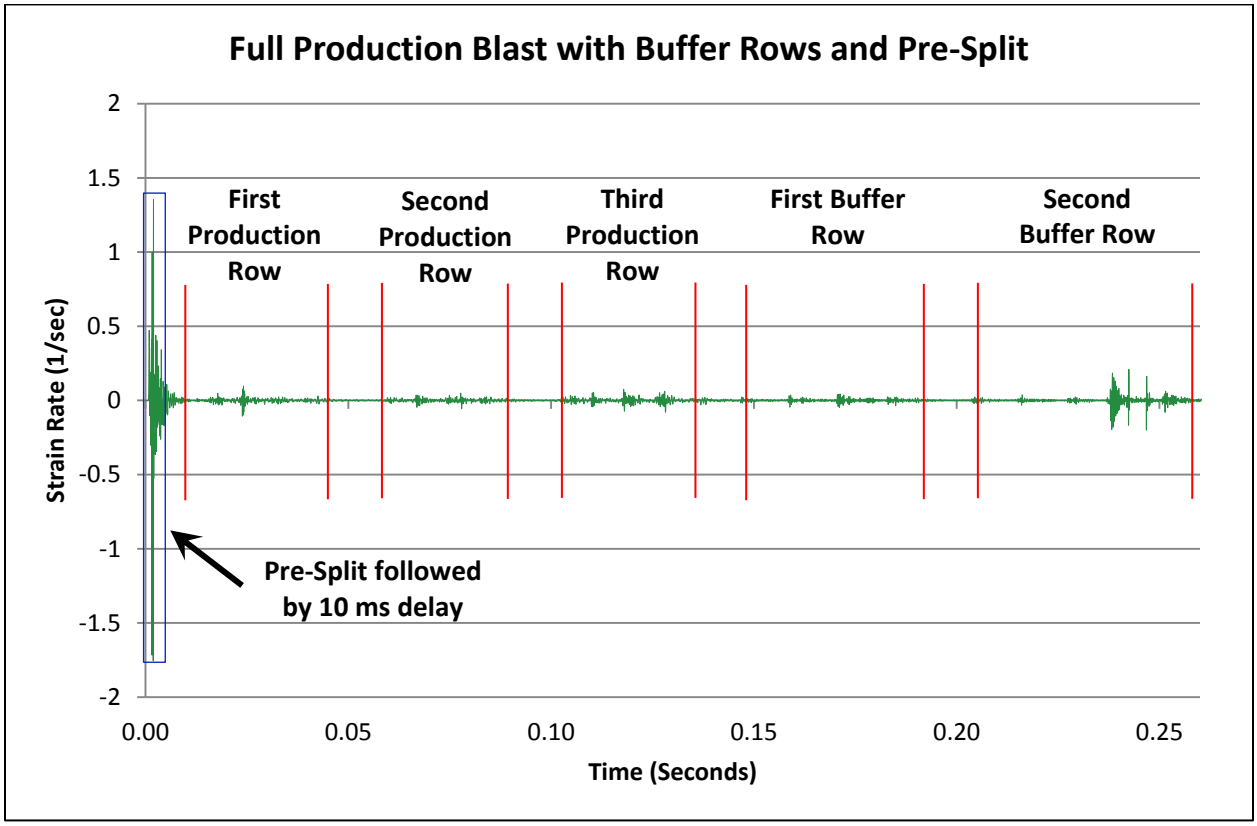

Figure 53 – Model results showing the strain rate measured behind the pre-split for a full blast model.

Table 15 – Summary of PPV measured at various distances behind the pre-split for the full blast model.

Distance Behind Presplit (m) and Corresponding Maximum PPV (mm/s)							
0.1m	*0.25m*	*0.5m*	*1m*	*2m*	*3m*	*4m*	*5m*
668	532	321	293	267	242	198	174

- Chapter 6: Conclusions -

6.1 Discussion & Conclusions

The stability of a final wall is vital to operations in an open pit mine. The walls are specially designed to have benches that will serve to catch any falling material and protect personnel and equipment working at the bottom of the open pit. The walls also host the ramp, which is the primary access to the bottom of the pit. Deterioration or instability on these walls can put an entire operation at risk. This is especially true in deep open pit mines with high walls. In underground mining, when an excavated stope wall is deemed to be unstable, the stope can be backfilled and adjacent mining can continue. Open pit mining is not as forgiving. If a significant wall failure occurs, the pit walls may need to be pushed back, which can take years to complete and will involve a large cost.

Blasting is by far the most widely used technology used to break and fragment rock in the mining industry. Given the violent nature of blasting and the high variability in the potential results, there is potential to cause significant blast-induced damage to the final pit wall. Blasts need to be designed specifically for the type of rock it is trying to break. Characteristics of the rock, such as natural jointing, joint orientation, joint conditions and the strength of the rock, all need to be accounted for.

The Blo-Up software is being developed by a consortium of companies to model the blast process from beginning to end. Blo-Up can be used as a means of re-tooling specific explosive properties, for modelling the outcome of specific blast designs, and for predicting blast-induced damage. Having the ability to model a blast to determine the potential outcome is advantageous

because it gives a better understanding of the blasting process and allows the blasting engineer to have a greater level of confidence in the blast design before field testing, therefore, avoiding the time consuming and costly 'trial and error' practice.

As detailed in this thesis, both small scale and large scale validation studies have been trialed with success using Blo-Up software. The research and trials completed have demonstrated the ability of the software to successfully model the outcome of a blast and produce results that are comparable with field observations. The field observations used for comparison were made at various diamond mines in the Southern Africa region. Problems detailed in this thesis were all observed in the field and recommendations made in the field follow the same steps detailed in this thesis to prevent final pit wall damage. The modelling results were not only used for purposes of validation of filed observations but were implemented to improve blast practices and results.

This thesis demonstrated that, in order to promote final wall stability, a blast must be properly balanced. Explosive energy must be evenly distributed to achieve optimal blasting results. Over confinement will lead to excessive dynamic loading applied to the final wall, which can lead to potential blast-induced damage. Even if a successful pre-split has been created, an over-confined production blast, caused by fast timing or out of sequence detonations along with excessive blasthole spacing, can still cause blast-induced damage in the final wall.

Natural jointing in the rock mass and specifically the orientation with respect to the pit walls can lead to significant damage sustained to the final wall if a pre-split is not properly designed to complement the rock mass. High pressure gasses from the explosive detonation will wedge open natural discontinuities and travel beyond the final wall limit before venting to atmospheric

pressure. Using less explosive, smaller hole diameters, and reducing the hole spacing, are all ways to better balance the blast energy and limit the amount of damage sustained to the final wall during the pre-split blast.

On a production scale, having a properly sequenced and timed blast is also important for final wall stability. Blasts that are too fast or have out of sequence detonations will result in over confinement of the system, which can lead to poor fragmentation, fly rock, and potential damage of the final wall. Broken material must have room to move towards a free face and time to clear the blast area before subsequent rows are detonated. Complex blast designs, out of sequence detonations, and fast timing between detonations can also result in significant blast-induced damage to the final wall. Box cuts and V-shaped blast patterns are inherently over confined situations and should be avoided if possible.

For predicting the effect of a blast in an open pit mine, especially those with adverse geological conditions, the use of modelling software would provide valuable insight to the outcome of a blast before the blast design is implemented and the blaster presses the button to initiate the detonation sequence, as demonstrated in this work. Explosive engineers, who normally rely on rules of thumb, empirical analysis, and past experiences obtained in the field, can use modelling software to design a blast for the specific rock mass characteristics encountered with a higher confidence level in predicting the outcome of the blast, once the rock mass is properly calibrated. Blo-Up software can assist in improving pit wall stability and in minimizing dilution, which will result in significant costs savings over the life of mine.

6.2 Limitations of the Software

One of the main limitations of the software is the length of time required to run a model. Run time increases dramatically as more holes are added to a model and as each hole is detonated due to tracking the trajectory of each broken particle. The progress is further slowed as the blast continues and individual pieces of broken material crash into each other and velocities of the broken material change. The long run time of the models limited the number of holes that could be placed in the model and the length of timing between detonations in the model. Algorithms, such as the one used to monitor PPV further increase the amount of time to complete a model and need to be optimized to reduce the influence on run time. To give an example, unrelated to this thesis, a 75 hole production blast model was built and run to completion in eight days. There are options to increase the speed of the software that are currently being explored; however this capability was not available at the time of writing this thesis.

Each time a model is run, some aspects of the solution will be slightly different. The distinct element method does not give the exact same solution each time a model is run. This observation supports results from various field testing programs for blasting as results are highly variable in the field. The non-determinism in the model is caused by the random order of accumulation of floating point numbers on multi-processor computers (Blo-Up is parallelized). The system is somewhat chaotic because it is sensitive to small changes in the initial conditions and these small changes can amplify, which is a consequence of distinct element method. Single point measurements can vary 20-30%, based on the author's experience. Since a single point is being measured, small changes in the system will exacerbate the problem, whereas regional measurements will average out and high variability is not as much of a factor to consider. This is

not necessarily a bad thing because blasting in itself and its results are highly variable in the field; therefore it is good to have a range of possible solutions that could be expected in the field.

Joints in the model are represented by user defined planes with weaker properties than the surrounding host material. Any lattice spring that is intersected by the joint planes are given a weaker tensile strength. In the field, joint sets will typically have very little tensile strength, which is the opposite of how the joints are modelled. Therefore, modelling joints accurately is a limitation of the software. The future plan is to represent the joint sets with Mohr Coulomb sliding failure criterion, however this code has not been implemented at this stage.

The Blo-Up software is a powerful tool; however the models must have reasonable data entered to get reasonable output. Accurate rock characteristics and explosive properties must be used. The sensitivity of the system to input parameters needs to be checked through a comprehensive sensitivity analysis to ensure that the overall system is well understood. All factors must be checked and calibrated in the model to match observation in the field. In addition, unless the user specifies, the model assumes all drilling and charging of holes is accurate, therefore drilling deviation in the field must be examined carefully and if necessary replicated in the models. Factors such as out of sequence detonations, amount of explosive used in each hole and the orientation of the drill holes have a significant effect on the outcome of a blast. If necessary these factors may need to be included if a post blast study is carried out.

6.3 Future Work

The research detailed has satisfied the objectives and scope of the thesis. That being said, there are many other opportunities to extend the study and pursue alternate avenues. Some of the future work topics can include:

- *Blasting in adverse geological lithologies:* further modelling and analysis of other complex rock mass conditions for better prediction of blast results. Large scale structures, such as faults or dykes intersecting an open pit can be very difficult to achieve good or acceptable blast results and will require specific focus.
- *Inclined pre-split holes:* verification, validation and calibration of the advantages that were achieved in this thesis with inclining the pre-split holes as a method of deflecting the force of a production blast. This topic should be investigated further with additional production designs.
- *Trim or cushion rows in the large scale layout:* expand modelling and analysis to incorporate a more detailed trim or cushion blast. Varying hole diameter, hole spacing, explosive charge, sequence and timing in trim blasting can be modelled to determine the effect of each parameter or a combination or parameters that can provide an acceptable blast result with minimizing blast-induced damage sustained to the surrounding rock mass or pit wall.
- *Damage indicators:* explore and verify using the numerical modelling software to examine if a stress-strain relationship could be applied to determine the amount of damage sustained by the surrounding rock mass.
- *Blasting in high locked in-stress rock conditions:* there are published reports (Arjang, 2006) of locked in-situ stresses at surface as high as 5-10MPa in the Canadian Shield, which would affect the outcome of a blast because cracking and damage will tend to favor the minor principal (sigma 3) stress orientation when high stresses are present in a rock mass.

- *Large scale blast designs:* further examination of large scale blast designs should be examined to determine optimal designs that can be applied in the field to reduce the amount of confinement of a blast. Longitudinal blast sequences, with two free faces exposed, would be ideal for providing this type of scenario as opposed to V-cut patterns or box cuts.
- *Examining toe damage from blasting:* the work presented in this thesis focused on reducing blast-induced damage sustained to the final wall at the bench scale. Given the high confinement at the bottom of a hole, there is likely to be damage sustained at the toe of the holes, which can affect the stability of the bench below prior to excavating the level. This type of damage should be investigated further.

References

Andrieux, P., 2012. Personal photos taken during a site visit to Southern Africa Diamond Mines.

Andrieux, P. & Hall, A., 2013. Contrôle des murs dans un massif rocheux fortement fracture. Presented at: 36e Session d'étude sur les techniques de sautage, Québec, November 2013. Page 18.

Arjang, B., 2006. Canadian crustal stresses and their application to mine design. Project 602510: Proceedings of the core project on deep mining. CANMET, Ottawa, Ontario. Page 43.

Bauer, A., & Calder P., 1977. Pit slope manual. Chapter 7 – Perimeter blasting. energy, Mines and Resources Canada, CANMET Report 77-14. Ottawa, ON, Canada. Page 82.

Bauer, A., & Calder, P. 1978. Open pit and blast seminar. Course #63-321. Queen's University, Department of Mining Engineering, Kingston, ON, Canada. Page 72.

Braithwaite, M., & Sharpe, G., 2009. Simulation of real detonations as an energy source term for the Hybrid Stress Blasting Model. FRAGBLAST 9; Proceedings of the 9th International Symposium on Fragmentation by Blasting. Jose A. Sanchidrian (ed.). Grenada, September 2009. Pages 721-727.

Brent G. F. & Smith G. E., 1996. Borehole pressure measurements behind blast limits as an aid to determining the extent of rock damage. FRAGBLAST 5: Proceeding of the 5th International Symposium on Fragmentation by Blasting. B. Mohanty (ed.). Montreal, Canada. Pages 103-112.

Brinkmann, J.R., Giltner, S.G., & Gibson P.A., 1987. Fundamental studies of blasting in narrow-stope gold mines. FRAGBLAST 2: Proceedings of the 2nd International Symposium on Rock

Fragmentation by Blasting. H. P. Rossmanith (ed.). Keystone, Colorado. CRC Press (pub.). Pages 498-520.

Cho, S. H., & Kaneko, K., 2004. Rock fragmentation control in blasting. The Mining and Materials Processing Institute of Japan. Vol. 45, No. 5, Pages 1722 - 1730.

Cunningham, C. V. B., 1983. The Kuz-Ram model for prediction of fragmentation from blasting. FRAGBLAST 1: Proceedings of the 1st International Symposium on Rock Fragmentation by Blasting. H. P. Rossmanith (ed.). Lulea University of Technology, Lulea, Sweden, August 22-26, 1983. CRC Press (pub.). Pages 439-453.

Cunningham, C. V. B., 1987. Fragmentation estimations and the Kuz-Ram model – four years on. FRAGBLAST 2: Proceedings of the 2nd International Symposium on Rock Fragmentation by Blasting. Keystone, Colorado, USA, August 23-26, 1987. Bethel, CT: Society for Experimental Mechanics. Page 475-487.

Dehghan Banadaki, M.M., 2010. Stress-wave induced fracture in rock due to explosive action. Ph.D. Thesis, Department of Civil Engineering, University of Toronto. Pages 85-94.

Dowding, C.H., 1996. Construction vibrations. Upper Saddle River, New Jersey: Prentice Hall. Chapter 13, Comparison of environmental and vibration-induced crack movement.

Dowding, C.H., 1985. Blast vibration monitoring and control. Hall, W.J., (ed.). Prentice-Hall Inc., Englewood Cliffs, NJ. Pages 1-288.

Dyno Nobel, 2010. Blasting and explosives quick reference guide 2010. Product and User Guide Booklet. Dyno Nobel Group. Pages 3-4.

Furtney, J. K., Cundall, P. A., & Chitombo, G. D., 2009. Developments in numerical modeling of blast induced rock fragmentation: Updates from the HSBM project. FRAGBLAST 9: Proceedings of the 9th International Symposium on Rock Fragmentation by Blasting. J. A. Sanchidrian (ed.). Granada, Spain, September 2009. CRC Press (pub.). Pages 335-342.

Furtney, J. K., Sellers, E., & Onederra I., 2012. Simple models for the complex process of rock blasting. Rock Fragmentation by Blasting: FRAGBLAST 10: Proceedings of the 10th International Symposium on Rock Fragmentation by Blasting. K. Singh and A. Sinha, (ed.). New Delhi, November 2012, CRC Press/Balkema (pub.). 2013. Pages 275-282.

Franklin, J., & Katsabanis, T., 1996. Measurement of blast fragmentation. FRAGBLAST 5: Proceedings of the 5th International Symposium on Rock Fragmentation by Blasting. B. Mohanty (ed.). Montreal, Canada. CRC Press/Balkema (pub.). Pages 25-29.

Hartman, H., 1992. SME Mining Engineering Handbook. Society for Mining, Metallurgy, and Exploration Inc, 1992. Page 732.

ICI Australia, 1990. Environmental effects of blasting. Handbook of blasting tables. Pages 33-35.

ISEE, 1998. Blaster's Handbook - 17th Edition. Published by the International Society of Explosives Engineers. R. Hopler (ed.). Cleveland, Ohio, USA. Page 744.

Itasca, 2012. Blo-Up user's guide - release 2.7. Itasca Consulting Group. Not published. Pages 1-142.

Jimeno, C. L., Jimeno, E. L., & Carcedo, F. J. A., 1995. Drilling and blasting of rocks. Y. V. De Ramiro (ed.). Balkema (pub.). Page 168.

Kapila, A. K., Bdzil, J.B., & Stewart, B.S., 2006. On the structure and accuracy of programmed burn. Combustion Theory and Modelling. Volume 10, Issue 2. Pages 289-321.

Krehl, P., 2001. History of shock waves. Handbook of Shock Waves. Gabi Ben-Dor (ed.). Volume 1, Chapter 1. Elsevier Inc. Pages 1-142.

Langefors, U., & Kihlstrom, B., 1976. The modern technique of rock blasting. 3rd Edition. New York, John Wiley and Sons. Page 438.

Lilly, P. A., 1986. An empirical method of assessing rock mass blastability. The AusImm/IE Aust. Newman Combined Group, Large Open Pit Mining Conference. J. R. Davidson (ed.). Pages 41-44.

Minchinton, A., & Lynch, P.M., 1996. Fragmentation and heave modeling using a coupled discrete element gas flow code. FRAGBLAST 5; Proceedings of the 5th International Symposium on Rock Fragmentation by Blasting. B. Mohanty (ed.). Montreal, August 1996. CRC Press/Balkema (pub.). Pages 71-80.

Mohanty, B., & Dehghan Banadaki, M.M., 2009. Characteristics of stress-wave-induced fractures in controlled laboratory-scale blasting experiments. Proceedings of the 2nd Asian-Pacific Symposium on Blasting Techniques. Wang X. (ed.). Metallurgical Industry Press, Beijing. Pages 43-49.

Morhard, R. C., 1987. Explosives and rock blasting. Field Technical Operations, Atlas Powder Company (pub.). Pages 1-662.

Ngo, T., Mendis, P., Gupta, A., & Ramsay, J., 2007. Blast loading and blast effects on structures – an overview. University of Melborne, Australia. Pages 76-91.

Olsson, M., Nie, S., Bergqvist, I., & Ouchterlony F., 2002. What causes cracks in rock blasting? FRAGBLAST 6: Proceedings 6th International Symposium on rock fragmentation by blasting. Johannesburg, South Africa. CRC Press/Balkema (pub.). Pages 221-233.

Onederra, I., Furtney, J., & Sellers, E., 2012. Modelling the extent of damage from fully coupled explosive charges. FRAGBLAST 10: Proceedings of the 10th International Symposium on Rock Fragmentation by Blasting. P.K. Singh & A. Sinha (ed.). New Delhi, India. Taylor and Francis Group, London, Pages. 267-274.

Onederra, I., Sellers, E., Furtnery, J., & Chitombo, G., 2012. Improved understanding of explosive-rock interactions using the hybrid stress blasting model. Journal of the Southern African Institute of Mining and Metallurgy, 112, 8. Pages 721-728.

Ouchterlony, F., Olsson, M., & Bavik, S.O., 1999. Bench blasting in granite with holes with axial notches and radial bottom slots. FRAGBLAST 6: Proceedings 6th International Symposium on rock fragmentation by blasting. Johannesburg, South Africa. CRC Press/Balkema (pub.). Pages 229-239.

Ouchterlony, F., Olsson, M., & Bergqvist, I., 2001. Towards new Swedish recommendations for cautious perimeter blasting. FRAGBLAST 6: Proceedings 6th International Symposium on rock fragmentation by blasting. Johannesburg, South Africa. CRC Press/Balkema (pub.). Pages 169-181.

Preece, D., 1993. Momentum transfer from flowing explosive gases to spherical particles during computer simulation of blast-induced rock motion. Proceedings of the 19th Annual ISEE Symposium. Explosives & Blasting Research. San Diego, January-February 1993. Pages 251-260.

Richards, A. B., Moore, A. J., 2013. Blast Vibration Course. Measurement – Assessment – Control. Terrock Consulting Engineers. File No. 27409591.doc. Pages 5-11.

Rorke, A. J., & Brummer, R. K., 1988. The use of explosives in rockburst control techniques. Proc. 2nd International symposium on rockburst and seismicity in mines. C. Fairhurst (ed.). Minneapolis, Minnesota. Balkema (pub.). Page 525-538.

Ruest, M., 2008. Numerical methods for simulating the flow of detonation products within an explicit fracture network formed by the coalescence of cracks during blasting. Ph.D. Thesis, The University of Queensland. Pages 65-101.

Ruest, M., Cundall, P., Guest, A., & Chitombo, G., 2006. Developments using the particle flow code to simulate rock fragmentation by condensed phase explosives. FRAGBLAST 8; Proceedings of the 8th International Symposium on rock fragmentation by blasting. B. Mohanty (ed.). Montreal, Canada. CRC Press/Balkema (pub.). Pages 140-151.

Rummel, F., König, E. and Thieme, B., 1992. Fracture mechanics parameters of EPS1 Soultz granite cores. Yellow Report 10, Ruhr - Universität, Bochum, unpublished report. Page 44.

Sellers, E., Furtney, J., Onederra, I., & Chitombo, G., 2012. Improved understanding of explosive – rock interactions using the hybrid stress blasting model. Journal of the South African Institute of Mining and Metallurgy. Vol. 112, Pages 721-728.

Sellers, E., Kotze, M., Dipenaar, L., & Ruest, M., 2009. Large scale concrete cube blasts for the HSBM model. FRAGBLAST 9: Proceedings of the 9th International Symposium on Rock Fragmentation. J.A. Sanchidrian (ed.). Grenada, Spain. CRC Press/Balkema (pub.). Pages 721-728.

Sharma, P. D., 2011. Mechanics of blasting and air-blast – it's concept and control while blasting. Retrieved from: http://miningandblasting.wordpress.com/2011/01/08/mechanics-of-blasting-and-air-blast-its-concept-and-control-while-blasting

Siskind, D., Stagg, M., Kopp, J., & Dowding, C., 1980. Structure response and damage Produced by ground vibration from surface mine blasting. Report of Investigation RI-8507. U.S. Bureau of Mines. U.S. Department of the Interior. Washington, DC, USA. Page 84.

St. J. Tose, S., 2006. A Review of the Design Criteria and Practical Aspects of Developing a Successful Pre-Split. Proceedings of the International Symposium on Stability of Rock Slopes in Open Pit Mining and Civil Engineering. Published by the South African Institute of Mining and Metallurgy. T. Stacey (ed.). Johannesburg, South Africa. Pages 525-545.

Srbulov, M., 2010. Ground vibration engineering – simplified analysis with case studies and examples. Kandilli, A.A., (ed.). Springer (Pub.), New York, USA. Pages 1-202.

Therin, X., 2012. Blasting Optimization. GeoDrilling International. Published September 4th, 2012. Pages 1-2.

Trivino, L., 2012. Study of Blast-Induced Damage in Rock with Potential Application to Open Pit and Underground Mines. Ph.D. Thesis, University of Toronto, Department of Civil Engineering. Pages 14-37.

U.S. Dept. of the Interiors Office, 2008. Blaster training module. Developed by: the Office of Technology Transfer, Western Regional Office, Office of Surface Mining, U.S. Department of the Interior. Denver, Colorado. May 6, 2008. Pages 1-26.

Workman, L. J., & Calder, P. N., 1992. Wall control. Calder & Workman Inc. Pages 23-75.

Yang, J., & Wang, S., 1996. A new constitutive mod-el for rock fragmentation by blasting – Fractal damage model. FRAGBLAST 8; Proceedings of the 8th International Symposium on rock fragmentation by blasting. B. Mohanty (ed.). Montreal, Canada. CRC Press/Balkema (pub.). Pages 95-100.

Yamin, G. A., 2005. Field measurements of blast-induced damage in rock. MASc Thesis. University of Toronto. Pages 1-153.

Yu, T., and Croxal, J., 1985. Kidd Creek blasthole stoping. Proceedings from the international symposium on large scale underground mining. Lulea, Sweden. Pages 97-106.

Appendix I – Iterations of Pre-Split Design

This appendix briefly outlines the iterations that were completed to arrive at an ideal pre-split design in homogeneous rock and in jointed rock.

Iteration for pre-split blasting in homogeneous kimberlite rock:

Kimberlite – 1.5m Hole Spacing

Decoupling ratio of 2 – Split factor = 0.50 kg/m^2

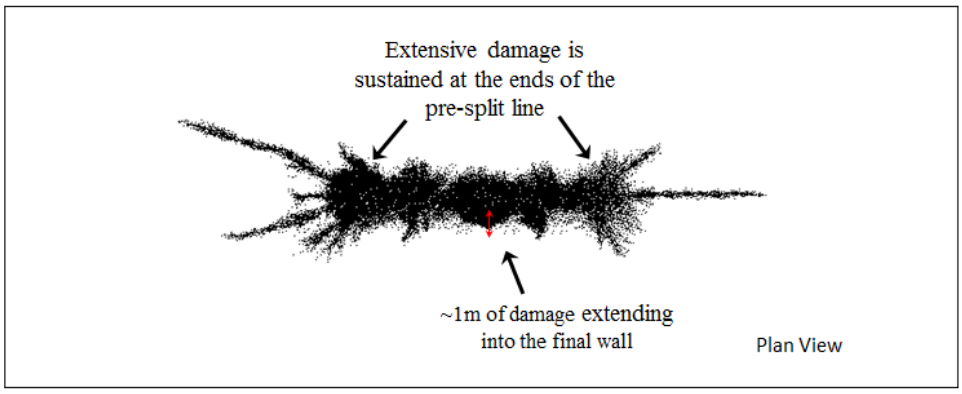

Notice the extensive amount of damage that is sustained to the final wall. In addition, at the ends of the rows there is more damage extending out at 30 degree angles to the pre-split line

Kimberlite – 1.5m Hole Spacing

Decoupling ratio of 3 - Split factor = 0.33 kg/m^2

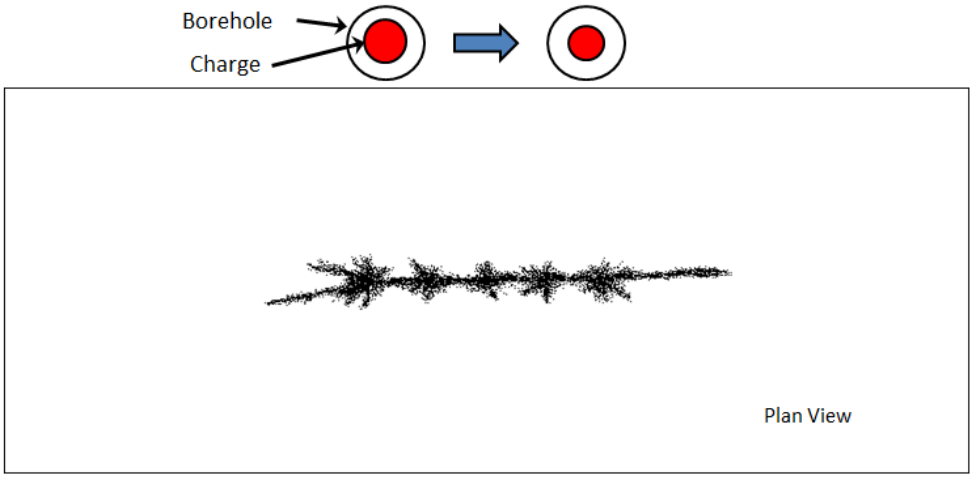

Far less damage occurring to the final wall – crack develops along the pre-split line. Ideal blasting results.

Kimberlite – 1.5m Hole Spacing

Decoupling ratio of 4 - Split Factor = 0.25 kg/m^2

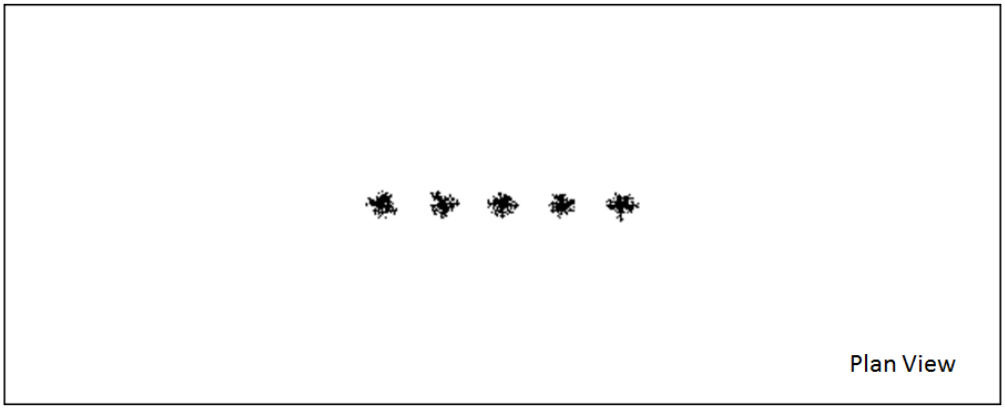

Fracturing does not bridge to adjacent holes due to a lack of explosive energy. The pre-split fracture will not occur based on the results of this model.

Kimberlite – 1.5m Hole Spacing

Decoupling ratio of 3 - Split Factor = 0.50 kg/m^2

150 mm Charge Diameter

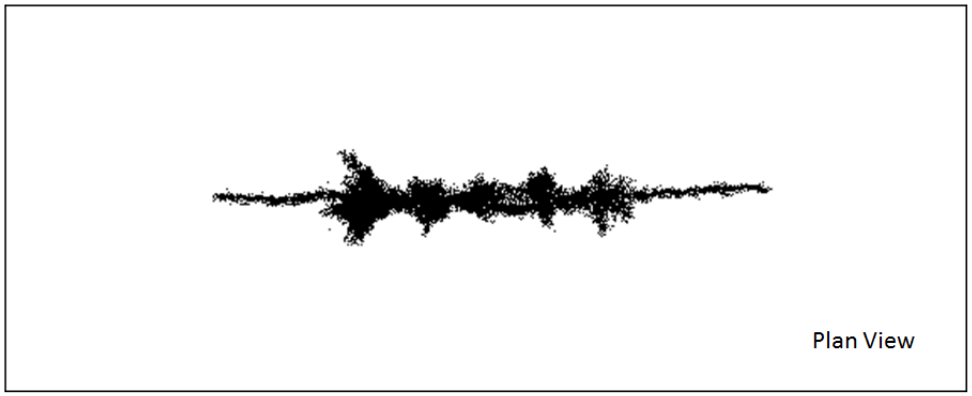

This model demonstrates a larger pre-split hole size. Due to the diameter of the hole, a decoupling ratio of 3 results in more explosive used than a hole of 100 mm.

Iterations for controlling damage at the end of the pre-split line:

Controlling Damage at End of Pre-Split Line

Decoupling ratio of 3 - Split factor = 0.33kg/m^2

Two additional holes drilled on either end of the pre-split line are left unloaded.

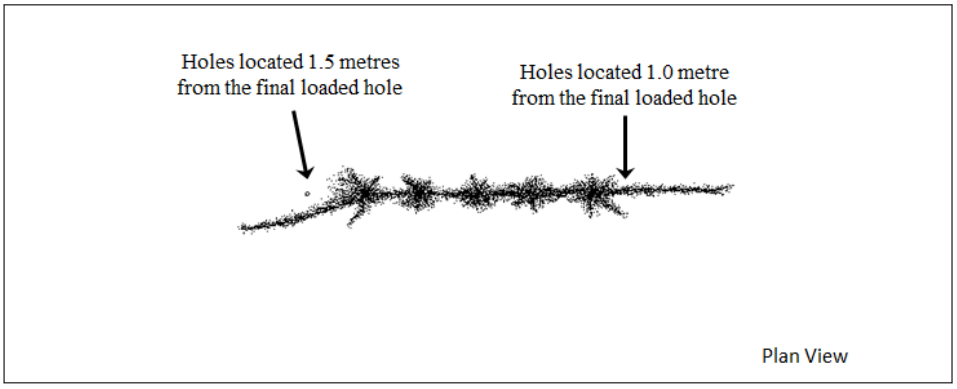

For comparison purposes, this model had a uncharged hole 1.5 metres from the left end of the pre-split and 1.0 metre from the right side of the pre-split. The left side is heavily damages because the uncharged hole was too far away to influence the direction of the fracture propagation.

Controlling Damage at End of Pre-Split Line

Decoupling ratio of 3 - Split factor = 0.33 kg/m^2

Two additional holes drilled on either end of the pre-split line are left unloaded.

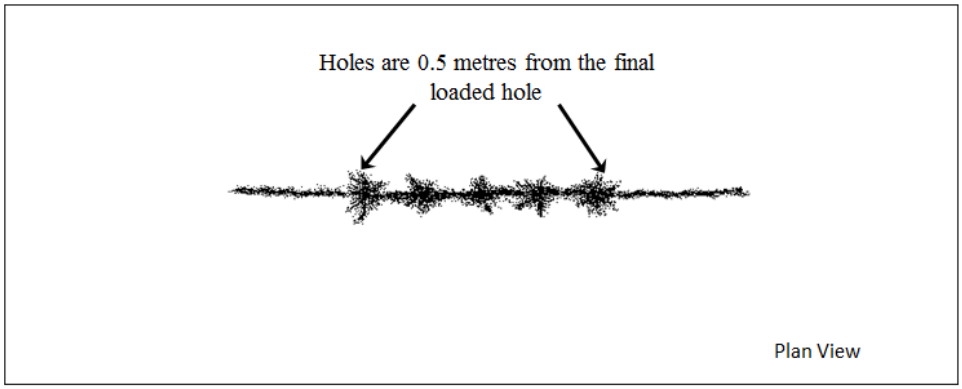

Far less damage occurring at the end of the pre-split line because the extra holes act as a free face, which the explosive energy can break to.

Iterations for a pre-split blast with two sub-vertical joint sets present in the rock mass:

Kimberlite – 1.5m Hole Spacing

2 vertical joint sets present in the rockmass at 45° to each other

Decoupling ratio of 2 - Split Factor = 0.50 kg/m^2

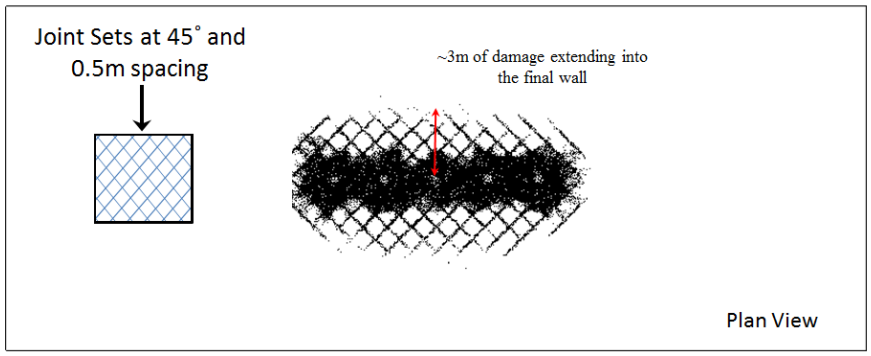

High pressure gasses exploit natural joint sets present in the rockmass. Expect to see ragged final walls, reduced catch benches and accelerated deterioration.

Kimberlite – 1.5m Hole Spacing

2 vertical joint sets present in the rockmass at 45° to each other

Decoupling ratio of 3 - Split Factor = 0.33 kg/m^2

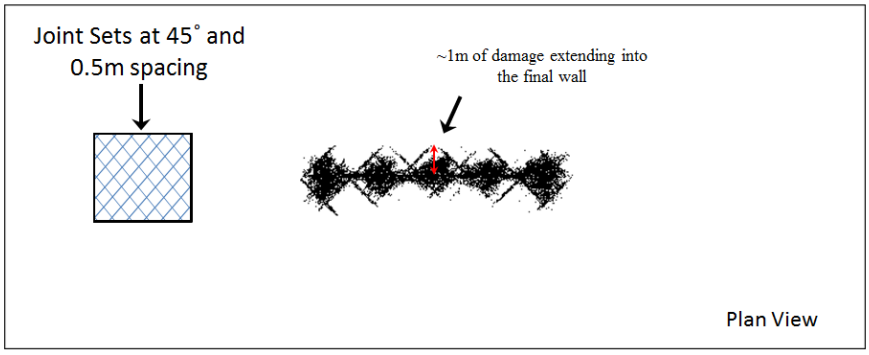

High pressure gasses exploit natural joint sets present in the rockmass. Expect to see ragged final walls, reduced catch benches and accelerated deterioration.

Kimberlite – 1.0m Hole Spacing

2 vertical joint sets present in the rockmass at 45° to each other

Hole spacing reduced to 1.0m and **decoupling**

Ratio increased to 5 - Split Factor = 0.50

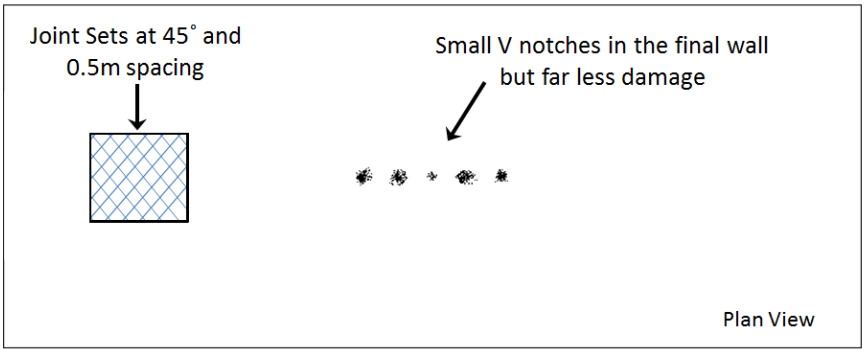

Holes are not close enough together to allow the pre-split fracture to propagate to surrounding holes.

Kimberlite – 0.8m Hole Spacing

2 vertical joint sets present in the rockmass at 45° to each other

Hole spacing reduced to 0.8m and **decoupling**

ratio increased to 5 - Split Factor = 0.38 kg/m^2

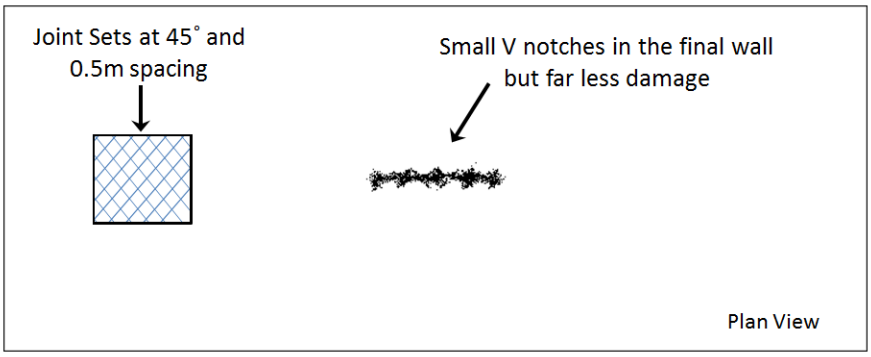

When the results of a blast are strongly influenced by weak geological features, holes drilled closer together and loaded lightly should be used in order to more evenly distribute the blast energy. Holes spaced further apart can result in excessive localized energy which will force open weak discontinuities over long distances.

Iterations for a pre-split blast with joint sets dipping into an open pit:

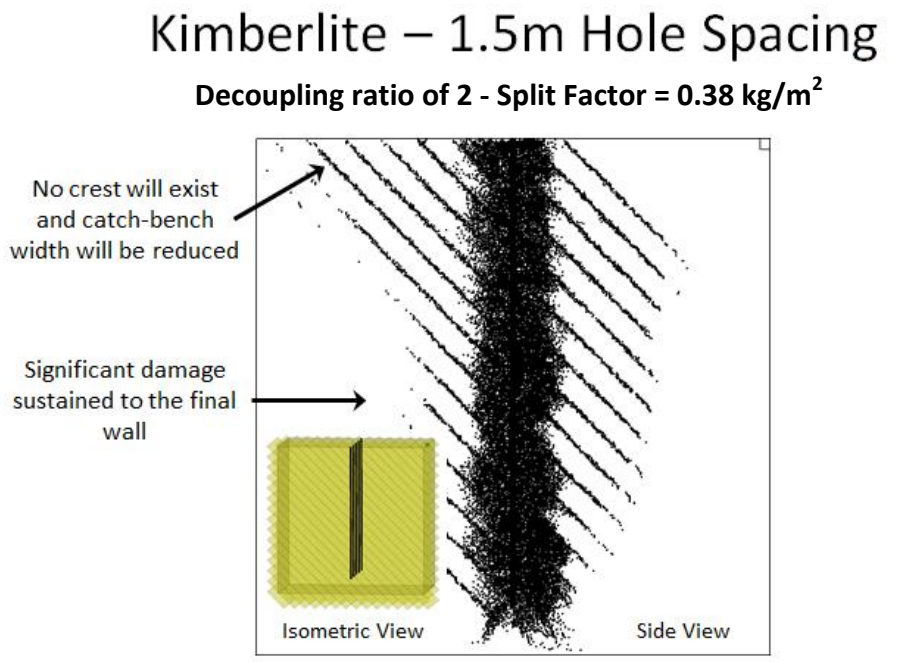

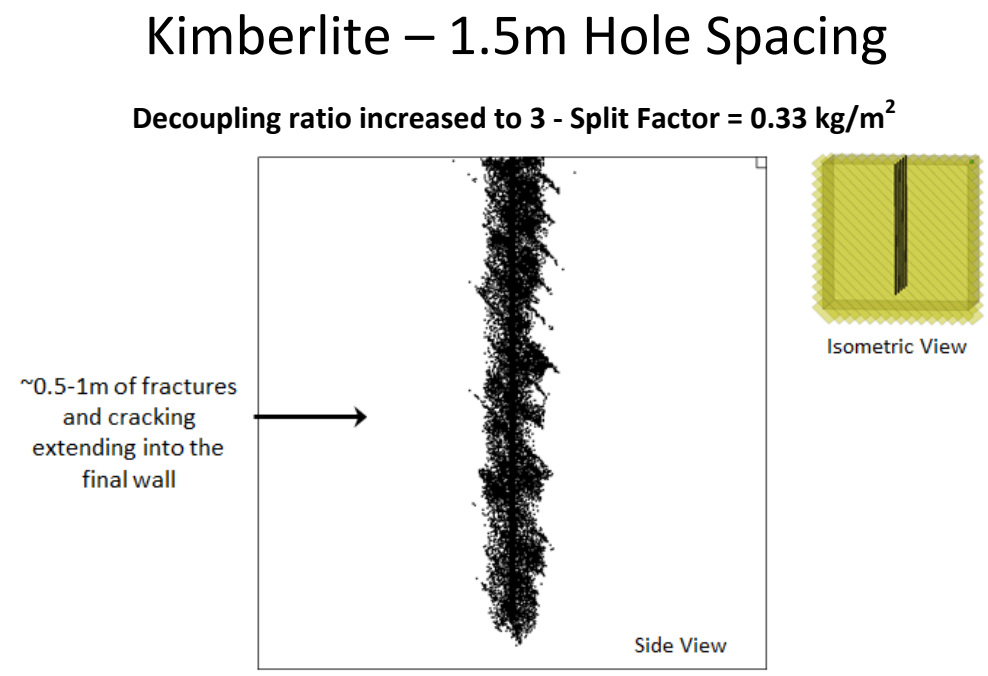

Kimberlite – 0.8m Hole Spacing

Decoupling ratio increased to 5 - Split Factor = 0.38 kg/m^2

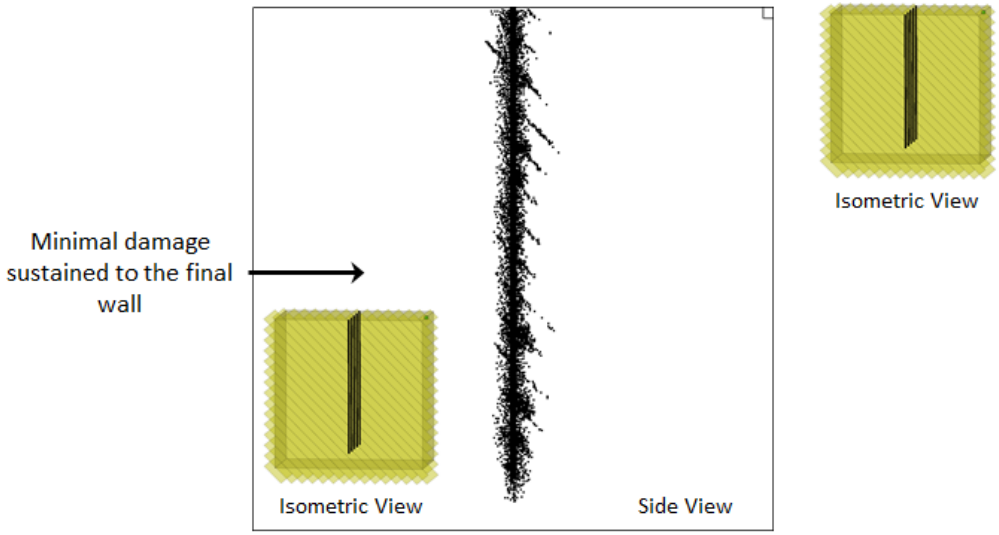

Appendix II – Algorithm to Contour the PPV in Each Lattice

This appendix presents the source code for the algorithm to contour the PPV in each of the PFC3D lattice nodes.

```
;signed-code 50dcbb3cc820b88b0ddbd555e06d73ab7d0cc7d5
; Blo-Up PPV Measurement
(defparameter *ppv-script-version* "1.2")
; This extension monitors the model and tracks the PPV of each lattice node.
; PPV is the maximum velocity vector magnitude occuring in a model.
; To get a plot of maximum velocity:
;   (1) Call this file (via File Menu > Run Script File)
;      *before* building the model
;   (2) Add the Diagnostics > Custom Marker Plot Item
; The function ppv-filter changes the region where the PPV is recorded.

(setf *read-default-float-format* 'double-float)
(defun ppv-filter (pos)
  "Return true for nodes which should have PPV tracked. pos in the
   origional positions of the node."
  (let* ((x-min -100) (x-max 100.0)
         (y-min -0.25) (y-max 0.25)
         (z-min -100.0) (z-max 100.0))
    (v3:bind (x y z) pos
             (and (< x x-max) (> x x-min)
                  (< y y-max) (> y y-min)
                  (< z z-max) (> z z-min)))))
(when (bu:model-built)
  (error "This extension must be loaded before a model is built"))
(defparameter *max-vel* nil
  "A scalar value for each node which is the maximum velocity
   magnitude experienced by this node")
(defparameter *filter-bit-vector* nil)
(defparameter *plot-skip* 1)
(defun max-vel-setup ()
  (setf *filter-bit-vector* (make-array (bu:node-count)
                                        :element-type 'bit
```

```
                                    :initial-element 0))
  (setf *max-vel* (make-array (bu:node-count)
                              :element-type 'double-float
                              :initial-element 0.0))
  (bu:node-loop n
   (when (ppv-filter (bu:node-location n))
     (setf (bit *filter-bit-vector* n) 1)))
  (bu:cycling-hooks-on))
(bu:add-function bu:*post-build-hooks* max-vel-setup)
(defun max-vel-cleanup ()
  (setf *max-vel* nil)
  (bu:cycling-hooks-off))
(bu:add-function bu:*reset-hooks* max-vel-cleanup)
(defun monitor-velocity ()
  "loop over the nodes and keep track of the maximum velocity each
   node reaches"
  (bu:node-loop n
   (when (eq 1 (bit *filter-bit-vector* n))
     (let ((vel (bu:node-velocity-mag n)))
       (when (> vel (aref *max-vel* n))
         (setf (aref *max-vel* n) vel))))))
(bu:add-function bu:*cycling-top-hooks* monitor-velocity)
(defun plot-maximum-velocity (plot-item)
  "Plot a point for each lattice node colored by the maximum velocity
   that node has experienced."
  (when (and (bu:model-built) (boundp '*max-vel*) *max-vel*)
    (bu:node-loop n
     (when (eq 1 (bit *filter-bit-vector* n))
       (when (zerop (mod n *plot-skip*))
         (bu:marker-plot-add-marker plot-item (bu:node-location n)
                                    (elt *max-vel* n)))))))
(bu:add-function bu:*marker-plot-item-list* plot-maximum-velocity)
```

```
(defun save-max-vel ()
  "save the PPV data"
  (with-prompt-for-output-file
    "choose a file to write the maximum velocity data to"
    "*.lisp"
    (format t "(defparameter *max-vel* nil)")
    (format t "(defparameter *filter-bit-vector* nil)")
    (format t "(setf *filter-bit-vector* ~a)" *filter-bit-vector*)
    (format t "(setf *max-vel* ~a)" *max-vel*)))
```

Appendix III – Algorithm to Record the PPV in a Specific Lattice Node

This appendix outlines the PPV script that runs while the model is cycling to record the maximum velocity magnitude a give node reaches.

```
;signed-code 6ec7053159f9de19b64b69bb6f22728245855e29
; Blo-Up PPV Measurement
(defparameter *ppv-script-version* "1.3")
; This extension monitors the model and tracks the PPV of some lattice
; nodes. PPV is the maximum velocity vector magnitude.
(load "util.fas")
(setf *read-default-float-format* 'double-float)
(when (bu:model-built)
  (error "This extension must be loaded before a model is built"))
(defparameter *ppv-points* nil
  "A list of integers. These are the node IDs where we monitor PPV")
(defparameter *ppv-input-points* nil
  "A list of list of numbers. These are the node locations where we   monitor PPV")
(defparameter *ppv-data* nil
  "Array of doubles for PPVs")
(defun ppv-setup ()
  (setf *ppv-points* nil)
  (when (not *ppv-input-points*) (error "no ppv locations given"))
  (setf *ppv-data* (make-array (length *ppv-input-points*)
                               :element-type 'double-float
                               :initial-element 0.0))
  (dolist (p *ppv-input-points*)  ;  find node ids
    (let* ((pv3 (v3:new (first p) (second p) (third p))))
      (push (bu:find-node-near pv3)  *ppv-points*))))
(defun ppv-monitor ()
  "loop over the nodes and keep track of the maximum velocity each
   (tracked) node reaches"
  (loop for i from 0 for node-id in *ppv-points* do
       (let ((vel (bu:node-velocity-mag node-id)))
         (when (> vel (aref *ppv-data* i))
           (setf (aref *ppv-data* i) vel)))))
(defun plot-ppv (plot-item)
```

```
  "Plot a point for each lattice node where the maximum velocity
   is monitored."
  (when (and (bu:model-built) (boundp '*ppv-points*) *ppv-points*)
    (loop for i from 0 for node-id in *ppv-points* do
      (bu:marker-plot-add-marker plot-item (bu:node-location node-id)
                                 (aref *ppv-data* i)))))
(defun ppv-write ()
  "save the PPV data"
  (bu:with-prompt-for-output-file
    "choose a file to write the maximum velocity data to"
    "*.txt"
    (loop for i from 0 for node-id in *ppv-points* do
         (format t "~a ~a~%" (bu:node-location node-id) (aref *ppv-data* i)))))
(defun ppv-cleanup ()
  (setf *ppv-data* nil)
  (setf *ppv-points* nil))
(defun ppv-activate ()
  (bu:add-function bu:*marker-plot-item-list* plot-ppv)
  (bu:add-function bu:*post-build-hooks* ppv-setup)
  (bu:add-function bu:*cycling-top-hooks* ppv-monitor)
  (bu:add-function bu:*reset-hooks* ppv-cleanup)
  (bu:cycling-hooks-on)
  (with-open-file
      (stream (bu:get-input-filename
               "PPV locations data file" "*.txt"))
    (setf *ppv-input-points* (util:read-delimited-numbers stream))))
(ppv-activate)
```

In addition to the PPV script, a measuring script must be loaded at the same time. The measuring script finds the nodes and springs for each sphere and the function update-stress calculates the stress. The equations used in update-stress are the same as those given in the PFC

manual for stress measurement spheres with the exception that the porosity is assumed to be zero in Blo-Up. The measuring script is detailed below:

```
(setf *read-default-float-format* 'double-float)
(load "util.fas")
(defpackage :measurement-sphere (:use :common-lisp)
            (:export :*measurement-sphere-script-version*
                     :*measurement-sphere-list*
                     :init
                     :get-stress
                     :activate
                     :deactivate
                     :plot-nodes
                     :plot-springs
                     :plot-contacts
                     :update-stress))
(in-package :measurement-sphere)
(defparameter *measurement-sphere-script-version* "1.3")
(setf *read-default-float-format* 'double-float)
(when (bu:model-built)
  (error "This extension must be loaded before a model is built"))
(defvar *measurement-sphere-list* nil)
(defstruct measurement-sphere
  pos (node-list nil)
  rad (spring-list nil)
  (spring-hash nil)
  (stress
   (make-array 6
               :element-type 'double-float
               :initial-element 0d0)))
(defun init (stream)
  (setf *measurement-sphere-list* nil)
```

```
  (dolist (sphere (util:read-delimited-numbers stream))
    (destructuring-bind (x y z rad) sphere
      (push (make-measurement-sphere :rad rad
                                     :pos (v3:new x y z))
            *measurement-sphere-list*)))
  (setf *measurement-sphere-list* (nreverse *measurement-sphere-list*)))
(defun reset ()
  (loop for sphere in *measurement-sphere-list* do
       (setf (measurement-sphere-node-list sphere) nil)
       (setf (measurement-sphere-spring-hash sphere) nil)
       (setf (measurement-sphere-spring-list sphere) nil)))
(defmacro measurement-sphere-bind (sphere &body body)
  `(destructuring-bind (pos rad spring-list node-list spring-hash stress)
       (list (measurement-sphere-pos ,sphere)
             (measurement-sphere-rad ,sphere)
             (measurement-sphere-spring-list ,sphere)
             (measurement-sphere-node-list ,sphere)
             (measurement-sphere-spring-hash ,sphere)
             (measurement-sphere-stress ,sphere))
     ,@body))
(defun build ()
  "find the nodes and springs in each measurement sphere"
  (bu:node-loop n
   (loop for sphere in *measurement-sphere-list* do
        (measurement-sphere-bind
         sphere
         (when (< (v3:distance pos (bu:node-location n)) rad)
           (push n (measurement-sphere-node-list sphere))))))
  (bu:spring-loop s
   (loop for sphere in *measurement-sphere-list* do
        (measurement-sphere-bind
         sphere
```

```
          (when (< (v3:distance pos (bu:spring-location s)) rad)
            (push s (measurement-sphere-spring-list sphere))))))
  ; build a map from node to attached springs, blo-up does not store this
  (flet ((node-sign (n1 n2)
           (if (> n1 n2) 1.0d0 -1.0d0)))
    (loop for sphere in *measurement-sphere-list* do
          (measurement-sphere-bind
           sphere
           (let* ((hash (make-hash-table)))
             (loop for n in node-list do
                   (setf (gethash n hash) nil))
             (loop for s in spring-list do
                   (let* ((n1 (bu:spring-node-one s))
                          (n2 (bu:spring-node-two s)))
                     (when (nth-value 1 (gethash n1 hash))
                       (push (list (node-sign n1 n2) s) (gethash n1 hash)))
                     (when (nth-value 1 (gethash n2 hash))
                       (push (list (node-sign n2 n1) s) (gethash n2 hash)))))
             (setf (measurement-sphere-spring-hash sphere) hash))))))
(defun find-contacts (sphere)
  "make a unique list of contact in measurement sphere"
  (let* ((contact-list nil))
    (loop for n in (measurement-sphere-node-list sphere) do
          (bu:node-contact-loop
           n contact
           (when (< (v3:distance (measurement-sphere-pos sphere)
                                 (bu:contact-location contact))
                    (measurement-sphere-rad sphere))
             (pushnew contact contact-list))))
    contact-list))
(defun update-stress ()
  "calculate and store the stress in all measurement spheres"
```

```
(dolist (sphere *measurement-sphere-list*)
  (measurement-sphere-bind
   sphere
   (loop for i below 6 do (setf (aref stress i) 0d0))
   (loop for n in node-list do
        (loop for s-data in (gethash n spring-hash) do
             (let* ((s (second s-data))
                    (sign (first s-data))
                    (np (bu:node-location n))
                    (sp (bu:spring-location s))
                    (d (v3:v3- sp np))
                    (f (bu:spring-force s)))
               (incf (aref stress 0) (* sign (aref d 0) (aref f 0)))
               (incf (aref stress 1) (* sign (aref d 1) (aref f 1)))
               (incf (aref stress 2) (* sign (aref d 2) (aref f 2)))
               (incf (aref stress 3) (* sign (aref d 0) (aref f 1)))
               (incf (aref stress 4) (* sign (aref d 0) (aref f 2)))
               (incf (aref stress 5) (* sign (aref d 1) (aref f 2))))))
     (loop for contact in (find-contacts sphere) do
          (let* ((n1 (bu:contact-node-one contact))
                 (n2 (bu:contact-node-two contact))
                 (n1p (bu:node-location n1))
                 (n2p (bu:node-location n2))
                 (cp (bu:contact-location contact))
                 (cf (bu:contact-force contact)))
            ;(format t "~a~%" cf)
            (loop for np in (list n1p n2p) for sign in (list 1 -1) do
                 (incf (aref stress 0) (* sign (aref (v3:v3- cp np) 0)
                                           (aref cf 0)))
                 (incf (aref stress 1) (* sign (aref (v3:v3- cp np) 1)
                                           (aref cf 1)))
                 (incf (aref stress 2) (* sign (aref (v3:v3- cp np) 2)
```

```
                                        (aref cf 2)))
                    (incf (aref stress 3) (* sign (aref (v3:v3- cp np) 0)
                                        (aref cf 1)))
                    (incf (aref stress 4) (* sign (aref (v3:v3- cp np) 0)
                                        (aref cf 2)))
                    (incf (aref stress 5) (* sign (aref (v3:v3- cp np) 1)
                                        (aref cf 2))))))
    (let* ((volume (* 4/3 pi (expt rad 3))))
       (loop for i below 6 do
            (setf (aref stress i) (/ (aref stress i) volume)))))))
(defun get-stress (sphere-number stress-tensor-component)
  (aref (measurement-sphere-stress
         (nth sphere-number *measurement-sphere-list*))
        stress-tensor-component))
(defun plot-nodes (plot-item)
  (loop for i from 0 for sphere in *measurement-sphere-list* do
       (measurement-sphere-bind
        sphere
        (loop for n in node-list do
             (bu:marker-plot-add-marker plot-item
              (bu:node-location n) i)))))
(defun plot-springs (plot-item)
  (loop for i from 0 for sphere in *measurement-sphere-list* do
       (measurement-sphere-bind
        sphere
        (loop for s in spring-list do
             (bu:marker-plot-add-marker plot-item
              (bu:spring-location s)
              (bu:spring-force-mag s))))))
(defun plot-contacts (plot-item)
  (loop for i from 0 for sphere in *measurement-sphere-list* do
       (loop for c in (find-contacts sphere) do
```

```
            (bu:marker-plot-add-marker plot-item
                                       (bu:contact-location c)
                                       (bu:contact-force-mag c)))))
;; (defun test-out ()
;;   "test function to printout spring hash"
;;   (with-prompt-for-output-file
;;       "txt" "*.txt"
;;       (loop for i from 0 for sphere in *measurement-sphere-list* do
;;            (print i)
;;            (measurement-sphere-bind
;;             sphere
;;             (loop for key being the hash-keys of spring-hash do
;;                  (print key)
;;                  (print (gethash key spring-hash)))))))
(defun activate ()
  (bu:add-function bu:*post-build-hooks* build)
  (bu:add-function bu:*reset-hooks* reset))
(defun deactivate ()
  (setf *measurement-sphere-list* nil)
  (bu:remove-function bu:*post-build-hooks* build)
  (bu:remove-function bu:*reset-hooks* reset))
(activate)
;(measurement-sphere-get-stress-tesnsor (car *measurement-sphere-list*))
;(map 'list #'measurement-sphere-get-stress-tesnsor  *measurement-sphere-list*)
```